universität wien

DISSERTATION/ DOCTORAL THESIS

Titel der Dissertation /Title of the Doctoral Thesis

„Analysis of the seismicity of the Vienna Basin Transfer Fault System with respect to completeness of records and aftershock sequences"

verfasst von / submitted by

Asma Nasir

angestrebter akademischer Grad / in partial fulfilment of the requirements for the degree of

Doktorin der Naturwissenschaften (Dr.rer.nat.)

Wien, 2022/ Vienna 2022

Studienkennzahl lt. Studienblatt / degree programme code as it appears on the student record sheet:	UA 791 426
Dissertationsgebiet lt. Studienblatt / field of study as it appears on the student record sheet:	Erdwissenschaften
Betreut von / Supervisor:	Univ. -Prof. Dr. Bernhard Grasemann
Betreut von / Supervisor:	Dr. Kurt Decker

Table of contents

Appendix A

Nasir, A. Lenhardt, W., Hintersberger, E., & Decker, K., **2013**. Assessing the completeness of historical and instrumental earthquake data in Austria and surrounding areas. Austria Journal of Earth Sciences, 106/1, 90-102. doi: 10.14470/FX099882

Appendix B

Nasir, A., Hintersberger, E., & Decker, K., **2020**. The Dobrá Voda earthquake (M=5.7) at the Vienna Basin Transfer fault: evaluation of the ESI2007 intensity and analysis of aftershock sequence. Austria Journal of Earth Sciences,113/1, 43-58.

Appendix C

Nasir, A., Hintersberger, E., and Decker, K., The temporal evolution of seismicity and variability of b-values along the Vienna Basin Transfer Fault System. (Submitted to Austrian Journal of Earth Sciences, **AJES22_03**)

Acknowledgments

To begin with, I wish to thank Kurt Decker for his guidance and encouragement during all phases of my work. In addition, I would like to thank Bernhard Grasemann for his helpful comments during the final phase of my work.

I am very grateful to my colleague Esther Hintersberger for helping me with my literature research. It is my pleasure to thank my friends and colleagues Stefi Neuhuber and many others at Geozentrum for their contribution, but also for creating an excellent working environment. It has been a pleasure to chat, eat, laugh, cook, and drink with all of you.

My parents deserve my deepest thanks for their understanding, interest, financial support, and unconditional love. The architect behind all of it, "my mother," deserves a big thank you for her unwavering support.

And last but not least, I would like to thank my dearly beloved husband Zaeem Saleem, without whom this project would not have been possible.

Thank you!

1. INTRODUCTION AND PROBLEM STATEMENT

Austria is generally characterized by moderate seismic activity with long recurrence intervals of damaging and strong earthquakes. The average recurrence interval of damaging earthquakes with M≥5/I_0≥VII-VIII is estimated with about 50 years (ZAMG, 2020). The national earthquake catalogue, covering the time since 1201, lists only two strong historical earthquakes: Rennweg, 1201 (M/I_0=6.1/IX) and Ried/Riederberg, 1590 (M/I_0=5.8/IX). The strongest instrumentally recorded earthquake is Schwadorf, 1927 (M=5.2/I_0=VIII; ZAMG 2020). The highest seismicity in Austria is associated with the active Vienna Basin Transfer Fault System (VBTF) in lower Austria, the Mur Mürz Fault in Styria (Gutdeutsch & Aric, 1988; Hinsch & Decker, 2010; Schenková et al., 1995; Sefara et al., 1998), the region north of the Periadriatc Fault System in southern Carinthia (Lenhardt, 1995) and the Inntal Fault in the Inn Valley in the Tyrol (Reiter et al., 2003). Among these faults, the Vienna Basin Transfer Fault System is associated with the highest level of seismic risk. In the 20th century, around 360 earthquakes with M≥3.4 were recorded in Vienna Basin among which 17 were damaging (ZAMG, 2020). The coincidence of a higher level of seismicity, the high level of values at risk, the dense population of more than 2 million people living in the area and the high vulnerability of Austria's main urban centres attracted continued research on the geological and seismological aspects of the Vienna Basin fault system, and the possible occurrences of strong earthquakes there (Gangl, 1974; Gutdeutsch & Aric, 1988; Decker et al., 2005; Hinsch & Decker, 2003, 2010; Hammerl & Lenhardt, 2013; Apoloner et al., 2014).

The VBTF is a seismically active sinistral fault passing between the Eastern Alps and the Western Carpathians in Austria and Slovakia. According to geological evidence derived from Quaternary basin analysis and geodetical data, the VBTF moves with slip rates of about 1-2 mm/year (Decker et al, 2005; Grenerczy et al., 2000; Grenerczy, 2002; Hinsch et al., 2003). Brittle deformation of the VBTF reaches to depth of about 8 to 12 km and the overall seismic slip velocity, estimated from the seismic energy released by the whole fault in the last century, is between 0.22-0.31 mm/yr indicating a marked seismic slip deficit (Hinsch & Decker, 2010). Hinsch and Decker (2003; 2010) further divided the VBTF into segments and found the seismic slip of individual segments varying from 0-0.77 mm/yr proving very significant seismic slip deficits for several, apparently non-moving fault segments that contrast from the fault segments with high seismic slip in the southernmost Vienna Basin and the Dobrá Voda area. Segments with zero seismic slip in historical times such as the Lassee segment East of Vienna are interpreted as locked segments. For the currently locked Lassee segment, Hinsch and Decker (2010) conclude that an earthquake with a magnitude in the range of approximately M=6.0-6.8 every 800 years is necessary to to move the segment at a slip rate of 1-2 millimetres per year. The recurrence intervals of such events, however, are longer than the time coverage of the

existing earthquake catalogue (1201-2020; ZAMG, 2020). The authors therefore conclude that earthquake records in Austria and adjacent Central Europe are too short to provide evidence of such rare events and that it is likely that the observed slip deficits reflect the limitations of the earthquake catalogue rather than tectonic differences between the individual segments of the VBTF. According to empirical scaling relations, these segments are large enough to cause earthquakes that are significantly stronger than those observed during the past few centuries and listed in the Austrian earthquake catalogues (ZAMG, 2020). Hinsch & Decker (2010) find that the maximum credible earthquake for the VBTF is in the range of M_{max}=6.8, which is significantly larger than the magnitude of the strongest recorded earthquake (M = 5.7). Their interpretation is corroborated by archaeological evidence of a M≥6 earthquake in the 4th century that destroyed the ancient Roman city of *Carnuntum*, located next to the VBTF and the locked Lassee fault segment (Kandler, 1989; Decker et al., 2006).

The outlined seismological characteristics of the Austrian territory and the VBTF (moderate seismicity, long recurrence intervals expected for strong earthquakes, the time limitation of earthquake records and the high relevance for seismic risk) motivated the detailed analysis of earthquake catalogues which is in the focus of my thesis. Earthquake catalogues are analysed with respect to (a) catalogue completeness, (b) the degree of reliance of recurrence intervals calculated for the strongest recorded earthquakes based on catalogue data, (c) the reliability to predict recurrence intervals of events stronger than the recorded ones based on Gutenberg-Richter (GR) relations derived from catalogues and (d) the effect of aftershock sequences on local seismicity.

Seismology is primarily concerned with earthquake catalogues. They provide a comprehensive database useful for numerous studies related to seismotectonics, seismicity, earthquake physics, and hazard analysis (Woessner et al., 2005). Therefore, chapter 2 (published in Nasir et al., 2013) examined the time coverage and completeness of historical and instrumental earthquake records for Austria and the surrounding regions focusing on the area around the VBTF finding that data cover too short periods of time and are too incomplete to capture the long-term seismicity of the fault zone. Strong earthquake of M≈6 and stronger occur at time intervals that are longer than the time spans covered by the earthquake catalogues. This conclusion was later supported by the evidence of prehistoric earthquakes on several splay faults of the VBTF (Hintersberger et al., 2012; 2013; 2018; Weissl et al., 2017). The conclusion is further in line with the seismic movement deficits observed by Hinsch & Decker (2003; 2010).

Chapter 2 (Nasir et al., 2013) of this thesis is based on a new composite catalogue for Austria and the Vienna Basin outside of Austria as well as a 100km wide buffer area outside the

boundary of Austria and the Vienna basin. The dataset is based on earthquake data from four different catalogues (ZAMG, 2009; ACORN, 2004; Van Gils & Leydecker, 1991; Shebalin et al., 1998), which cover different record length with a first entry in 1048 AD. Existing approaches in the research of seismic hazard assessment and earthquake catalogue analysis are generally based on the Poisson model since seismic activity is considered to be stochastic in nature (Vere-Jones, 1970). This requires only considering independent earthquakes and excluding dependent seismic events such as fore- and aftershocks, which are included in earthquake catalogues as well. Aftershocks and foreshocks have therefore been removed from the composite catalogue for a reliable estimate of the a- and b-parameters of the Gutenberg-Richter (1942).

The assessment of catalogue completeness and the reliability of the calculated G-R-relation used and compared two different methods for completeness correction. These are the analysis of time series ("temporal course of earthquake frequency", TCEF, Grünthal et al., 1998) and the statistical analysis proposed by Stepp (1972). Since the raw data includes both historical and instrumental events and most of the earthquake record in Austria is pre-instrumental, these computations are first made for intensity. The main focus of this thesis is to assess the completeness of historical and instrumental earthquake data, establish a declustered catalogue after applying completeness corrections and provide a precise estimate of a and b-value of Gutenberg and Richter relations derived from the catalogue. The Stepp (1972) method allows evaluating the minimum observation interval needed for reliable estimations of recurrence periods and estimates the time period for which the catalogue is supposed to be complete. TCEF analyses the cumulative number of earthquakes of an intensity or magnitude class over time (Lenhardt, 1996; Gasperini & Ferrari, 2000; Grünthal et al., 1998). Increases or decreases of the number of earthquakes of a certain intensity/magnitude class over time allow estimating periods of catalogue completeness. However, TCEF does not provide indications of minimum observation intervals required for calculating reliable interevent times.

Aftershock identification and the assessment of the temporal length of the aftershock sequences of large earthquakes is an important aspect of earthquake catalogue interpretation and requires catalogue declustering. It impacts the Gutenberg-Richter (1942) predicted frequency of earthquakes in a certain region and, thereby, seismic hazard assessment. For Austria and the VBTF this is shown by Nasir et al. (2013). Aftershocks are usually identified either by using the empirical Omari's law (Ogata, 1983) or by the combination of spatial (Wells and Coppersmith, 1994) and temporal windows (Gardner & Knopoff, 1974). However, for diffused plate boundaries and intraplate regions with low deformation rates, it is still questionable if aftershocks after a major event may continue for much longer time as predicted by these temporal windows. For intraplate settings with fault slip rates with 1 mm/yr or less,

Stein & Liu (2009) suggest aftershock durations of hundred(s) of years. Chapter 3 of this thesis therefore reviews the applicability of the Stein & Liu (2009) model to the Dobrá Voda segment, the northern most segment of the VBTF System (Decker et al., 2005; Fojtikova et al., 2010; Hinsch & Decker, 2010). The aftershock study is performed after applying the ESI 2007 Environmental Intensity Scale to the earthquake to better constrain the epicentral intensity for the Dobrá Voda earthquake to I_0=IX (Nasir et al., 2020). The intensity assessment is based on the environmental effects caused by the 1906 Dobrá Voda earthquake such as hydrological effects and surface cracks that were described by contemporary authors.

In Chapter 4 of the thesis, the VBTF is assessed by dividing the fault zone into segments to analyse the aftershock patterns of strong events and to determine the Gutenberg-Richter (GR) parameters characterizing the seismicity of the different segments. The seismically active VBTF shows an exceptional pattern of seismic activity with significant earthquake activity in the south and a deficit of earthquakes at the centre. Historical seismicity of VBTF in the southern Vienna Basin apparently features a long-term decline of seismic activity. This gave rise to the speculation that the observed earthquakes belong to an extended aftershock sequence subsequent to a strong, historically not recorded earthquake (Seth Stein, 2010, pers. comm.), comparable to the observation of Stein & Liu (2009) for slow moving active faults. Chapter 4 therefore examines if evidence of long-term decline of seismic activity exists for other segments of the VBTF than the Dobrá Voda segment. Chapter 4 further determines and compares the b-value of Gutenberg Richter (1942) relation of the different fault segments. The Gutenberg-Richter b-values are important for estimating seismicity rates for seismic hazard analysis. The b-value is also related to stress levels and shows changes precursory to the occurrence of large earthquakes (Barrientos et al., 2020). However, the reliability and precision to determine b-value is critically dependant on the availability of long enough earthquake data. The VBTF is therefore assessed after applying completeness corrections to the earthquake catalogues (e.g., Stepp, 1972; Grünthal et al., 1998). These corrections were already performed for VBTF by Nasir et al., 2013. The renewed analysis became necessary due to the use of updated earthquake catalogues (ZAMG, 2020) and extended regional coverage of the area under investigation („extended VBTF“). Data were then analysed to identify possible long aftershock sequences and determine Gutenberg-Richter (GR) b-values. Results, however, did not detect temporal seismicity patterns indicating that strong earthquakes had occurred in the past. The long aftershock sequence of the 1906 Dobrá Voda earthquake remained the only one identified.

2. GEOLOGY AND SEISMICITY IN AUSTRIA

2.1 Seismicity in Austria

For seismic studies, earthquake catalogues are the most important product, which plays a vital role in probabilistic and deterministic hazard analysis. It is important, however, that earthquake catalogues are consistent. Austria has historical records of seismic activity as far back as 1201. Instrumental records started after the Laibach/Ljubljana (1895) earthquake (I_0=VIII-IX; Suess, 1887) and increased after the installation of Weichert Seismographs in 1903 and 1905 (Hammerl et al., 2001). The Laibach/Ljubljana (1895) earthquake also triggered systematic efforts to collect macroseismic data in the former Austro-Hungarian Empire (Hammerl et al., 2001).

Figure 1 and Table 1 show the strong earthquakes with M≥5 that occurred in Austria. The oldest recorded earthquake is 1201 (M=6.1) with an inferred epicentre near Rennweg (Carinthia; ZAMG, 2020). There are the two strong earthquakes with the same epicentral area at Kinderberg in 1267 (M= 5.4) and 1885 (M=5), and two earthquakes (M= 5.2, 5.8) in 1590 with an epicentre near Ried/Riederberg (ZAMG, 2020).

YEAR	M	D	Lat	Long	Z	M	Io	EPICENTER
1201	5	4	47.05	13.62	8	6.1	9	Rennweg
1267	5	8	47.51	15.45	8	5.4	8	Kindberg
1590	9	15	48.26	16.07	6	5.2	8	Ried
1590	9	15	48.26	16.07	6	5.8	9	Ried
1670	7	17	47.28	11.51	6	5.2	8	Hall in Tirol
1768	2	27	47.82	16.24	9	5	7	Wiener Neustadt
1885	4	30	47.51	154.5	8	5	7	Kindberg
1886	11	28	47.32	10.84	8	5.1	7.5	Nassereith
1927	7	25	47.53	15.49	11	5.1	7	Wartberg
1927	10	8	48.07	16.58	6	5.2	8	Schwadorf
1930	10	7	47.36	10.66	9	5.3	7.5	Namlos
1936	10	3	47.07	14.7	8	5	7	Obdach
1938	11	8	47.96	16.4	10	5	7	Ebreichsdorf
1939	9	18	47.77	15.91	10	5	7	Puchberg
1964	10	27	47.63	15.81	15	5.3	6.5	Semmering
1972	4	16	47.71	16.18	10	5.3	7.5	Pitten
1983	4	14	47.66	15.13	10	5	6.5	Weichselboden

Table 1: Earthquakes with M≥5 in Austria (from ZAMG 2020 earthquake catalogue).

2.2 Major active faults in Austria

Austria is geologically subdivided into the Bohemian Massif, the Molasse Zone, the Helvetic and Penninic units forming the external Alpine thrust sheets, the Austro-Alpine unit including the

Northern Calcareous Alps and the Austroalpine crystalline units, and Southern-Alpine units (Janoschek & Matura, 1980).

The main active faults in Austria are shown in Figure 1 and listed Table 2. Fault data is taken from the SHARE online data base (SHARE, http://diss.rm.ingv.it/share-edsf/SHARE_WP3.2_Database.html). One of the most active faults is the Vienna Basin Transfer Fault (VBTF), which is a 450 km long NE-SW-striking sinistral strike-slip fault system. In the SW, the VBTF crosses through the central part of the southern Vienna Basin and links up with the Mur-Mürz Fault System. Further north, it limits the Vienna Basin to the east (Figure 1). The Vienna basin itself is almost 180 km long. The fault system was established in the Miocene (between Badenian and Pannonian, ca. 15 to 6 Ma) when it formed the Vienna Pull-Apart basin at a major releasing bend of the fault (Royden, 1988; Wessely, 1988).

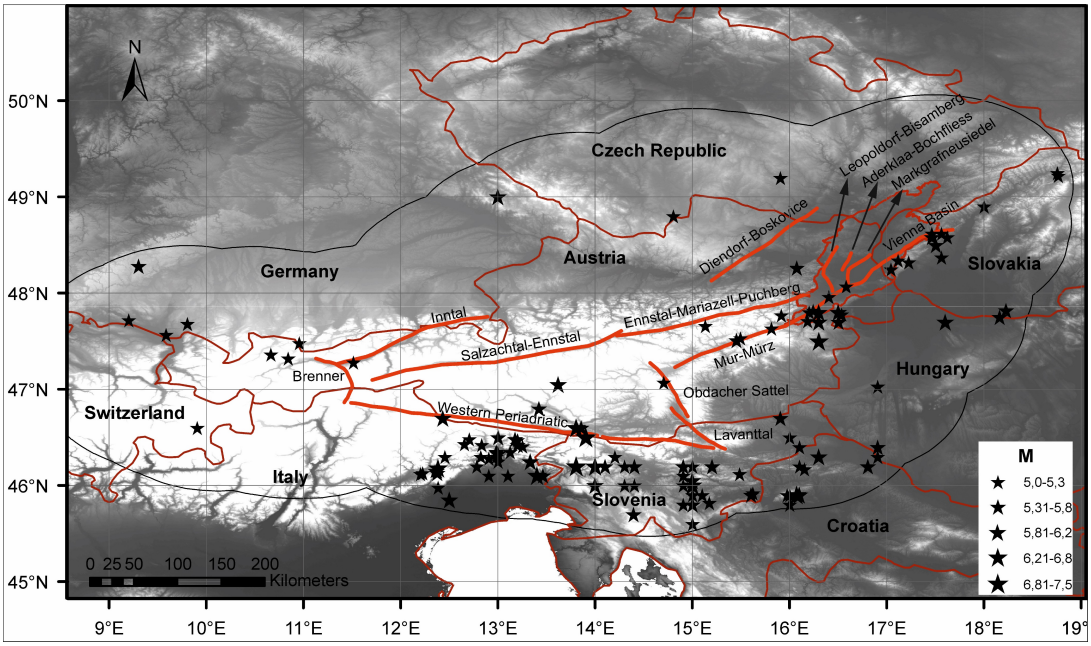

Figure 1: Major active fault and strong earthquakes in Austria and the surrounding areas. Faults are denoted by red lines. The fault data has been taken from (http://diss.rm.ingv.it/share-edsf/SHARE_WP3.2_Database.html). Black stars in the figure denote earthquakes of M≥5 from the manually compiled composite catalogue for Austria and a buffer area of 100 km (ZAMG, 2020; ACORN, 2004; Van Gils & Leydecker, 1991; Shebalin et al., 1998; Nasir et al., 2013).

The main faults shown in Figure 1 are shortly characterized as follows:

The Vienna Basin Transfer Fault: The historical and instrumental seismicity along the VBTF is characterized by M_{max}=5.2/I_{max}=VIII (ACORN, 2004; AEC, 2015). The strongest historical earthquakes associated with the VBTF are the earthquake of *Carnuntum* in the 4th Century AD

(M≥6, Decker et al., 2006; Decker et al., 2015) and the Dobrá Voda 1906 earthquake (I_0=IX-X; Nasir et al., 2020). The maximum magnitude derived from maximum rupture area (Table 2) is M_w=6.8 (Beidinger et al., 2009; http://diss.rm.ingv.it/share-edsf/SHARE_WP3.2_Database.html). The Slip rates, derived from GPS measurements (Grenerczy et al., 2005) and geological modelling (Decker et al., 2005) show a sinistral movement along the VBTS with a velocity in the order of 1.5-2.0 mm/yr. The seismic displacement rates obtained from historical and instrumentally recorded earthquakes show significantly lower displacement velocities of ca. 0.2-0.3 mm/yr on the average for the whole fault (Hinsch & Decker, 2003; 2010). The authors conclude a significant seismic movement deficit from the difference between geodetically and geologically derived slip velocities and the seismic slip velocities. They further conclude that the historical and instrumental earthquake records cover too short periods of time and are too incomplete to capture the long-term seismicity of the VBTF. The presumption that the time coverage of earthquake catalogues is too short to cover the seismic cycle of the VBTF and that catalogue incompleteness is a further reason for the observed seismic slip deficit are a starting point for the thorough investigations into the completeness of the earthquake data in the Vienna basin by Nasir et al., (2013).

No.	Fault Name	Z (km)	Strike (deg)	Dip (deg)	Rake	Slip rate (mm/a)	M_{max}	Code
1	Vienna Basin Transfer Fault	0-12	210-230	60-90	340-360	1-2	6.9	ATC001
2	Markgrafneusiedel Fault	0-11	0-50	40-70	270-290	0.05-0.1	7	ATC002
3	Aderkla-Bockfliess	0-6	180-220	40-70	270-290	0.01-0.05	6.2	ATC003
4	Mur-Mürz	0-11	240-250	60-90	0-20	1-2	6.5	ATC004
5	Leopoldsdorf-Bisemberg	0-9	350-30	40-60	260-280	0.05-0.2	6.8	ATC005
6	Ennstal-mariazell-puchberg	0-13	240-270	60-90	340-350	0.01-0.1	6.1	ATC006
7	Salzachtal-Ennstal	0-11	235-270	50-80	340-350	0.01-0.1	6.1	ATC007
8	Obdacher Sattel	05-12	130-155	60-80	150-170	0.1-1	5.6	ATC008
9	Lavanttal	05-12	290-320	60-80	150-170	0.1-1	5.6	ATC009
10	Western Periadriatic	0-19	260-300	70-90	130-170	0.5-1	7	ATC010
11	Eastern Periadriatic	0-19	270-300	70-90	130-170	0.5-1	7	ATC011
12	Brenner	3.5-16.5	110-170	30-50	260-280	0.5-1	6.8	ATC012
13	Inntal	4.5-11.5	50-80	60-80	10-30	0.5-1	6.1	ATC013
14	Diendorf-Boskovice	0-15	220-250	70-90	0-20	0.01-0.05	7	ATC014

Table 2: Active faults in Austria according to the SHARE Database (http://diss.rm.ingv.it/share-edsf/SHARE_WP3.2_Database.html)

The Mur-Mürz Fault is the south-eastern continuation of the sinisitral VBTF strike slip fault (Fig. 1). The fault is 30-40 km long and 11 km deep as derived from an instrumental seismic data (http://diss.rm.ingv.it/share-edsf/SHARE_WP3.2_Database.html). Based on GPS, geodetic data and regional dynamic is 1-2 mm/yr with maximum magnitude M_w= 6.5 (Sefara et al., 1998; Tóth et al., 2006; http://diss.rm.ingv.it/share-edsf/SHARE_WP3.2_Database.html).

The Salzachtal-Ennstal-Mariazell-Puchberg fault is a sinistral strike slip fault system (Fig. 1) in the Eastern Alps with length of 400km (Frost et al., 2009). The fault formed under ductile to brittle deformation conditions. The depth of the eastern part of the active fault system (Ennstal evaluated from speleothems (Plan et al., 2010) and on earthquake data (Lenhardt et al., 2007) is 0-13 km. The seismic slip velocity assumed from regional dynamics is 0.01-0.1 mm/yr and maximum magnitude M_w=6.1 based on tectonically damaged speleothems and macroseismic earthquake data (Plan et al., 2010; http://diss.rm.ingv.it/share-edsf/SHARE_WP3.2_Database.html). The western part of the fault system, the **Salzachtal-Ennstal** fault has a depth of 0-11 km, which is based on geomorphology and seismic data (Lüschen et al., 2004). The maximum magnitude at this fault M_w=6.1 is evaluated from earthquake data (Lenhardt et al., 2007).

The Lavanttal and Obdacher Sattel faults are major NW-SE-striking dextral strike slip faults in the Austroalpine units east of the Tauern Window (Fig.1; http://diss.rm.ingv.it/share-edsf/SHARE_WP3.2_Database.html). For these faults a minimum depth and maximum depth of 5 km and 12 km, respectively, is inferred from earthquake data (Reinecker & Lenhardt, 1999; Lenhardt et al., 2007). The maximum magnitude estimated from regional seismological data is M_{max}=5.6. Vrabec et al. (2006) estimate a slip rate of 0.1-1 mm/yr based on seismicity and geological considerations (http://diss.rm.ingv.it/share-edsf/SHARE_WP3.2_Database.html).

The Western and Eastern Periadriatic Fault System are crustal-scale strike slip faults forming the plate boundary between the Adriatic Plate and the Austroalpine Units at the surface over a length of more than 400 km (Fig. 1; http://diss.rm.ingv.it/share-edsf/SHARE_WP3.2_Database.html). The depth derived from geomorphology and seismic data is 0-19 km (Willinghofer & Cloetingh, 2003; Lüschen et al., 2004). The maximum magnitude M_w=7 based on historical seismic records from Guidoboni et al., (2007). The slip rate assumed from GPS data is 0.5-1 mm/yr (Vrabec et al., 2006; Caporali et al., 2009; http://diss.rm.ingv.it/share-edsf/SHARE_WP3.2_Database.html).

The Brenner Fault is a crustal-scale normal fault delimiting the Tauern Window towards the West (Fig. 1; http://diss.rm.ingv.it/share-edsf/SHARE_WP3.2_Database.html). The depth range of seismogenic faulting is estimated to be between 3.5-16.5 km derived from earthquake data (Reiter et al., 2005). The slip rate derived from GPS data is 0.5-1 mm/yr (Reiter et al., 2005). The maximum magnitude M_w=6.8 is inferred from maximum rupture area (Wells & Coppersmith, 1994; http://diss.rm.ingv.it/share-edsf/SHARE_WP3.2_Database.html).

The Inntal Fault System is a strike slip fault connected to the Sub-Tauern Ramp Fault System (Fig. 1) north of the Tauern Window in the Tyrol, Austria. The depth 4.5-11.5km is evaluated from earthquake data (Lenhardt et al., 2007) and geophysical data (http://diss.rm.ingv.it/share-edsf/SHARE_WP3.2_Database.html). The slip rate based on GPS data is 0.5-1 mm/yr (Reiter et al., 2005) and the maximum magnitude inferred from fault dimension (Wells & Coppersmith, 1994) is M_w=6.1 (Lenhardt et al., 2007).

The Diendorf-Boskovice Fault is a strike slip fault (Fig. 1) of 200 km length which forms the eastern margin of Bohemian Massif, Austria (Hintersberger & Decker, 2017). The depth 0-15 km assumed from geomorphology, regional geology, and geodynamics (Lankreijer et al., 1999). The slip rate and maximum magnitude inferred from regional geodynamics and regional seismological data is 0.01-0.05 mm/yr and M_w=7 respectively (http://diss.rm.ingv.it/share-edsf/SHARE_WP3.2_Database.html).

2.3 Active faults of the Vienna Basin Transfer Fault System

2.3.1 *The Vienna Basin Transfer Fault and its fault segments*

The Vienna Basin Transfer fault (VBTF) is NNE-SSW striking left-lateral active fault in Vienna Basin (Hintersberger et al., 2012). The historically moderate seismicity (I_{max}/M_{max}=VIII-IX/5.7) is concentrated on the southern (Wiener Neustadt-Mitterndorf-Schwadorf) (ACORN, 2004; AEC, 2015) and northern (Dobrá Voda) sections of the VBTF, while the central section of the fault (Arbesthal- Lassee-Zohor-Solosnica) recorded almost no earthquakes in the past 500 years (Beidinger & Decker., 2011). The Dobrá Voda segment (Slovakia) is the currently most active part of the fault and is interpreted as a restraining bend showing reverse faulting (Fojtikova et al., 2010; Beidinger & Decker, 2011; Hinsch & Decker, 2010).

For the Lassee segment, geological and geomorphological data indicate horizontal quaternary displacement rates of 1-2 mm/yr (Beidinger et al., 2011). New data include evaluations of two paleoseismological trenches and lidar-based elevation data. The results show at least 3 major earthquakes (M>6) in the last 90 thousand years, whereby the youngest is not older than 40 thousand years and reaches the recent surface of the earth (Hintersberger et al., 2012; 2013). Assuming that the latter offset arose as a result of the recent earthquake can be concluded on it that seismic movement at the VBTS is mainly caused by earthquakes M≈7 and return periods of several thousand years (Decker et al., 2015).

Active faults in central Europe are typically very slow and the Large earthquakes occur at recurrenece intervals of several hundred to several thousand years. The average recurrence interval for M_w=6 earthquakes estimated from Figure 2 for the VBTF with its average slip velocity in the order of 1 mm/yr is about few hundred years, for M=6.5 little less than 1000 years and for M=7 more than 1000 years. These recurrence intervals exceed the length of available earthquake catalogues. The historical records in central europe mostly cover time scales between 500 to 1000 years.

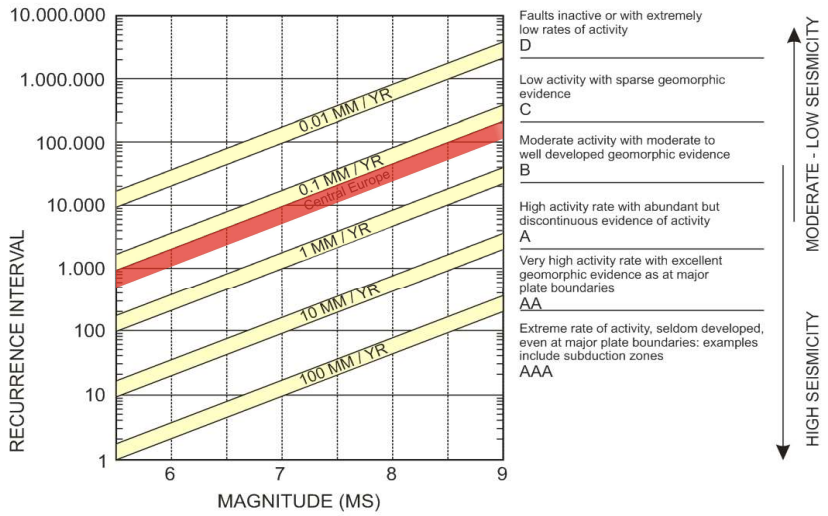

Figure 2: Magnitude vs. recurrence interval plot for different fault slip velocities and earthquakes in low to high seismicity areas . Red bar shows that the expected recurrence times for strong earthquakes (M≈6-7) are in the order of 500 to several thousand years for slip velocities of 0.1 mm/yr which are typical for faults in central Europe (Slemmons & Depolo, 1986).

Below is the list of active faults that are part of the VBTF, that were verified so far:

2.3.2 *Leopoldsdorf fault*

The Leopoldsdorf Fault System comprises a set of normal faults at a releasing bend of the VBTF (Decker et al., 2015). The reflection seismic data reveals that the fault extends between 0-9 km depth. The active slip velocity is estimated with 0.05-0.2 mm/yr (Hinsch et al., 2005) and a maximum magnitude M_w=6.8 inferred from maximum rupture area (Wells & Coppersmith, 1994). Activity of the Leopoldsdorf Fault System is inferred from the offset and tilting of fluvial paleo-landscapes in the hanging wall of the listric fault (Decker et al., 2015). Among others, the late Pleistocene terraces of the Danube are displaced by the fault system (Hinsch et al., 2005). Quaternary activity is also documented by offsets of Middle Pleistocene loess and late Pleistocene (possibly also Holocene) Danube gravel, which was exposed in historical sand and

construction pits (Decker et al., 2015). Biostratigraphic dating of the displaced sediments and historically reported offsets at individual faults show slip velocities in the range of a few hundredth of a millimetres per year (Plachy, 1981; Decker et al., 2015).

2.3.3 *Bisamberg-Nussdorf fault*

The Bisamberg-Nussdorf fault system consists of several east-dipping faults on the western margin of the Vienna basin on the border between the Miocene Pull-Apart basin and the flysch units further west (Decker et al., 2015). The quaternary activity of the fault is inferred from geomorphological data (tilting of the Pleistocene Gänserndorf terrace, offset Pleistocene terrace sediments, morphological fault levels; Decker et al., 2005; Decker et al., 2015) and outcrop data documented from several historical outcrops in the Vienna city area (Decker et al., 2005; Hinsch et al., 2005). From the tilting and the offset of the Gänserndorf Terrace an average slip velocity of about 0.15 mm/yr is estimated (Hintersberger et al., 2013; Decker et al., 2015).

2.3.4 *Aderklaa-Bockefliess fault*

The Aderkla-Bockfliess faults are normal faults (Fig. 1) in the north-central Vienna Basin that dip towards Northwest. The faults offset the Pleistocene Gänserndorf Terrace (Weissl, 2017) having 6 km depth (Decker et al., 2015). The slip velocity based on the geological and geomorphological data is about 0.01-0.05 mm/yr (Weissl, 2017). A maximum magnitude of M_w=6.2 is inferred from the maximum rupture area of the fault (Wells & Coppersmith, 1994). The quaternary activity of the Aderklaa-Bockfliess faults is evident from the linear fault scarp west of the Gänserndorf terrace, the offset of the basal Quaternary unconformity and up to 40m thick Quaternary growth strata of the Aderklaaer Basin (Decker et al., 2005; Weissl et al., 2015). A trench across the fault shows downthrown gravel of the Gänserndorf Terrasse (Weissl et al., 2015). The basis of the Gänserndorf Terrace is vertically offset by ~ 10m at the fault revealing an average displacement rate of 0.03 mm/yr. More recent surface offsets were reported from the NNW continuation of the fault through deformation bands with a few centimetres offset in the late Pleistocene loess (14-15 ka) (Weissl et al., 2015; Decker et al., 2015).

2.3.5 *Markgrafneusiedel fault*

The Markgrafneusiedl Fault (MF) is normal branch fault of the VBTF (Fig. 1), which is located at central Vienna Basin (Decker et al., 2015). The fault is 16km long (Spahić et al., 2013). The depth obtained from geophysical data is 11km (Hinsch et al., 2005) and the slip rate which is based on Quaternary geology and paleoseismology data is 0.05-0.1 mm/yr. The maximum magnitude M=7 which is inferred from paleoseismological data and fault geometry (Hintersberger et al., 2012; 2018).

The fault delimits and cuts the Late Pleistocene Gänserndorf Terrace to the east. Although neither historically nor instrumentally recorded earthquakes are known to be associated with this fault, it has an outstanding linear tectonic fault scarp with up to 17m high due to Quaternary movement along the MGNS (Decker et al., 2015). Three Paleoseismological trenches shows that five earthquakes with magnitudes between M ~ 6.3 and M ~ 7.0 have occurred on this fault in the period between 13.8 ± 1.4 ka and 104 ± 12 ka. An average displacement rate of less than 0.1 mm/yr is well constrained by geomorphological and paleoseismological data (Hintersberger et al., 2018; Decker et al., 2015).

3. METHODS USED TO ANALYSE SEISMICITY

3.1 Compilation of the earthquake catalogue

The compiled composite catalogue of the area considered for completeness analysis covers Austria, the Slowak part of the VBTF and a 100 km wide buffer outside of the Austrian borders and the VBTF (Figure 3). The seismicity of Austria and the VBTF was analysed using four different catalogues, the recent Austrian earthquake catalogue named ZAMG (1201-2020) with an intensity range of I_0=II-IX (ZAMG, 2020) supplemented by the ACORN (1600-2004) earthquake catalogue (Lenhardt et al., 2007) covering the area of Eastern Alps, Western Carpathians and Bohemian Massif (Czech Republic, Slovakia, Hungary and Austria), the European catalogue (Van Gils & Leydecker, 1991) covering the area of Germany, Switzerland and Italy with a data length from 479 BC to 1981 AD and the SE-European Catalogue (Shebalin & Leydecker, 1998) that covers the area of Slovenia, Croatia and Hungary with a data length from 342BC to 1990AD.

The compiled composite catalogue has been declustered and further used for completeness analyses according to the procedure proposed by Stepp (1972) and the TCEF method (Temporal Course of Earthquake Frequency; Grünthal et al., 1998; Lenhardt et al., 1996; Gasperini & Ferrari, 2000; Nasir et al., 2013).

The compiled earthquake catalogue includes both historical and instrumental earthquake data, which cannot be considered complete and consistent due to several reasons. Incompleteness of historical earthquake can be due to a threshold of records (Gutdeutsch & Hammerl., 1997, 1999). This threshold depends on population density, the local intensity of earthquakes, social and political circumstances, the interest of chronologist who could take note of event and other natural disaster which distract the attention from earthquakes (Hammerl et al., 2001).

Instrumental records of seismic events are available from about 1905 onwards as shown in Figure 4.

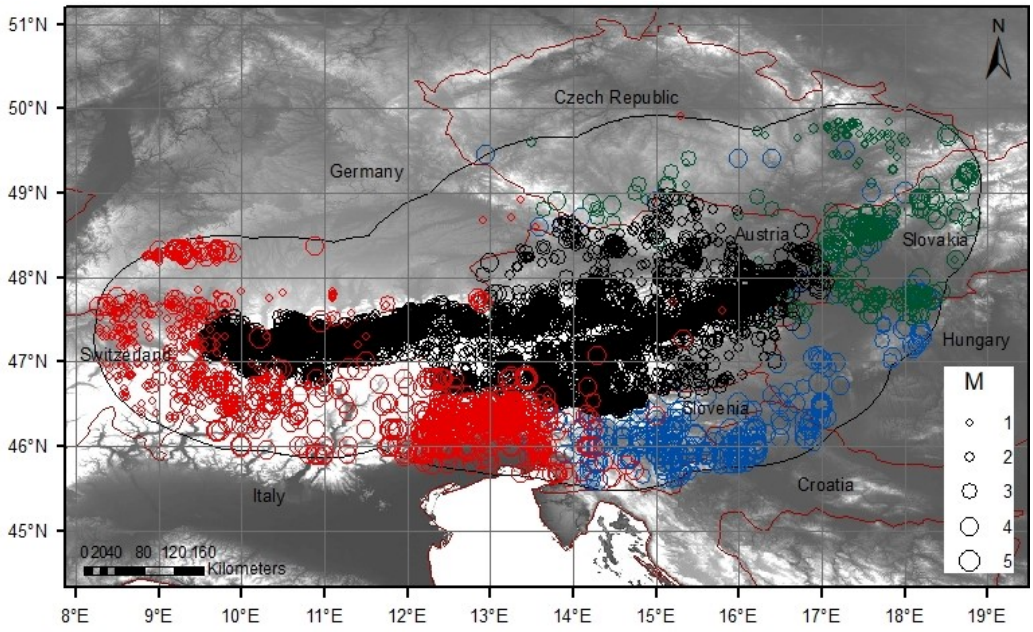

Figure 3: Composite catalogue for Austria based on data from four different earthquake catalogues (ZAMG, 2020; ACORN, 2004; Van Gils & Leydecker, 1991; Shebalin et al., 1998). It also includes the data from surrounding regions such as Vienna basin outside the Austria and a buffer region 100km outside the boundary of Austria and Vienna basin. The magnitude range is from 1–6.1 (ZAMG; 1201 – 2020); (Green) ACORN Earthquake Catalogue (1267 – 2004 AD) with magnitude ranges from 0-5.8 (Lenhardt et al., 2007); (Red) European Earthquake catalogue for Austria and a 100 km buffer area outside the boundary of Austria (479BC - 1981 AD). The magnitude range is from 0-6.8 (Van Gils & Leydecker, 1991). (Blue) Southeast European Earthquake Catalogue (342BC – 1990AD) with magnitude range of 1.6-7.5 (Shebalin & Leydecker, 1998).

Catalogue	I_{min}	I_{max}	Start	End
ZAMG	III	IX	1201	2020
ACORN	II	VIII	1600	2004
European	IV	X	497	1981
SE-European	III	IX	342	1990
Composite	III	X	1048	2020

Table 3: Earthquake catalogues used to compile a dataset for Austria, the VBTF and a 100 km wide margin around Austria.

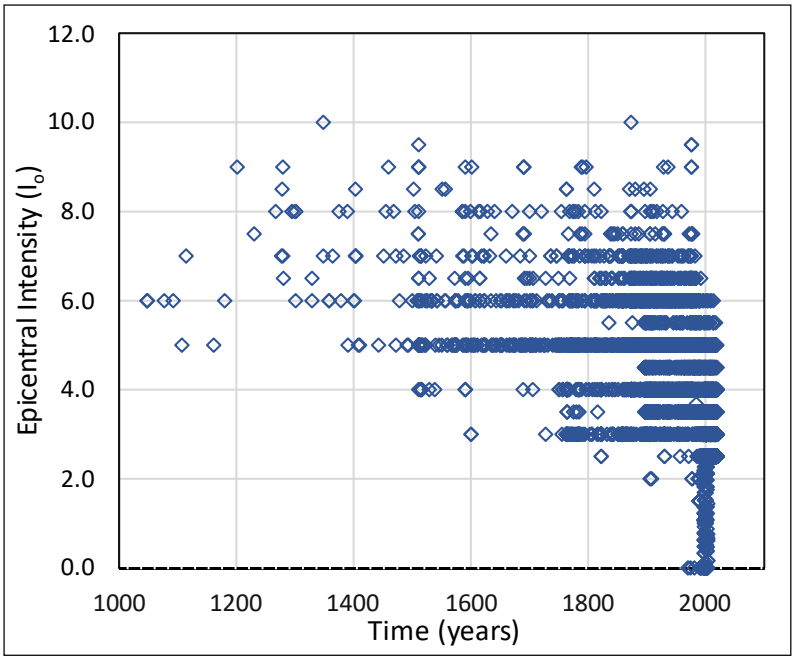

Figure 4: Distribution of earthquake records over time versus Epicentral Intensity (I_0) from 1048 to 2020 (ZAMG, 2020). The plot shows a significant improvement of records from 1905 on, which is related to the installation of seismographs in the former Austrian Empire. Data from the compiled composite catalogue (Figure 3, Table 3).

The compiled catalogues include both historical seismic data (about 70%) and instrumental seismic data (30%). For historical events, the primary data in the earthquake catalogues is exclusively intensity. However, for all computations, for example completeness analysis and calculations of b-values of Gutenberg-Richter relations, the historical earthquake data needs to be converted into magnitude. Although some assessment like completeness estimates can be done using intensity scale as in Nasir et al. (2013), calculations of Gutenberg-Richter parameters require conversions into magnitude. Most but not all earthquakes in the different catalogues are listed with both intensity and magnitude. Missing earthquake magnitudes have been converted using the following empirical conversion equations for the region of central Europe:

Germany (Grünthal et al., 1988)	$M = 0.63 * I_o + 0.5$	(European Catalogue by Van Gils & Leydecker, 1991)
Austria (Wolfgang Lenhardt)	$M = 2 / 3 * I_o$	(Austrian catalogue by ZAMG, 2020)
Switzerland (Rottner´s relation)	$M = 0.5 * I_o + 1.5$	(SE-Europe Catalogue by Shebalin & Leydecker)
Hungary (Karnik, 1968)	$M = 0.6 * I_o + 0.3$	(ACORN catalogue by Lenhardt et al., 2007)

The catalogues used to compile a comprehensive database have different regional intensity-magnitude conversions. To ensure that any further interpretation of magnitude is based on consistent data, the differences between the different correlations were assessed. Using the

manually compiled earthquake catalogue 2020, these formulas are derived from intensity magnitude relations for the pre-instrumental earthquakes (1048-1905) and instrumental earthquakes (1906-2020). The correlation of intensity-magnitude for individual catalogue is also determined as shown in Table 4.

The results show that the correlation between intensity and magnitude (I/M correlation) of the composite catalogue 2020 for pre-instrumental and instrumental earthquake data is $M=0.696I_o$ and $M=0.578I_o$ respectively (Figure 5a; 5b). The difference of I/M correlation of pre-instrumental and instrumental earthquakes is 0.12. Similarly, the coefficients derived for I/M correlations of the individual catalogues by ZAMG (2020), the European catalogue, the SE-European catalogue and ACORN also differ from historical to instrumental earthquakes from 0.02, 0.021 and 0.011 respectively (Table 4).

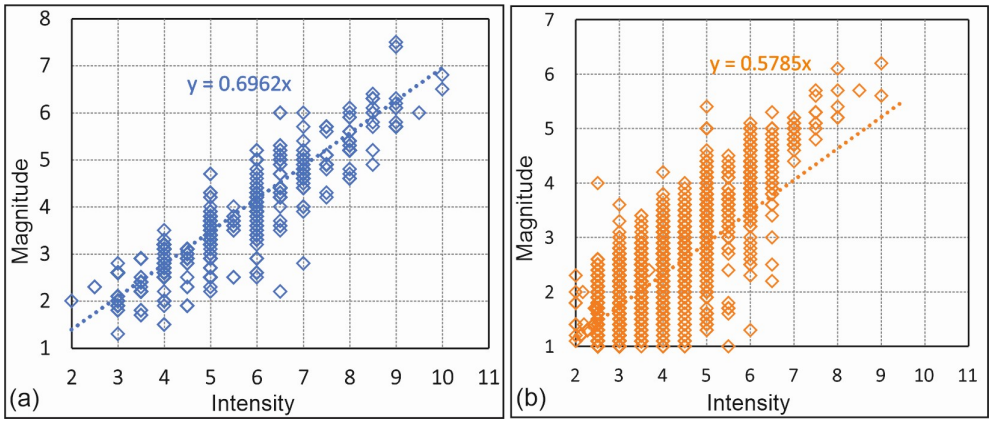

Figure 5: Intensity vs. magnitude plots for pre-instrumental earthquakes (before 1905, blue symbols) and instrumental data (1906 to present, orange symbols). Data from the compiled composite catalogue by Nasir et al., in prep. Figure 5a shows the earthquakes until 1905 from available catalogue data excluding events listed with M=0. Figure 5b shows earthquakes from 1906 till 2020.

It has been noticed that most of the of pre-instrumental earthquakes in the European catalogue are not listed with magnitude. In order to evaluate the a- and b- value of Gutenberg-Richter relation (1942) and applying completeness corrections with respect to magnitude, a correlation has been established using $M=0.72I_0$ for earthquakes till 1905 to convert the intensity into magnitude of European catalogue (Table 4).

The epicentral depth plays a major role for evaluating magnitude and intensities. A simple test of the catalogue reveals the expected result that higher intensities of events with shallow depth

yield lower magnitudes as compared to higher intensities associated with larger depths. The hypocentral depths distribution in Figure 6 shows that most of the earthquakes from the composite catalogue cluster at 10 and 15 km depth which has been considered as shallow seismicity.

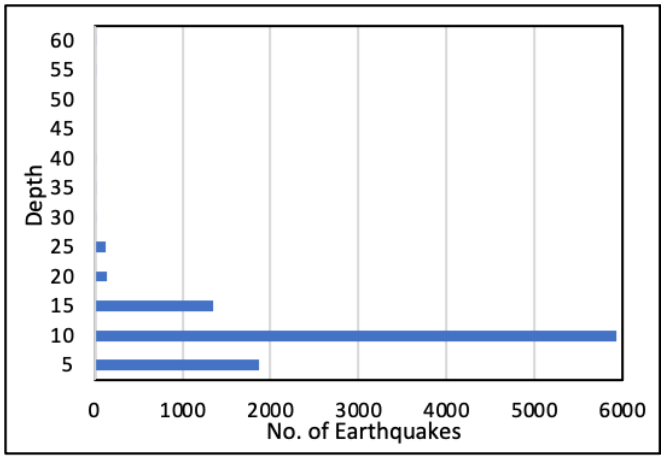

Figure 6: Number of earthquake vs. hypocetral depth (in kilometer) of earthquakes from the composite catalogue compiled for this study.

Catalogue	I/M relation derived from catalogue		Formula used by countries
	untill 1905	from 1906	Regional Formulas
Composite	$M=0.0696*I_o$	$M=0.5785*I_o$	
ZAMG	$M=0.6466*I_o$	$M=0.6277*I_o$	$M = 2 / 3 * I_o$
ACORN	$M=0.7826*I_o$	$M=0.6983*I_o$	$M = 0.6 * I_o + 0.3$
European	$M=0.7225*I_o$	$M=0.6998*I_o$	$M = 0.63 * I_o + 0.5$
SE-Europe	$M=0.6785*I_o$	$M=0.6674*I_o$	$M = 0.5 * I_o + 1.5$

Table 4: Empirical formulas derived from I/M cross plots for different catalogues and the time windows until 1905 (historical) and 1906-2020 (instrumental). The correlations listed in columns 2 and 3 were used to convert intensity into magnitude for events for which only intensity is listed in a catalogue. Composite catalogue compiled by Nasir et al., in prep. ZAMG: ZAMG,2020; ACORN: Lenhardt et al., 2007; European catalogue: Van Gils & Leydecker 1991; SE-Europe: Shebalin et al, 1998. The right column lists empirical relations established by other authors (ZAMG: Lenhardt, 1995; ACORN: Karnik, 1968; European catalogue: Grünthal et al., 1988; SE-Europe: Rottner´s relation).

3.2 Declustering of earthquake catalogue

The declustering of earthquake catalogues by removing fore- and aftershocks of major events is very important because estimations of the mean annual rate of seismic activity and the determination of seismicity parameters (a- and b-values in Gutenberg-Richter relation) generally

assume that earthquakes record a Poisson distribution therefore, they need to be independent from each other (Gardner & Knopoff, 1974; Öncel & Alptekin, 1999; Keilis-Borok et al., 1982). Such independence is not true for fore-and aftershocks of major earthquakes.

The compiled earthquake catalogue 2020 (Nasir et al., in prep.) is declustered using Wells & Coppersmith (1994) empirical relation between fault dimension and magnitude:

$$\text{Log (length)} = (M - 4.32) / + 1.54$$

The fault length derived for the magnitude of an event is used to constrain the spatial window and the distance from the mainshock in which fore- and aftershocks may be expected. Events at larger distances are not regarded as dependent fore- or aftershocks.

The time window used to evaluate the temporal evaluation of aftershock sequences is derived from the relation by Gardner & Knopoff (1974) stating the time window in days after the mainshock in which aftershocks are expected (Table 5). Both, the spatial and time window are used to deculstering the catalogue manually.

Mag	L (km)	T (days)
4.5	10	83
5.0	10	155
5.5	10	290
6.0	12	510
6.5	26	790
7	54	915

Table 5: Spatial and temporal windows used for identifying foreshocks and aftershocks. The distance from mainshock is derived from the empirical relation by Wells & Coppersmith (1994; Log (length in km) = (M - 4.32) / 1.54 rounded up to 10km to account for imprecise epicentre records. The temporal windows are evaluated according to Gardner & Knopoff (1974).

3.3 Completeness corrections

After removal of fore- and aftershocks from the compiled catalogue, the completeness corrections according to the method by Stepp (1972) and TCEF (Lenhardt, 1996; Gasperini and Ferrari, 2000) were applied on the dataset.

Furthermore, the same completeness corrections were applied on the sub-region of Austria corresponding to the VBTF which extends into Slovakia.

3.3.1 Stepp completeness correction

The Stepp completeness correction (Stepp, 1972) is the method which is used to determine catalogue completeness. In this method the entire earthquake catalogue is divided into different arbitrary time windows keeping in mind that the time windows have enough earthquake data to analyse any individual magnitude class (Figure 7; Table 6). To calculate the stability of the mean rate of occurrence (λ) of earthquake which occur in predefined magnitude range in series of time windows (T). If the value of λ does not change the standard deviation (SD) varies as 1/√T. On the other hand, if λ varies the SD divert from 1/√T as shown in the graph in Figure 7. The length of time interval where no deviation from straight line slope occurs outlines the catalogue completeness time interval (Stepp, 1972; Nasir et al., 2013). The lines in Figure 7 shows the 1/√T slope. The data point which lies on this 1/√T slop defines the completeness of the catalogue of each magnitude class. A MATLAB code has been written for Stepp completeness correction (Appendix 1).

Magnitude	Time (years)	N	N_0
2<M≤3	1940-2020	787	21362
3<M≤4	1825-1970	1661	11800
4<M≤5	1600-1930	377	1348
5<M≤6	1500-1920	86	306
6<M≤7	N/A	6	N/A

Table 6: Rate of earthquake occurrences for different magnitude classes derived from the Stepp correction of the declustered composit catalogue (Stepp, 1972). N: Number of recorded earthquake of a magnittude class within the completeness period T. N_0= cumulative number of earthquakes of the magnitude class extrapolating the recurrence interval derived from the completeness time period T to the total length of the catalogue (972 years; 1048-2020). For the highest magnitude class the observation period is too short to define a reliable average reccurrence period (N/A).

The completeness period for each magnitude class of the composite catalogue 2020 (Nasir et al., in prep.) is analysed for the period between 1048-2020 (972 years). The time length is divided into 22-time windows. All time windows contain a number of earthquakes which is sufficient for the calculation. From Figure 7, it has been observed that for 1<M≤2, the completeness is not reached at any time. Similarly, earthquakes with magnitude 6<M≤7 do not reveal a stable average recurrence interval Indicating the observation time covered by the

catalogue (972 years) is too short to constrain the recurrence interval reliably. The same is true for the strongest earthquakes (7<M≤8) with only two recorded events. The intervals with complete records (Table 6) are for 2<M≤3 (1940-2020), 3<M≤4 (1825-1970), 4<M≤5 (1600-1930) and 5<M=6 (1500-1920).

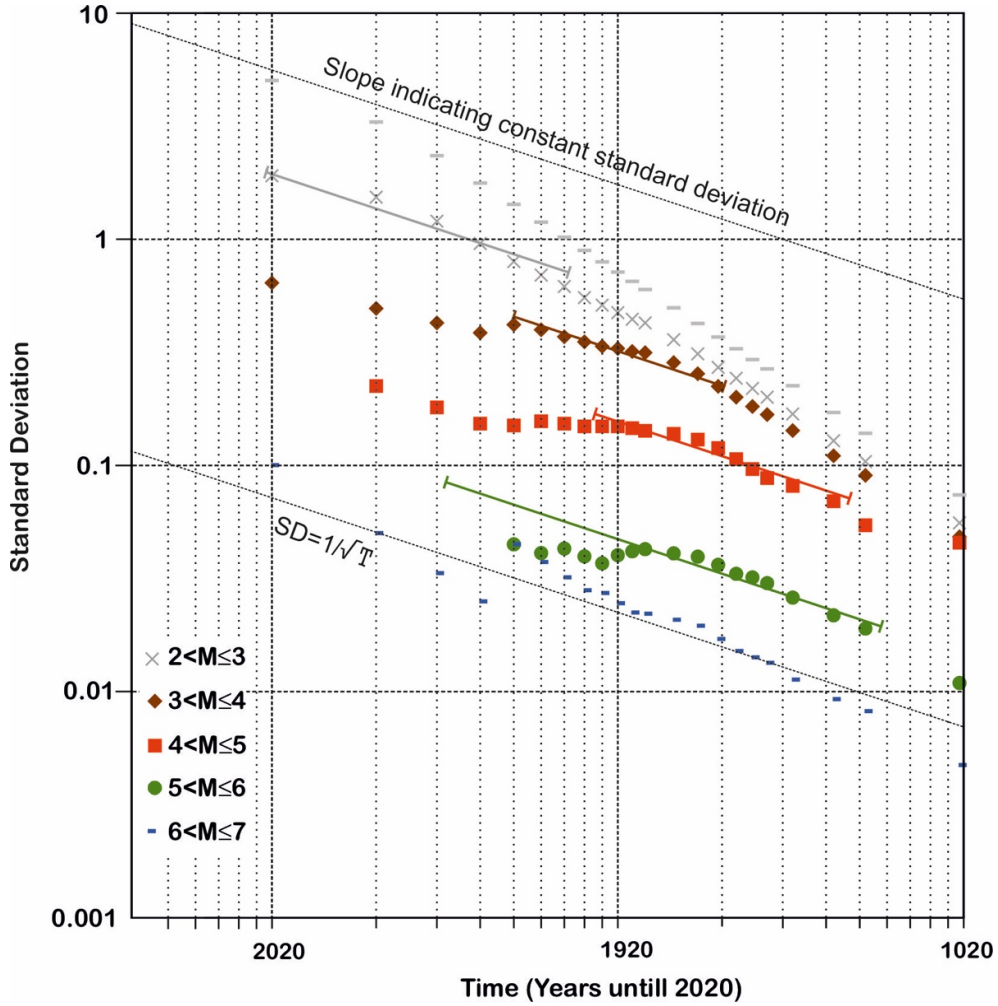

Figure 7: Assessment of the completeness of the compiled composite earthquake catalogue (1048-2020) using the Stepp (1972) method for different magnitude classes. Straight lines indicate constant standard deviations for the recurrence intervals of earthquakes of a certain magnitude class. Upper left ends of lines indicate the minimum observation time needed for reliable estimates of recurrence intervals, lower right ends indicate the interpreted start of the period of complete observations. Black dotted lines show the 1/√T slope.

3.3.2 TCEF completeness correction

The TCEF is a very common method used for catalogue completeness in Europe (Gaperini & Ferrari, 2000; Lenhardt, 1996). It is a statistical analysis performed for each individual magnitude class.

Magnitude	Time (years)	N	N_0
1<M≤2	1995-2020	5034	256686
2<M≤3	1995-2020	1425	68492
3<M≤4	1891-2020	1641	15219
4<M≤5	1873-2020	380	2949
5<M≤6	1768-2020	106	454
6<M≤7	1689-2020	16	46

Table 7: Rate of earthquake occurrences for different magnitude classes derived from the TCEF correction of the declustered composit catalogue (2020). N: Number of recorded earthquake of a magnittude class within the completeness period T. N_0= cumulative number of earthquake of magnitudes ≥ M_0 extrapolating the recurrence interval derived from completeness time period T to the total length of the catalogue (972 years; 1048-2020).

In this method, the cumulative number of earthquakes of a certain magnitude class is plotted against time. Changes in slope show increases or decreases in recorded numbers and, therefore, provide indications of the completeness of the earthquake catalogue. The data is said to be complete for time intervals corresponding to the steepest slope (Grünthal et al., 1998; Nasir et al., 2013). A MATLAB code has been written for TCEF completeness correction (Appendix 2).

The TCEF evaluation for the compiled composite catalogue 2020 and different magnitude classes is shown in Figure 8 and Table 7. The plot indicates completeness of earthquake record as follows: 1<M≤2 (1995-2020), 2<M≤3 (1995-2020), 3<M≤4 (1891-2020), 4<M≤5 (1873-2020), 5<M≤6 (1768-2020) and 6<M≤7 (1689-2020). The graphs in Figure 8 indicate that most of the earthquake data became complete after the start of systematic recording of earthquakes in the former Austrian Hungarian empire after the earthquake of Ljubljana (1895). For magnitude 7<M≤8 only two events constrain the slope of the TCEF curve.

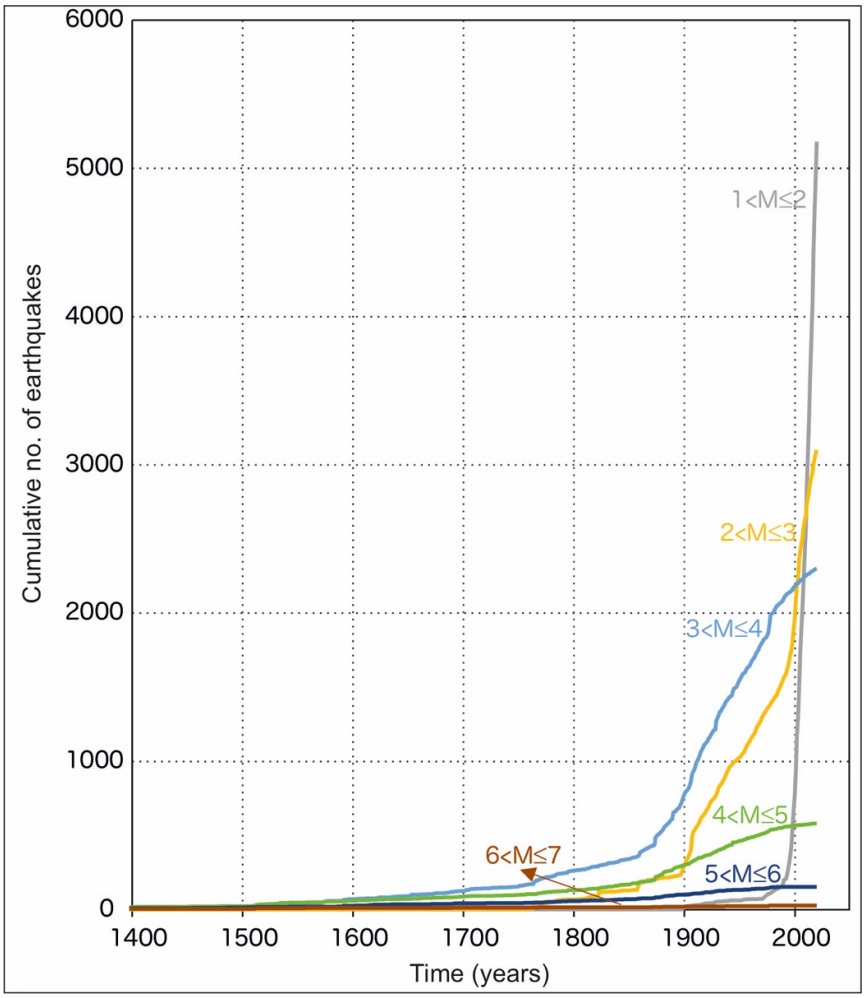

Figure 8: Time vs. Cumulative number of earthquakes plot for earthquakes of different magnitude classes. Data from the compsite catalogue 2020. The time interval with the steepest slope of the curves regarded as the time period with complete earthquake records of a certain magnitude class.

3.4 Comparison of Gutenberg-Richter parameters derived from different completeness corrections

After the assessment of catalogue completeness, the a- and b-value of Gutenberg -Richter relation (Gutenberg & Richter, 1954) is calculated for the considered completeness period:

$$\text{Log}_{10}(\lambda_M) = a - bM$$

The Gutenberg-Richter relation shows the occurrence of earthquakes with magnitude greater and equal to M. In equation λ_M is the mean annual rate of exceedance of M. a and b are constants. 10^a is the yearly earthquake of magnitude greater or equal to 0 and b shows the relative likelihood of small and large earthquakes (Gutenberg & Richter, 1954), however to obtain the parameters of Gutenberg Richter, a manual programming in MATLAB is used (Appendix 3).

Following declustering and applying different completeness analyses to the entire study area, considerable differences are found in the estimated seismicity parameters, such as the mean annual rate of seismic activity and the resulting intensity-frequency coefficients (a- and b-values in the Gutenberg-Richter relation). Figure 9 and Table 8 summarize the GR a- and b-values from the datasets after declustering and completeness corrections according to the results of the Stepp (1972) and TCEF completeness assessment.

Comparing the declustered uncorrected catalogue with the results obtained after applying completeness corrections (Figure 9) shows difference of the Gutenberg-Richter b-value of 0.05 and 0.19 for the Stepp and TCEF corrections respectively. The a-values differ by 0.64 and 1.86 respectively. Comparison of the resulting Gutenberg-Richter relations shows that calculating seismicity parameters from the uncorrected dataset underestimates the occurrence frequencies of earthquakes of all magnitude classes. The observed differences lead to the following conclusions:

(1) In addition to providing completeness intervals, the Stepp (1972) Test also incorporates insight into how many earthquakes must be observed in order to derive reliable average recurrence intervals for a given magnitude class. The test excludes the highest magnitude class ($6<M\leq7$) because it identifies that the observation period is too short for constraining a stable average interevent time for these strong and rare earthquakes. To reach stable estimates of mean recurrence intervals, Stepp (1972) recommends minimum time intervals covering at least five to fifteen mean return periods. As the composite catalogue observes fewer earthquakes, occurrence rates are likely underestimated. The datapoint for $6<M\leq7$ is therefore not included in the regression calculating the Gutenberg-Richter parameters resulting in a shallower linear slope of the Gutenberg-Richter curve.

(2) The TCEF method assumes that all earthquakes of the highest intensity class were observed during the length of the catalogue. It therefore includes the magnitude class ($6<M\leq7$), independently on whether the observation period is long enough to determine its completeness. Results therefore differ substantially from the Stepp Test. After the TCEF-correction, including $6<M\leq7$ in the estimation of seismicity parameters results in a slight overestimation of events for lower magnitudes and an underestimation of larger events. Applying TCEF and Stepp corrections, the b-value of Gutenberg-Richter relation differs by 0.14.

Catalogue/Correction Method	GR-Parameters	
	a-value	b-value
DC uncorrected	2.39	0.55
DC Stepp correction	3.05	0.60
DC TCEF correction	4.25	0.74

Table 8: Comparison of the Gutenberg-Richter a- and b-values calculated from the declustered uncorrected catalogue (DC), the declustered catalogue corrected after applying the Stepp (1972) test, and the declustered catalogue after applying TCEF completeness correction.

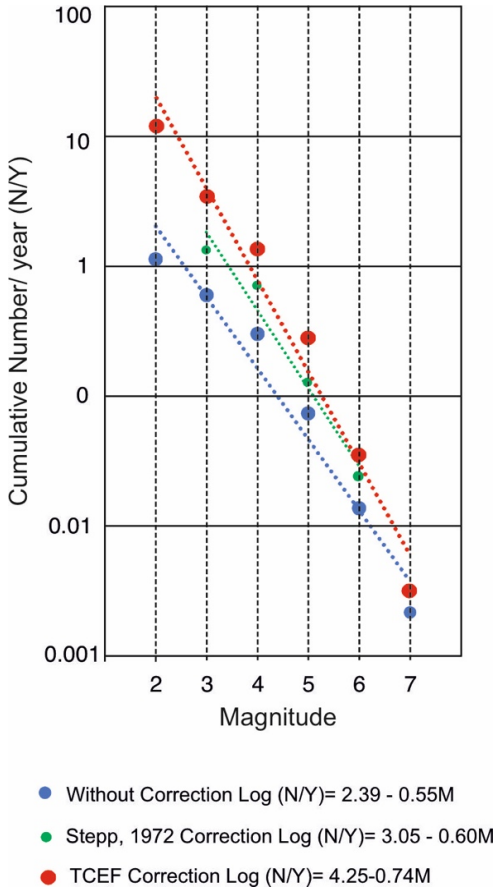

Figure 9: Comparison of the Gutenberg-Richter relations calculated from the declustered catalogue without using any completeness correction (blue symbols and dotted line), applying Stepp correction (green symbols and dotted line) and applying TCEF correction (red symbols and dotted line). Since the Stepp test shows that historical observation periods are too short for establishing recurrence intervals that are reliable, the Gutenberg-Richter regression based on the Stepp test does not include magnitude class $6<M\leq7$.

(3) Without any completeness correction, the declustered composite catalogue 2020 tends to underestimate the a- and b-parameters (Figure 9). Differences are particularly noteworthy for the a-values (Table 8).

Based on these observations the Stepp (1972) method is preferred over the TCEF analysis. It is regarded to provide more reliable data for calculating mean recurrence intervals due to its ability of considering minimum observation times necessary to calculate stable average recurrence periods for rare strong earthquakes.

4. THE 1906 DOBRÁ VODA EARTHQUAKE AND ITS AFTERSHOCK SEQUENCE AT THE VBTF

The earthquake at Dobrá Voda (1906, M=5.7/I_0=VIII-IX, ACORN, 2004) northeast of the Vienna Basin region is the strongest historical earthquake recorded at the VBTF. The earthquake occurred in the Brezovské Karpaty area about 60 km NE of Bratislava, in Slovakia. The 1906 Dobrá Voda earthquake occurred at the fault segment of the VBTF of the same name a time marked by the transition from macroseimic to instrumental earthquake records, being one of the first earthquakes in the region with instrumentally determined surface-wave magnitude (Réthly, 1907). Nasir et al. (2020) focus on the evaluation of epicentral intensity based on ESI 2007 environmental effects to confirm the intensity of the Dobrá Voda earthquake and the analysis of a long aftershock sequence which influenced the seismicity of 20th century.

4.1 Evaluation of the ESI 2007 intensity

Contemporary description of reactions of the population, damages to buildings, but also, on the natural environment such as permanent and temporary hydrological effects on wells and springs, formation of surface cracks (Réthly, 1907) are used to compare the epicentral intensity derived from the classic macro seismic scale with the ESI (Michetti et al., 2007) based on effects on the environment (Figure 10).

From the Dobrá Voda area, reports confirm numerous hydrological effects of the earthquake such as spring water coloured red, development of a sulphur spring, increase of water output, falling-dry of wells etc., surface cracks and landslides. These effects are used for the assessment of the environmental earthquake intensity according to Michetti et al. (2007). Contemporary pictures show some of these effects and help to determine the intensity according to ESI 2007 (Table 9). The minimum area affected by environmental effects is 2500 km². The evolution of the historical descriptions using the ESI 2007 criteria results in intensity estimates between $I_{(ESI)}$=VIII and $I_{(ESI)}$=X (Nasir et al., 2020). As two of the four observed hydrological changes were permanent, the resultant epicentral intensity following the ESI would be $I_{0\ (ESI)}$=IX-X (Michetti et al., 2007; Table 9).

		Primary effects		Secondary Effects			
Intenisty	**Description**	**Surface displacement /deformation**	**Hydrological anomalies**	**Soil cracks**	**slope movement**	**liquid faction**	**area (km²)**
VIII	heavily damaging	Observed rarely	significant, mostly temporary	50cm wide area, several hundred meter long	rock falls and landslides up to more than 100.000 m³.	not rare up to 1m wide	100
IX	destructive	observed commonly	strong, mostly temporary	100cm wide, several hundred meter long	rock falls and landslides up to more than 1000.000 m³.	common up to 3m	1000
X	very destructive	leading	strong, partly permanent	more than 100cm wide, several hundred meter long	rock falls and landslides up to more than 1.000.000 m³.	very common, larger areas, subsidence	5000

Table 9: Definition of intensity classes VIII to X according to ESI 2007 (Michetti et al., 2007; Nasir et al., 2020).

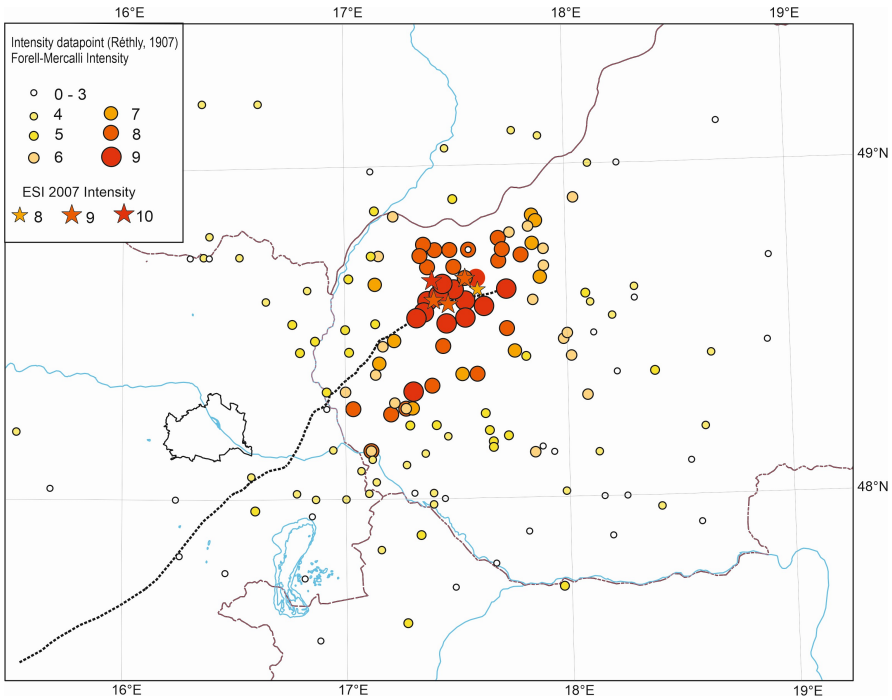

Figure 10: Map of intensity datapoints for the 1906 Dobrá Voda earthquake (Réthly, 1907; Nasir et al., 2020). Intensity values related to the 12-part Forel-Mercalli scale (Cancani, 1904, taken from Réthly, 1907; colored circles) and to the ESI scale (Michetti et al., 2007; stars). The felt area is almost 30.000 km².

4.2 Analysis of aftershock sequence

Earthquake data for the Dobrá Voda segment is taken from the ACORN catalogue (2004), covering the border region between Slovakia, the Czech Republic, and Austria. Aftershock determination classically uses spatial windows scaled by the magnitude of the main shock (Wells & Coppersmith, 1994; Nasir et al., 2013). To account for the uncertainties of epicentral locations derived from macroseismic historical data, we decided to select earthquakes in a 13 km radius around the mainshock (Figure 11) as potential aftershocks. For comparison, we further selected earthquakes up to 26 km of epicentral distance. Figure 11 shows the seismic activity around the mainshock discriminating the area within 13 km (green circles) and 26 km (blue circles) radial distance from the epicentre. However, most of the earthquakes are within 5-10 km to the mainshock.

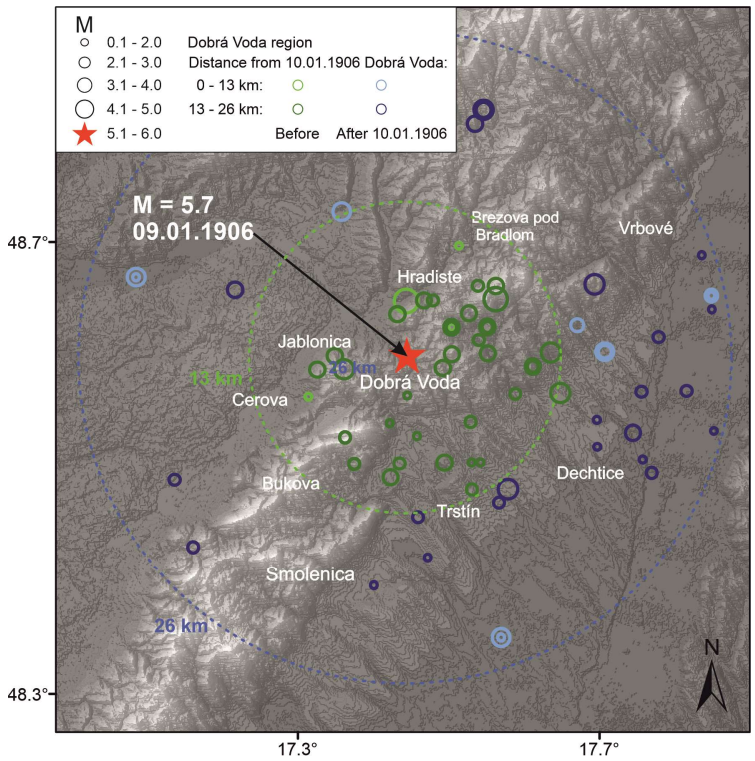

Figure 11: Seismicity in the vicinity of the epicentre of the Dobrá Voda 1906 earthquake (M/I_0= 5.7/VIII-IX; from Nasir et al., 2020). Green circle shows the seismicity within radius of 13 km and blue circle show seismicity within 26 km radius.

For historical times before the 20th century, the threshold for completeness of earthquake information is M>4.0 with 20 earthquakes in the 26 km radius before the Dobrá Voda 1906 earthquake (Figure 11, 12). The onset of smaller earthquake recordings with magnitudes down to M≈2.5 (≈I_0=III-IV) starts around 1895 in the entire former Austrian areas (Nasir et al., 2013).

On the other hand, within the 13 km radius, only 6 earthquakes with M≈2.5 are observed before the Dobrá Voda 1906 earthquake with the first entry in 1874. However, after the main shock, earthquakes are mostly observed within 13 km distance of the main shock for the next 70 years. Possible data gaps with no earthquake recordings exist for the war times of 1914-1918 (WWI) and 1938-1945 (WWII). The earthquakes outside the 13 km radius restart again after the mainshock around 1975 (Nasir et al., 2020).

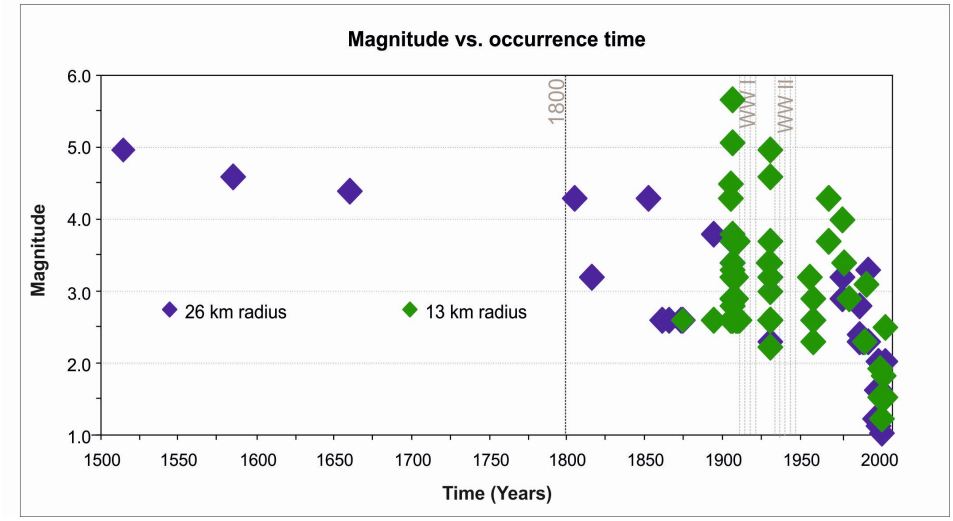

Figure 12: Magnitude vs. occurrence time plotted for earthquakes in vicinity of 1906 Dobrá Voda M=5.7 earthquake (Nasir et al., 2020). Blue and green symbols denote events that occurred within 13 and 26 km, respectively.

Aftershock identification and the assessment of the temporal length of the aftershock sequences of large earthquakes is an important aspect of earthquake catalogue declustering. It impacts the Gutenberg-Richter predicted frequency of earthquakes in a certain region and, thereby, seismic hazard assessment. Aftershocks are usually identified either by using the empirical Omari's law (Ogata, 1983) or by the combination of spatial (Wells & Coppersmith, 1994) and temporal windows (Gardner & Knopoff, 1974).

However, for diffused plate boundaries and intraplate regions with low deformation rates, it is still questionable if aftershocks after a major event may continue for much longer time as predicted by these temporal windows. For intraplate settings with fault slip rates with 1 mm/yr or less, Stein & Liu (2009) suggest aftershock durations of hundred(s) of years. Nasir et al. (2020) therefore review the applicability of the Stein & Liu (2009) model to the Dobrá Voda segment, the northernmost segment of the Vienna Basin Transfer Fault (VBTF) System (Decker et al., 2005; Hinsch & Decker, 2010).

5. AFTERSHOCK SEQUENCES AT THE VIENNA BASIN TRANSFER FAULT SYSTEM

Aftershock activity is generally triggered by a large earthquake. In the aftermath of a large earthquake, this aftershock activity leads to a local increase of seismic activity, which is later on decays back to a lower level labelled as 'normal' background seismicity (Stein & Liu, 2009). The length of an aftershock sequence can vary from a few months at plate margins to several years and even decades and centuries in intraplate regions (Stein & Lui, 2009), depending not only on the magnitude of the causing earthquake, but apparently also on the regional level of background seismicity. At the northern end of the Vienna Basin, the 1906 Dobrá Voda mainshock (M=5.7) has caused elevated seismicity in its near vicinity which is still recorded today (Nasir et al., 2020). Nasir et al. (in prep.) therefore analyse whether the seismic activity on other parts of the VBTF (Figure 13) can be explained as the result of a (pre-)historic strong mainshock.

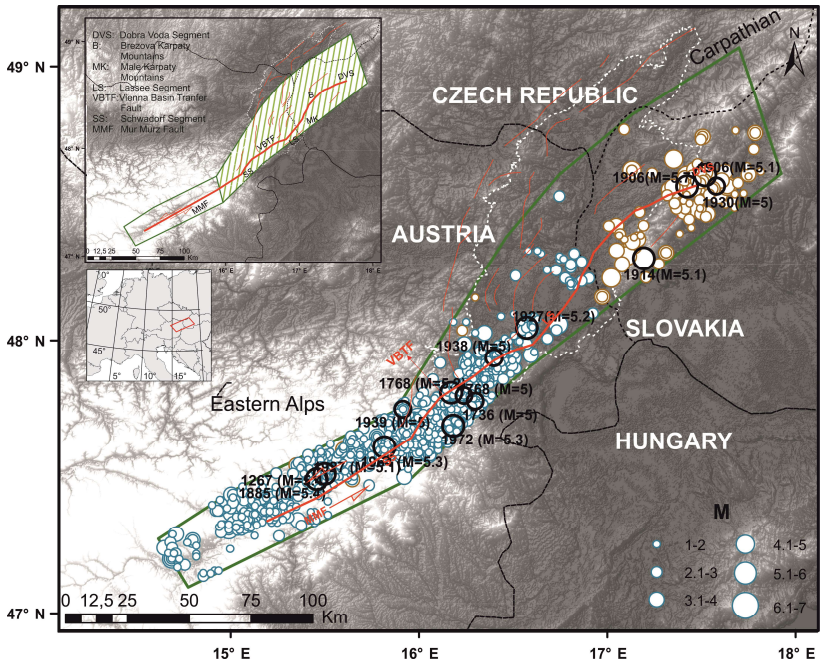

Figure 13: Distribution of earthquakes at Vienna Basin. Blue circles show earthquakes from Austrian earthquake catalogue, brown circles are earthquakes from ACORN earthquake catalogue and black circles are earthquake of M≥5. Green polygon shows the extended Vienna Basin Transfer Fault (VBTF) which pass through region of Austria and Slovakia. Green lines in the polygon are the Vienna Basin region generally used.

The extent of the VBTF in Austria and Slovakia is shown in Figure 14. Nasir et al. (in prep.) divide the fault into eight arbitrary segments of approximately 50 km length each to characterize the temporal evolution of seismicity for all segments and identify long aftershock sequences, which

are comparable to the aftershock sequence of the 1906 Dobrá Voda earthquake. Analyses were originally motivated by discussions with Seth Stein (pers. comm.) who tentatively interpreted the historical seismicity in the southern Vienna Basin as a persisting aftershock sequence subsequent to a strong (M≈6-7) earthquake that occurred prior to the onset of historical earthquake records.

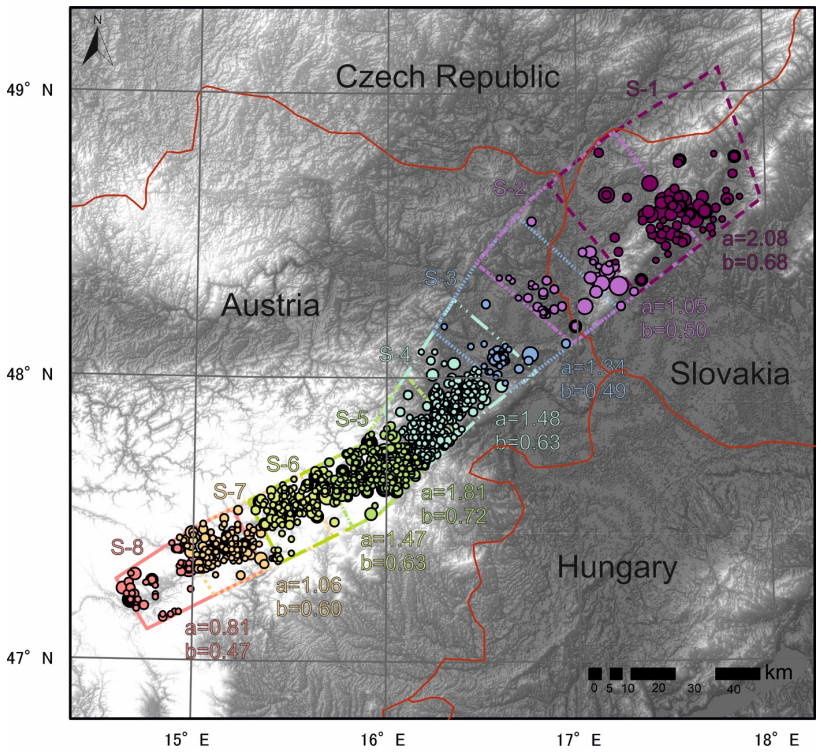

Figure 14: Segmentation of extended VBTF. Arbitrarily selected segments are about 50 km long and overlap each other. See text for explanation of segment selection. The a- and b-values of Gutenberg-Richter relation (Gutenberg & Richter, 1942) is shown next to each segment from S1: Segment 1 to S8: Segment 8.

Analyses are based on arbitrarily selected segments of the VBTF with lengths of 50 km. Segment lengths were chosen by considering that (a) long aftershock sequences may be expected from strong earthquakes with magnitudes M≈6.0-6.8 (M=6.8 corresponds to the maximum credible earthquake for the VBTF proposed by Hinsch & Decker, 2010) and (b) earthquakes of this magnitude range result from slip of faults with lengths between about 14 and 44 km according to empirical scaling relations for strike-slip faults (Wells & Coppersmith, 1994). Defining overlapping segments for the analyses should ensure to avoid omitting any information regarding aftershock patterns subsequent to a main shock that occurred a segment boundary. Segment boundaries therefore do not correspond to tectonically defined fault segments as

those proposed by Hinsch & Decker (2010) or Beidinger et al. (2010). The southwestern continuation of the VBTF into the Mur-Mürz fault is also included in the analysis.

In the corresponding manuscript, Nasir et al. will address the questions raised above using a newly compiled up-to-date earthquake catalogue (ZAMG, 2020) and (ACORN,2004), which covers the full extent of the VBTF in Austria and Slovakia including its continuation into the Mur-Mürz Fault. As the major part of the 754-years-long earthquake catalogue is based on intensity, an updated empirical formula is established to convert Intensity into magnitude (see chapter 4). Data is consequently subjected to completeness corrections using TCEF and Stepp (1972) as also described in chapter 4.

The manuscript further determines and compares the b-value of Gutenberg Richter (1942) relation of the different fault segments stating marked differences between the segments. The Gutenberg-Richter b-values are important for estimating seismicity rates for seismic hazard analysis. The b-value is also related to stress levels and shows changes precursory to the occurrence of large earthquakes (Barrientos et al., 2020).

Along the Mur-Mürz-VBTF system, the smallest b-values of 0.47 and 0.49 are calculated for the segments at the SW end of Mur-Mürz fault and the Lassee-Segment of the VBTF. The Schwadorf segment revealed the largest b-value with 0.72. The most prominent finding is that b-values of fault strands with very high seismic slip deficits (as determined by Decker & Hinsch, 2010) are much lower than values obtained from fault strands that slipped and caused earthquakes in historical times.

The finalization of the manuscript and the final discussion of the results are still under process.

6. RESULTS

This cumulative thesis consists of three papers in which I analyse the seismicity of Austria and Vienna Basin, focusing on the Vienna Basin Transfer Fault system, in terms of the completeness of earthquake records and aftershock sequences.

The article by Nasir et al. (2013; Appendix A) assessed catalogue completeness for a composite catalogue for Austria and the surrounding regions using TCEF and statistical analyses according to Stepp (1972). Most of the earthquake data is pre-instrumental in nature. Therefore, to avoid

the uncertainties resulting from intensity-magnitude conversions the computation and analysis is accomplished in intensity.

When comparing both completeness corrections, it should be stressed that the TCEF includes all earthquakes of the higher intensity classes based on the assumption that all of the strongest earthquakes have been observed during the whole catalogue length. Due to this reason the highest intensity class is also included for Gutenberg-Richter analysis. The Stepp method (Stepp, 1972), on the other hand, only considers intensity classes for which stable recurrence periods can be calculated from the earthquake record. As this is not the case for earthquakes of higher intensity, the Stepp, 1972, test does not include the highest intensity class for Gutenberg-Richter analysis due to the fact that the historical observation period is too short to calculate a statistically meaningful recurrence interval for these events.

Both completeness corrections therefore reveal significant differences in the resulting Gutenberg-Richter relations and different recurrence estimates for strong earthquakes. The GR results shows that there is only a minor difference in a- and b- values for the clustered and declustered catalogue. The GR a- and b-values after TCEF correction underestimates the lower intensities and overestimates the higher intensities. The Stepp test is regarded more reliable due to the fact that it is only considering intensities, for which stable recurrence periods can be computed from the time coverage of the underlying earthquake catalogue. Results suggest that data for earthquakes of I_0=VII and VIII are only complete for the period after 1750, lower intensities are only complete from 1900 on. Comparison of the completeness of the whole catalogue with the Vienna Basin sub-region suggests that the completeness for the entire catalogue is overestimated by both applied methods. In the Vienna Basin, I_0=VII and VIII is only complete since 1900; I_0<VII earthquakes are even incomplete for the 20th century. Observation time is too short to determine recurrence intervals for I_0=X (whole region) and I_0=IX (Vienna Basin). It is concluded that historical observations are not significant for determining stable recurrence rates for large earthquakes in areas with slow and very slow faults.

The study by Nasir et al. (2020; Appendix B) analysed the 1906 Dobrá Voda (M=5.7) earthquake which is the dominant earthquake at the northern part of the Vienna Basin and has influenced the local seismic activity in the 20th century. Environmental effects caused by the 1906 Dobrá Voda mainshock and its strongest aftershock in 1906 described by contemporary authors include hydrological effects and surface cracks. Application of the ESI 2007 intensity scale to these effects help better constrain the epicentral intensity for the Dobrá Voda mainshock and its strongest aftershock. Analyses reveal epicentral intensities of I_0=IX and I_0=VIII for the main shock and the strongest aftershock, respectively. The new intensity estimates are regarded

more appropriate to describe the maximum intensity of the events than the value listed in the ACORN and CNEC catalogues (ACORN, 2004; Grünthal et al., 2009). Earthquakes prior to the main shock are sparse and mostly scattered around the entire region. After the mainshock, earthquakes are mainly concentrated within 13 km of epicentral distance for ca. 70 years. Comparison of aftershock determination methods suggests that the aftershock sequence might have lasted longer than predicted by the Omori law, as suggested by Stein & Liu (2009) for slow-moving faults in intraplate regions.

Nasir et al. (submitted to Austrian Journal of Earth Sciences, JAES22_03; Appendix C) divided the VBTF regionally into eight arbitrary segments of approximately 50 km length each in order to identify potential long aftershock sequences comparable to the Dobrá Voda 1906 earthquake. Such aftershock sequences might result from unrecorded strong earthquakes. The segments overlap each other for not missing information regarding aftershock patterns that may result from earthquakes that occurred next to segment boundaries. The working hypothesis is that the cause of the documented heterogeneous earthquake activity with seismicity particularly concentrating along the southern part of the VBTF might reflect long aftershock sequences subsequent to one or several strong earthquakes that occurred prior to the time covered by the earthquake catalogue. Aftershock activity is generally triggered by a large earthquake. In the aftermath of a large earthquake, this aftershock activity leads to a local increase of seismic activity which later on decays back to a lower level labelled as 'normal' background seismicity (Stein & Liu, 2009). The length of an aftershock sequence can vary from a few months at plate margins to several years and even decades and centuries in intraplate regions (Stein & Lui, 2009), depending not only on the magnitude of the causing earthquake, but apparently also on the regional level of background seismicity. At the northern end of the VBTF, the 1906 Dobrá Voda mainshock (M=5.7) has caused elevated seismicity in its near vicinity which has been still recorded till today (Nasir et al., 2020).

The analysed segments of the Vienna Basin Transfer Fault (apart from Dobrá Voda) and the Mur-Mürz Fault do not show seismicity patterns which could be interpreted as long aftershock sequences subsequent to a so-far unknown strong earthquake. The 1906 Dobrá Voda (M=5.7) earthquake lies in segment 2 causing the long aftershock pattern observed in segments 2 and 3. Segment 3 also revealed a temporal seismicity pattern indicating an about 10-20 years long aftershock sequence after a mainshock in 1890 (M=4.5). In segment 8 several moderate earthquakes occurred, e.g., in 1899 (M=4.1), 1995 (M=4.2) and 2004 (M=3.8), each characterized by a short aftershock sequence. Apparently, these earthquakes are not strong enough to cause long aftershock sequences.

7. ZUSAMMENFASSUNG

Die kumulative Doktorarbeit fokussiert auf die Analyse der Seismizität in Österreich und entlang des Wiener Becken-Transferstörungssystems (VBTF). Nasir et al. (2013) bewerten die Vollständigkeit des Erdbebenkatalogs und vergleichen die Methoden zur Korrektur unvollständiger Kataloge nach Stepp (1972) und aufgrund des zeitlichen Verlaufs der Erdbebentätigkeit (TCEF). Die Anwendung dieser Methoden führte zu signifikanten Unterschieden in den aus dem korrigierten Erdbebenkatalog berechneten Gutenberg-Richter (GR)-Beziehungen. GR a- und b-Werte nach TCEF-Korrektur unterschätzen die niedrigeren Intensitäten und überschätzen die höheren Intensitäten. Der Stepp-Test erscheint zuverlässiger, da er nur Intensitäten berücksichtigt, für die aus der Zeitabdeckung des zugrunde liegenden Erdbebenkatalogs stabile Rekurrenz Intervalle berechnet werden können.

Nasir et al. (2020) analysieren das Erdbeben von 1906 in Dobrá Voda (M=5.7), das die lokale seismische Aktivität während des 20. Jahrhunderts beeinflusste. Die durch das Erdbeben und sein stärkstes Nachbeben verursachten Umweltauswirkungen werden mit der Umweltintensitätsskala ESI 2007 verglichen, um die epizentralen Intensitäten besser einzugrenzen. Diese Intensitätsschätzungen werden als geeigneter angesehen, die maximale Intensität der Ereignisse zu beschreiben, als die in bestehenden Katalogen aufgeführten Werte. Nach dem Hauptbeben konzentrieren sich Erdbeben für etwa 70 Jahre hauptsächlich in einer Entfernung von 13 km vom Epizentrum des Hauptbebens. Die Daten deuten darauf hin, dass die Nachbebensequenz viel länger dauerte als vom Omori-Gesetz vorhergesagt. Die Nachbebensequenz folg vielmehr der Vorhersage von Stein & Liu (2009) für sich langsam bewegende Störungen in Intraplattenregionen.

Nasir et al. (einzureichen beim Austrian Journal of Earth Sciences; Appendix C) teilte die VBTF regional in acht willkürliche Segmente von jeweils ca. 50 km Länge ein, um mögliche lange Nachbebensequenzen vergleichbar mit dem Erdbeben von Dobrá Voda 1906 zu identifizieren. Solche Nachbebensequenzen können aus nicht aufgezeichneten starken Erdbeben resultieren. Die Segmente werden überlappend gewählt, um sicher zu gehen, dass keine Informationen zu Nachbebenmustern fehlen, die aus Erdbeben resultieren, die in der Nähe der Segmentgrenzen aufgetreten sind. Die Arbeitshypothese ist, dass die Ursache der dokumentierten heterogenen Erdbebenaktivität, die sich insbesondere auf den südlichen Teil der VBTF konzentriert, lange Nachbebensequenzen nach einem oder mehreren starken Erdbeben widerspiegeln könnten. Solche starken Erdbeben könnten vor der im Erdbebenkatalog erfassten Zeit aufgetreten sein. Nachbeben-Aktivitäten werden im Allgemeinen durch Starkbeben ausgelöst, die durch die Nachbebenaktivität zu einem lokalen Anstieg der seismischen Aktivität führt. Die erhöhte

Aktivität fällt später auf ein niedrigeres Niveau zurück, das als „normale“ Hintergrundseismizität bezeichnet wird (Stein & Liu, 2009). Die Länge einer Nachbebensequenz kann von einigen Monaten an Plattenrändern bis zu mehreren Jahren und sogar Jahrzehnten und Jahrhunderten in Intraplattenregionen variieren (Stein & Lui, 2009). Die Dauer hängt von der Stärke des verursachenden Erdbebens und dem regionalen Niveau der Hintergrundseismizität ab. Am nördlichen Ende des VBTF hat Erdbeben von 1906 Dobrá Voda (M=5.7) eine erhöhte Seismizität in seiner näheren Umgebung verursacht, die noch heute sichtbar ist (Nasir et al., 2020). Die analysierten Abschnitte der Wiener Becken Transfer-Störung (außer Dobrá Voda) und der Mur-Mürz Störung zeigen jedoch keine Seismizitätsmuster, die als lange Nachbebensequenzen nach einem bisher unbekannten starken Erdbeben interpretiert werden könnten. Das Erdbeben von 1906 in Dobrá Voda (M=5.7) liegt in Segment 2 und verursacht das in den Segmenten 2 und 3 beobachtete lange Nachbebenmuster. M=4.5). In Segment 8 ereigneten sich mehrere mittelschwere Erdbeben, z. B. 1899 (M=4.1), 1995 (M=4.2) und 2004 (M=3.8), die jeweils durch eine kurze Nachbebenfolge gekennzeichnet waren. Offenbar sind diese Erdbeben nicht stark genug, um lange Nachbebenfolgen zu verursachen.

8. REFERENCES:

ACORN, **2004**. Catalogue of Earthquakes in the Region of the Alps - Western Carpathians – Bohemian Massif for the period from 1267 to 2004. Computer File, Vienna (Central Institute for Meteorology and Geodynamics, Department of Geophysics) Brno (Institute of Physics of the Earth, University Brno).

Apoloner, M.T., Bokelmann, G., Bianchi, I., Brückl, E., Hausmann, H., Mertl, S., & Meurers., R., **2014**. The 2013 earthquake series in the Southern Vienna Basin: location. Advances in Geosciences, 36, 77-80.

AEC, **2015**. Austrian Earthquake Catalogue. Computer-Datei, Abteilung Geophysik, Zentralanstalt für Meteorologie und Geodynamik, Wien.

Barrientos, L.A., & Nava, A.A., **2020**. Gutenberg-Richter b value studies along the Maxican Subduction Zone and data constraints. Geofisica Internacional, 59(4), 285-298.

Beidinger, A., **2009**. Geophysical, geomorphologic and geological investigations along the Lassee-Segment of the Vienna Basin Transfer Fault System (VBTF) (Doctoral thesis, University of Vienna).

Beidinger, A., & Decker, K., **2011**. 3D geometry and kinematics of the Lassee flower structure: Implications for segmentation and seismotectonics of the Vienna Basin strike-slip fault, Austria. Tectonophysics, 499(1-4), 22-40.

Cancani, A., **1904**. Sur l'emploi d'une double echelle sismique des intensitès, empirique et absolue. Gerlands Beiträge zur Geophysik, 2, 281-283.

Caporali, A., Aichhorn, C., Barlik, M., Becker, M., Fejes, I., Gerhatova, L., Ghitau, D., Grenerczy, G., Hefty, J., Krauss, S., Medak, D., Milev, G., Mojzes, M., Mulic, G., M., Nardo, A., Pesec, P., Rus, T., Simek, J., Sledzinski, j., Solaric, M., Stangl, G., Stopar, B., Vespe, F., & Virag, G., **2009**. Surface kinematics in the Alpine–Carpathian–Dinaric and Balkan region inferred from a new multi-network GPS combination solution. Tectonics, 474(1-2), 295-321.

Decker, K., Persson, H., & Hinsch, R., **2005**. Active tectonics and Quaternary basin formation along the Vienna Basin Transform fault. Quaternary Science Reviews, 24(3-4), 305-320.

Decker, K., Gangl, G., & Kandler, M., **2006**. The earthquake of Carnuntum in the fourth century AD–archaeological results, seismologic scenario and seismotectonic implications for the Vienna Basin fault, Austria. Journal of Seismology, 10(4), 479-495.

Decker, K., Hintersberger, E., & Weissl, M., **2015**. Paläoseismologische Untersuchungen am Lassee-Abschnitt der Wiener Becken Störung – Implementierung neuer Methoden für die Erdbebeninformation. Endbericht NC 81-2012 - Paläoseismologie Wiener Becken. Unpublished Report, University Vienna, 146pp.

Decker, K., Grupe, S., & Hintersberger, E., **2015**. Characterizing active faults in the Urban area of Vienna. 6th th international INQUA meeting on Plaeoseismology, Active Tectonics and Archaeoseismology, Pescine, Fucino Basin, Italy.

Fojtikova, L., Vavrycuk, V., Cipicar, A., & Madaras, J., **2010**. Focal mechanisms of microearthquakes in the Dobrá Voda seismoactive area in the Malé Karpaty Mts. (Little Carpathians), Slovakia. Tectonophysics, 492, 213–229.

Frost, E., Dolan, J., Sammis, C., Hacker, B., Cole, J., & Ratschbacher, L., **2009**. Progressive strain localization in a major strike-slip fault exhumed from mid seismogenic depths: Structural observations from the Salzach-Ennstal-Mariazell-Puchberg fault system, Austria. Journal of Geophysical Research, 114, B04406.

Gangle, G., **1974**. Seismotektonische Untersuchungen am Alpenostrand. Mitteilungen der Österreichischen Geologischen Gesellschaft Wien, 66/67, 33-48.

Gardner, J.K., & Knopoff, L., **1974**. Is the sequence of earthquakes in southern California, with aftershocks removed, poissonian? Bulletin of the Seismological Society of America, 64, 1363-1367.

Gasperini, P., & Ferrari, G., **2000**. Deriving numerical estimates from descriptive information: the computation of earthquake parameters. In Catalogue of Strong Italian Earthquakes from 461 B.C. to 1997, Annali di Geofisica, 43, 729-746.

Gutdeutsch, R., & Aric, K., **1988**. Seismicity and Neotectonics of the East Alpine-Carpathian and Pannonian Area: Chapter 15, 183-194.

Gutdeutsch, R., & Hammerl, C., **1997**. Über die Aufzeichnungsschwelle historischer Beben. Mitteilungen der Deutschen Physikalischen Gesellschaft, 2, 2-9.

Gutdeutsch, R., & Hammerl, C., **1999**. An uncertainty parameter of historical earthquakes–the record threshold. Journal of Seismology, 3(4), 351-362.

Grenerczy, G., Kenyeres, A., & Fejes, I., **2000**. Present crustal movement and strain distribution in Central Europe inferred from GPS measurements. Journal of Geophysical Research 105 B9, 21.835–21.846.

Grenerczy, G., **2002**. Tectonic processes in the Eurasian–African plate boundary zone revealed by space geodesy. In: Stein, S., Freymueller, J.T. (Eds.), Plate Boundary Zones. AGU Monograph Geodynamics Series, Vol. 30, 67–86, American Geophysical Union.

Grenerczy, G., Sella, G., Stein, S., & Kenyeres, A., **2005**. Tectonic implications of the GPS velocity field in the northern Adriatic region. Geophysical Research Letters, 32, L16311.

Guidoboni, E., Ferrari, G., Mariotti, D., Comastri, A., Tarabusi, G., & Valensise, G., **2007**. Catalogue of Strong Earthquakes in Italy (461 BC-1997) and Mediterranean Area (760 BC-1500). INGV-SGA. Available from http://storing.ingv.it/cfti4med/.

Grünthal, G., **1988**. Erdbebenkatalog-des Territoriums der Deutschen Demokratischen Republik und angrenzender Gebiete von 823 bis 1984. Akademie Der Wissenschaften Der DDR, Forschungsbereich Geo- und Kosmoswissenschaften, Zentralinstitut Für Physik Der Erde Potsdam. Manuscript Nr 99. ISSN 0514-8790. 179pp.

Grünthal, G., Mayer-Rosa, D., & Lenhardt, W., **1998**. Abschätzung der Erdbebengefährdung für die D-A-CH-Staaten - Deutschland, Österreich, Schweiz. Bautechnik, 75(10), 753-767.

Gutenberg, B., & Richter, C. F., **1942**. Earthquake magnitude, intensity, energy, and acceleration. Bulletin of the Seismological society of America, 32(3), 163-191.

Grünthal, G., Wahlström, R., & Stromeyer, D., **2009**. The unified catalogue of earthquakes in central, northern, and northwestern Europe (CENEC) - updated and expanded to the last millennium. Journal of Seismology, 13(1), 517-541.

Hammerl, C. (Ed.)., **2001**. Die Zentralanstalt für Meteorologie und Geodynamik 1851-2001: 150 Jahre Meteorologie und Geophysik in Österreich. Graz (Leykam), 840 pp., ISBN-10 3701174377.

Hammerl, C., & Lenhardt, W., **2013**. Erdbeben in Niederösterreich von 1000 bis 2009 n. Chr. Abhandlungen der Geologischen Bundesanstalt, 67, 3-297.

Hinsch, R., & Decker, K., **2003**. Do seismic slip deficits indicate underestimated seismic potential along the Vienna Basin Transform Fault System? Terra Nova, 15, 343-349.

Hinsch, R., Decker, K., & Peresson, H., **2005**. 3-D seismic interpretation and structural modeling in the Vienna Basin: implications for Miocene to recent kinematics. Austrian Journal of Earth Sciences, 97, 38-50.

Hinsch, R., & Decker, K., **2010**. Seismic slip rates, potential subsurface rupture areas and seismic potential of the Vienna Basin Transfer Fault. International Journal of Earth Science, 100, 1925-1935.

Hintersberger, E., & Decker, K., **2012**. The central Vienna Basin Transfer Fault-lack of knowledge or seismic gap? In AGU Fall Meeting Abstracts, 2012. T33A-2638.

Hintersberger, E., Decker, K., Lomax, J., Fiebig, M., & Lüthgens, C., **2013**. Fault linkage model of strike-slip and normal faults in the Vienna Basin based on paleoseismological constraints. In EGU General Assembly Conference Abstracts, EGU2013-12755.

Hintersberger, E., & Decker, K., **2017**. Estimation of recent activity and segmentation along the Diendorf Fault System (Austria) based on multiple parameters. In EGU General Assembly Conference Abstracts (p. 14746).

Hintersberger, E., Decker, K., Lomax, J., & Lüthgens, C., **2018**. Implications from palaeoseismological investigations at the Markgrafneusiedl Fault (Vienna Basin, Austria) for seismic hazard assessment. Natural Hazards and Earth System Sciences, 18(2), 531-553.

Janoschek, W.R., & Matura, A., **1980**. Outline of the geology of Austria. Abhandlungen der Geologischen Bundesanstalt, Wien, 26 C.G.I., 34, 7/1/1998.

Kandler, M., **1989**. Eine Erdbebenkatastrophe in Carnuntum? Acta Archaeologica Academiae Scientiarum Hungaricae. 41: 313–336. Akademia Kiado, Budapest

Kárník, V., & Hübnerová, Z., **1968**. The probability of occurrence of largest earthquakes in the European area. Pure and Applied Geophysics, 70(1), 61-73.

Keilis-Borok, V. I., Knopoff, L. & Rotwain, I.M., **1982**. Burst of aftershocks, long term precursors of strong earthquakes. Nature, 283, 259-263.

Lenhardt, W., Švancara, J., Melichar, P., PazdÍrková, J., Havíř, J., & Sýkorová, Z., **1996**. Erdbebenkennwerte zur Berechnung der Talsperren Österreichs. Bundesministerium für Land- und Forstwirtschaft, Österreichische Staubeckenkommission. Zentralanstalt für Meteorologie und Geodynamik, Unpublished Report, 85pp.

Lenhardt, W., **1996**. Erdbebenkennwerte zur Berechnung der Talsperren Osterreichs. unpublished. report, Zentralanstalt fur Meteorologie und Geodynamik (ZAMG), Vienna, 86.

Lankreijer, A., Bielik, M., Cloetingh, S., & Majcin, D., **1999**. Rheology predictions across the western Carpathians, Bohemian massif, and the Pannonian basin: implications for tectonic scenarios. Tectonics, 18(6), 1139-1153.

Lüschen, E., Lammerer, B., Gebrande, H., Millahn, K., & Nicolich, R., **2004**. Orogenic structure of the Eastern Alps, Europe, from TRANSALP deep seismic reflection profiling. Tectonophysics, 388, 85-102.

Lenhardt, W., Švancara, J., Melichar, P., Pazdírková, J., Havíř, J., & Sýkorová, Z., **2007**. Seismic activity of the Alpine-Carpathian-Bohemian Massif region with regard to geological and potential field data. Geologica Carpathia, 58(4), 397-412.

Michetti, A. M., Esposito, E., Guerrieri, L., Porfido, S., Serva, L., Tatevossian, R., & Roghozin, E., **2007**. Environmental seismic intensity scale-ESI 2007. Memorie descrittive della carta geologica d'Italia, 74, 41.

Nasir, A., Hintersberger, E., & Decker, K., **2020**. The 1906 Dobrá Voda Earthquake (M=5.7) at the Vienna Basin Transfer Fault: evaluation of the ESI2007 intensity and analysis of the aftershock sequence. Austrian Journal of Earth Sciences, 113(1), 43-58.

Nasir, A., Lenhardt, W., Hintersberger, E., & Decker, K., **2013**. Assessing the completeness of historical earthquake and instrumental data in Austria and the surrounding areas. Austrian Journal of Earth Sciences, 106(1), 90-102.

Ogata, Y., **1983**. Estimation of the parameters in the modified Omori formula for the aftershock frequencies by the maximum likelihood procedure. Journal of Physics Earth, 31, 115-124.

Öncel, A. O., & Alptekin, Ö., **1999**. Effect of aftershocks on earthquake hazard estimation: an example from the North Anatolian fault zone. Natural Hazards and Earth System Sciences, 19(1), 1-11.

Plachy, H., **1981**. Neue Erkenntnisse zur Tektonik im Wiener Raum. Mitteilungen der Österreichischen Geologischen Gesellschaft, 74/75, 231-243.

Plan, L., Grasemann, B., Spötl, C., Decker, K., Boch, R., & Kramers, J., **2010**. Neotectonic extrusion of the Eastern Alps: constraints from U/Th dating of tectonically damaged speleothems. Geology, 38(6), 483-486.

Royden, L.H., **1988**. Late Cenozoic tectonics of the Pannonian basin system. In: Royden LH, Horvath F (eds) The Pannonian basin: a study in basin evolution. AAPG Memoir 45. American Association of Petroleum Geologists and Hungarian Geological Society, Tulsa, 27-48.

Réthly, A., **1907**. Erdbeben in Ungarn 1906 (in Hungarian with German abstracts). K. Ungar. Reichsanstalt für Meteorologie und Erdmagnetismums (Kir. Orsz. Meteorológiai és Földmágnességi Intézet), 109.

Reinecker, J., & Lenhardt, W. A., **1999**. Present-day stress field and deformation in eastern Austria. International Journal of Earth Sciences, 88(3), 532-550.

Reiter, F., Ortner, H., & Brandner, R., **2003**. Seismically active Inntal fault zone: inverted European rift structures control upper plate deformation. Sciences geologiques: Memoire, 54, 233-234.

Reiter, F., Lenhardt, W. A., & Brandner, R., **2005**. Indications for activity of the Brenner Normal Fault zone (Tyrol, Austria) from seismological and GPS data. Austrian Journal of Earth Sciences, 97, 16-23.

Suess, F.E., **1887**. Das Erdbeben von Laibach am 14. April 1895. Jahrbuch der k.k. geologischen Reichsanstalt 1896, 412-614.

Stepp, J.C., **1972**. Analysis of completeness of earthquake sample in the Puget Sound area and its effect on statistical estimates of earthquake hazard. In Proceedings of the 1st International Conference on Microzonazion, Seattle, 2, 897-910.

Schenková, Z., Schenk, V., Pospíšil, L., & Kottnauer, P., **1995**. Seismogeological pattern of a transition area between the Eastern Alps and the Western Carpathians. Tectonophysics, 248(3-4), 235-245.

Shebalin, N.V., & Leydecker, G., **1998**. Earthquake catalogue for Central and Southeastern Europe 342 BC-1990 AD. European commission, Report No. ETNU CT, 93-0087, Brussels.

Sefara, J., Kovac, M., Plasienka, D., & Sujan, M., **1998**. Seismogenic zones in the Eastern Alpine–Western Carpathian–Pannonian junction area. Geologica Carpathica 49(4), 247–260.

Stein, S., & Liu, M., **2009**. Long aftershock sequences within continents and implications for earthquake hazard assessment. Nature, 462(5), 87-89.

Spahić, D., Grasemann, B., & Exner, U., **2013**. Identifying fault segments from 3D fault drag analysis (Vienna Basin, Austria). Journal of Structural Geology, 55, 182-195.

SHARE, 2021. SHARE, http://diss.rm.ingv.it/share-edsf/SHARE_WP3.2_Database.html

Slemmons, D.B., & DePolo, C., **1986**. Evaluation of Active Faulting and Associated Hazards In: Wallace, R.E. (Panel Chairman) Active Tectonics, National Academy Press, Washington, D.C., 45-62.

Tóth, L., Győri, E., Mónus, P., & Zsíros, T., **2006**. Seismic hazard in the Pannonian region. In The Adria Microplate: GPS Geodesy, Tectonics and Hazards (pp. 369-384). Springer, Dordrecht. In: Pinter, N., Grenerczy, G., Weber, J., Stein, S., Medak, D. (eds) The Adria Microplate: GPS Geodesy, Tectonics and Hazards (pp. 369-384). Springer, Dordrecht.

Van Gils, J.M., & Leydecker, G., **1991**. Catalogue of European earthquakes with intensities higher than 4. Commission of the European Communities- Nuclear science and technology. 14, ISBN 92-826-2506-0 Catalogue number: CD-NA-13406-EN-C. Brussels-Luxenbourg 1991, 353.

Vere-Jones, D., **1970**. Stochastic models for earthquake occurrence. Journal of Royal Statistical Society: Siries B (Methodological), 32, 1/1/1945.

Vrabec M., & Fodor L., **2006**. Late Cenozoic tectonics of Slovenia: structural styles at the Northeastern corner of the Adriatic microplate. In: Pinter N., Gyula G., Weber J., Stein S., Medak D. (eds) The Adria Microplate: GPS Geodesy, Tectonics and Hazards. Nato Science Series: IV: Earth and Environmental Sciences, 61, Springer, Dordrecht. https://doi.org/10.1007/1-4020-4235-3_10.

Weissl, M., Hintersberger, E., Lomax, J., Lüthgens, C., & Decker, K., **2017**. Active Tectonics and Geomorphology of the Gaenserndorf Terrace in the central Vienna Basin (Austria). - Quaternary International, 451, 209-222.

Wessely, G., **1988**. Structure and development of the Vienna Basin in Austria: Chapter 24. AAPG Special volumes, 113, 333-346.

Wells, D. L., &Coppersmith, K. J., **1994**. New empirical relationship among magnitude rupture length, rupture width, rupture area, and surface displacement. Bulletin of Seismological Society of America, 84, 974-1002.

Willingshofer, E., & Cloetingh, S., **2003**. Present-day lithospheric strength of the Eastern Alps and its relationship to neotectonics. Tectonics, 22, 1075.

Woessner, J., & Wiemer, S., **2005**. Assessing the quality of earthquake catalogues: Estimating the magnitude of completeness and its uncertainty. Bulletin of the Seismological Society of America, 95(2), 684-698.

Weissl, M., Hintersberger, E., Lomax, J., & Decker, K., **2015**. Geomorphological and paleoseismological investigations on the Gaenserndorf Terrace in the central Vienna Basin (Austria), Abstracts 6th International INQUA Meeting on Paleoseismology, Active Tectonics and Archaeoseismology, 19-24 April 2015, Pescina, Fucino Basin, Italy. Miscellanea INGV 27, 201 5. 534-528.

Weissl, M., Hintersberger, E., Lomax, J., Lüthgens, C., & Decker, K., **2017**. Active tectonics and geomorphology of the Gaenserndorf Terrace in the Central Vienna Basin (Austria). Quaternary International, 451, 209-222.

ZAMG, **2009**. Earthquake catalogue of felt earthquakes 1200– 2009 A.D. (Austria). Computer File. Central Institute of Meteorology and Geodynamics (ZAMG), Vienna, Austria.

ZAMG, **2020**. Earthquake catalogue of felt earthquakes 1200– 2020 A.D. (Austria). Computer File. Central Institute of Meteorology and Geodynamics (ZAMG), Vienna, Austria.

Attachment 1

Programming for the Stepp completeness correction

1. Stepp MATLAB Script

```
clear all

%Input source file
data = xlsread(input('please enter source file   :  '));
%check for NaN
i=length(data);
while i>0,
    if isnan(data(i,2)),
       data(i,:)=[];
    end;
    i=i-1;
end;

%Define length of catalogue
t_all = data(:,2);
tmin = min(t_all);
tmax = max(t_all);
t = tmax-tmin+1;

%Define time windows - DEFAULT
tii=1499;
tjj=1699;
tkk=1749;
tll=1899;
ti=tmin;
tj=(tii+1:100:tjj);
tk=(tjj+1:50:tkk);
tl=(tkk+1: 25:tll);
tm=(tll+1:10:tmax);
t_win = cat(2,ti,tj,tk,tl,tm,tmax+1);

%Define I or M, we define I at the moment
%I = column 12, M = column 11
x = input('please choose Intensity (1) or Magnitude (2) ');

if x == 1, y=12;
else y=11;
end

%intensity/magnitude data
h = data(:,y);
hmin = min(h);
hmax = max(h);

%cummulative number of each time window (DEFAULT)
h_list=hmin:1:(hmax+1.5);
h_count=[];
h_cumGR=[];
```

```
i=1; j=1;

 while i<length(t_win),
     h_sublist=[];
    % sublist for all earthquakes in one time window
    while (j<=length(data) && t_all(j)>=t_win(i) &&
t_all(j)<t_win(i+1)),
      h_sublist=cat(1,h_sublist,h(j));
      j = j+1;
    end

      %how many earthquakes of a certain intensity in a certain time
      %window
      h_subcount = histc(h_sublist,(hmin-0.5):1:(hmax+0.5));
      % cumulative number for a certain time window
      h_subcum = cumsum(flipud(h_subcount));
      h_count = cat(2,h_count,h_subcount);
      h_cumGR = cat(2,h_cumGR,h_subcum);
      i = i+1;
 end;

%Number of earthquakes in every time window (DEFAULT)
t_label=t_win;
t_label(length(t_label))=[];
[t_label',h_cumGR(length(h_subcum),:)']

figure(1)
bar(h_cumGR(length(h_list),:))
title('total number of earthquakes in each time window')


i = input('Do you want to change time window?  (1)Yes   (2)No   :');

%change time windows, if necessary... (MANUAL)
if i == 1,
    tw=[]; % defining new time window
    tin=1;
    while tin < tmax,
    tin = input('change time window:  ');
    tw = cat(1,tw,tin);
    end

%Renaming of the new time windows (MANUAL)
    t_win=tw;
    t_label=t_win;
    t_label(length(t_label))=[];


%cummulative number of each time window (MANUAL)
h_list=hmin:1:(hmax+0.5);
h_count=[];
h_cumGR=[];
i=1; j=1;

 while i<length(t_win),
     h_sublist=[];
    % sublist for all earthquakes in one time window (MANUAL)
    while (j<=length(data) && t_all(j)>=t_win(i) &&
t_all(j)<t_win(i+1)),
      h_sublist=cat(1,h_sublist,h(j));
      j = j+1;
    end
```

```
      %how many earthquakes of a certain intensity in a certain time
      %window
      h_subcount = histc(h_sublist,(hmin-0.5):1:(hmax+0.5));
      % cumulative number for a certain time window
      h_subcum = cumsum(flipud(h_subcount));
      h_count = cat(2,h_count,h_subcount);
      h_cumGR = cat(2,h_cumGR,h_subcum);
      i = i+1;
 end;

%Number of earthquakes in every time window (MANUAL)
[t_label,h_cumGR(length(h_subcum),:)']

figure(2)
bar(h_cumGR(length(h_list),:))
title('total number of earthquakes in each time window - MANUAL')
end;
%TIME WINDOW DEFINITION FINISHED


%Cumulative number of earthquake for each intensity class
i=1;
h_indcount=[];
while (i<=length(h_subcum))
    h_subcount= cumsum(fliplr(h_count(i,:)));
    h_indcount = cat(1,h_indcount,h_subcount);
    i=i+1;
end

% Calculation of standard deviation
sd=[];
diff_time=fliplr(tmax-t_label+1);

j=1; %number of intensity classes (max = 12)
while j<=length(h_subcum),
    i=1; %number of time window (max = 21)
    num=[];
    while i<=length(diff_time),
        n = sqrt(h_indcount(j,i))/diff_time(i);
        num = cat(1,num,n);
        i=i+1;
    end
    sd = cat(2,sd,num);
    j=j+1;
end
figure(3)
loglog(diff_time,1./sqrt(diff_time),diff_time,sd,'o')
title('Stepp plot: stand. var. vs time windows');
xlabel('time');
ylabel('standard deviation (sqrt(#)/t)');

% Define new completeness period
tc=[]; % completeness time period
nc=[]; % number of events within the completeness time period
i=1;
tc_flip=fliplr(t_label);

while i<=hmax+1.5,
   for n = 0:hmax+1.5
    tcmin  = input(['Please enter minimum completeness time for Io/M--
', int2str(n)]);
```

```
    tcmax  = input(['Please enter maximum completeness time for Io/M--
', int2str(n)]);


    if tcmax >= 2000,
        tc = cat(1,tc,t);
        nc = cat(1,nc,h_indcount(i,find(tc_flip==tcmin))-
h_indcount(i,1));
    else
        tc = cat(1,tc,tc_flip(find(tc_flip==tcmax)-1)-
tc_flip(find(tc_flip==tcmin)));
        nc = cat(1,nc,h_indcount(i,find(tc_flip==tcmin))-
h_indcount(i,find(tc_flip==tcmax)-1));
    end
    i=i+1;
   end
end;


%Calculation of recurrence rates
num_eq=nc*t./tc;
cum_numeq=cumsum(flipud(num_eq));
cum_numeq=flipud(cum_numeq);

%plotting
figure(4)
semilogy(h_list,cum_numeq,'o')
if y==12,
    xlabel('Intensity'),
else xlabel('Magnitude'),
end
ylabel('log of cumulative number')
title('GR plot')

h_reg=[ones(size(h_list')), h_list'];
t_reg=log10(cum_numeq);

j=length(cum_numeq);
while j>0,
    if cum_numeq(j) == 0,
        h_reg(j,:)=[];,
        t_reg(j,:)=[];,
    end,
    j=j-1;
end

%Excluding data points from regression
i=input('Neglect data during regression? (1)Yes (2)No');
if i==1,
     a=input('Give number of low mag/int to exclude');,
     b=input('Give number of large mag/int to exclude');,
     if b>0,
         h_reg(length(h_list)-b+1,:)=[];,
         t_reg(length(h_list)-b+1,:)=[];,
     end,
     if a>0,
         j=1,
         while j<=a,
         h_reg(1,:)=[];,
         t_reg(1,:)=[];,
         j=j+1;
         end,
     end,
```

```
end

%Regression
[B,Bint,R,Rint,Stats]=regress(t_reg,h_reg)

%Plot Regression vs. Data
figure(5)
plot(h_reg(:,2),(h_reg(:,1)*B(1)+h_reg(:,2)*B(2)),h_list,log10(cum_nume
q),'o')
xlim([hmin-1,hmax+1]);
ylim([log10(min(cum_numeq))-0.5,log10(max(cum_numeq))+0.5]);
legend('GR-relation','earthquake data')
ylabel('log of cumulative number')
title('GR plot')
if y==12,
    xlabel('Intensity'),
else xlabel('Magnitude'),
end;
```

2. Explanation to use the Script

```
%Input source file
```

Input the source file which is of format given below

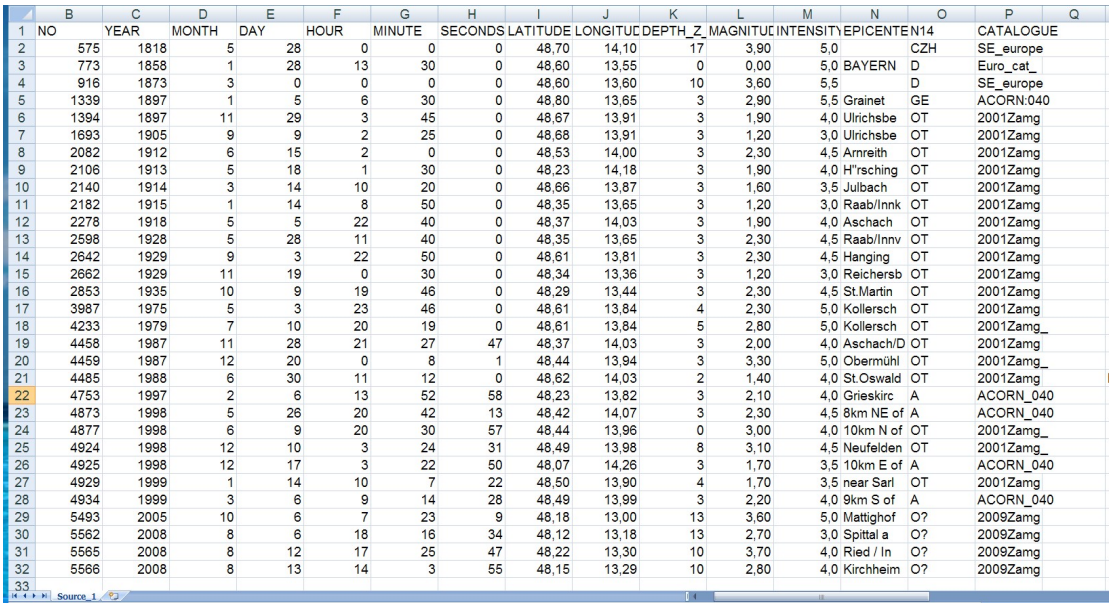

	B	C	D	E	F	G	H	I	J	K	L	M	N	O	P	Q
1	NO	YEAR	MONTH	DAY	HOUR	MINUTE	SECONDS	LATITUDE	LONGITUD	DEPTH_Z	MAGNITUD	INTENSITY	EPICENTE	N14	CATALOGUE	
2	575	1818	5	28	0	0	0	48,70	14,10	17	3,90	5,0		CZH	SE_europe	
3	773	1858	1	28	13	30	0	48,60	13,55	0	0,00	5,0	BAYERN	D	Euro_cat_	
4	916	1873	3	0	0	0	0	48,60	13,60	10	3,60	5,5		D	SE_europe	
5	1339	1897	1	5	6	30	0	48,80	13,65	3	2,90	5,5	Grainet	GE	ACORN:040	
6	1394	1897	11	29	3	45	0	48,67	13,91	3	1,90	4,0	Ulrichsbe	OT	2001Zamg	
7	1693	1905	9	9	2	25	0	48,68	13,91	3	1,20	3,0	Ulrichsbe	OT	2001Zamg	
8	2082	1912	6	15	2	0	0	48,53	14,00	3	2,30	4,5	Arnreith	OT	2001Zamg	
9	2106	1913	5	18	1	30	0	48,23	14,18	3	1,90	4,0	H"rsching	OT	2001Zamg	
10	2140	1914	3	14	10	20	0	48,66	13,87	3	1,60	3,5	Julbach	OT	2001Zamg	
11	2182	1915	1	14	8	50	0	48,35	13,65	3	1,20	3,0	Raab/Innk	OT	2001Zamg	
12	2278	1918	5	5	22	40	0	48,37	14,03	3	1,90	4,0	Aschach	OT	2001Zamg	
13	2598	1928	5	28	11	40	0	48,35	13,65	3	2,30	4,5	Raab/Innv	OT	2001Zamg	
14	2642	1929	9	3	22	50	0	48,61	13,81	3	2,30	4,5	Hanging	OT	2001Zamg	
15	2662	1929	11	19	0	30	0	48,34	13,36	3	1,20	3,0	Reichersb	OT	2001Zamg	
16	2853	1935	10	9	19	46	0	48,29	13,44	3	2,30	4,5	St.Martin	OT	2001Zamg	
17	3987	1975	5	3	23	46	0	48,61	13,84	4	2,30	5,0	Kollersch	OT	2001Zamg	
18	4233	1979	7	10	20	19	0	48,61	13,84	5	2,80	5,0	Kollersch	OT	2001Zamg_	
19	4458	1987	11	28	21	27	47	48,37	14,03	3	2,00	4,0	Aschach/D	OT	2001Zamg	
20	4459	1987	12	20	0	8	1	48,44	13,94	3	3,30	5,0	Obermühl	OT	2001Zamg_	
21	4485	1988	6	30	11	12	0	48,62	14,03	2	1,40	4,0	St.Oswald	OT	2001Zamg	
22	4753	1997	2	6	13	52	58	48,23	13,82	3	2,10	4,0	Grieskirc	A	ACORN_040	
23	4873	1998	5	26	20	42	13	48,42	14,07	3	2,30	4,5	8km NE of	A	ACORN_040	
24	4877	1998	6	9	20	30	57	48,44	13,96	0	3,00	4,0	10km N of	OT	2001Zamg_	
25	4924	1998	12	10	3	24	31	48,49	13,98	8	3,10	4,5	Neufelden	OT	2001Zamg_	
26	4925	1998	12	17	3	22	50	48,07	14,26	3	1,70	3,5	10km E of	A	ACORN_040	
27	4929	1999	1	14	10	7	22	48,50	13,90	4	1,70	3,5	near Sarl	OT	2001Zamg	
28	4934	1999	3	6	9	14	28	48,49	13,99	3	2,20	4,0	9km S of	A	ACORN_040	
29	5493	2005	10	6	7	23	9	48,18	13,00	13	3,60	5,0	Mattighof	O?	2009Zamg	
30	5562	2008	8	6	18	16	34	48,12	13,18	13	2,70	3,0	Spittal a	O?	2009Zamg	
31	5565	2008	8	12	17	25	47	48,22	13,30	10	3,70	4,0	Ried / In	O?	2009Zamg	
32	5566	2008	8	13	14	3	55	48,15	13,29	10	2,80	4,0	Kirchheim	O?	2009Zamg	
33																

Source_1

Figure 1. Example (screenshot) of input in MATLAB application file.
Assignement of colums in the code:
Column C= Column 2 = year
Column L = Column 11= magnitude
Etc.

```
%check for NaN
```

The script will check the second column (Year) as shown above, empty row will not be counted.

```
%Define length of catalogue
```

t_all will select the year column and tmin, tmax find the minimum and maximum year
't' will count the time period(years).

```
%Define time windows (Default)
```

In this section we already defined the time window.

```
%Define I or M, we define I at the moment
%I = column 12, M = column 11
```

We can choose the column of intensity by pressing 1 and by pressing 2 we can choose magnitude for calculation of GR-Relation.
hmin will find the minimum intensity/magnitude of the catalogue used.
hmax will find the maximum of intensity/magnitude of the catalogue used.

```
%cummulative number of each time window(Default)
```

It will count the number of earthquake event in every time window and while loop run every time to count earthquake events of every time window and will display it in a list as shown below:

```
        1048          47
        1500          99
        1600          88
        1700          39
        1750          62
        1775          60
        1800          52
        1825          58
        1850         133
        1875         334
        1900         338
        1910         254
        1920         245
        1930         259
        1940         165
        1950         223
        1960         251
        1970         274
        1980         219
        1990         368
        2000         415
%Number of earthquakes in every time window
```

In this section a histogram between time windows and cumulative number of earthquakes of each time window will be displayed.

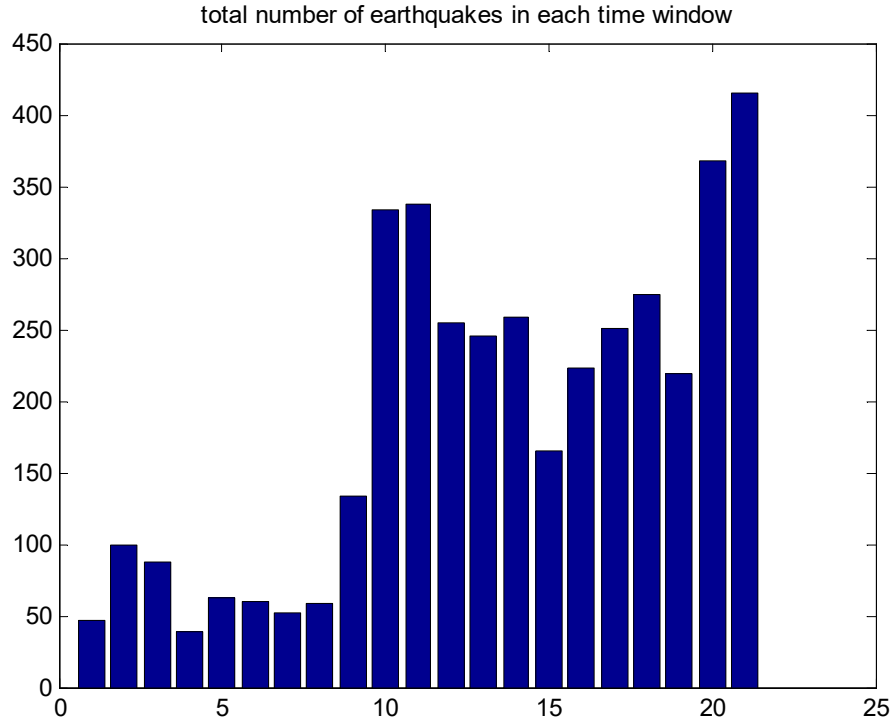

Figure 2: Histogram of Time windows (x-axis) and cumulative number of earthquake(y-axis) of each time window.

```
%change time windows, if necessary... (MANUAL)
```

If we think that we can continue with the by default time windows then we do not need to define time window otherwise we can define manually. After defining we will do the same process as described above until histogram.

```
%Cumulative number of earthquakes for each intensity class and
Calculation of standard deviation
```

We will cumulate number of earthquakes of every intensity class for each time window and calculate standard deviation.
After that we will make a logarithmic plot between different time windows and standard deviation.

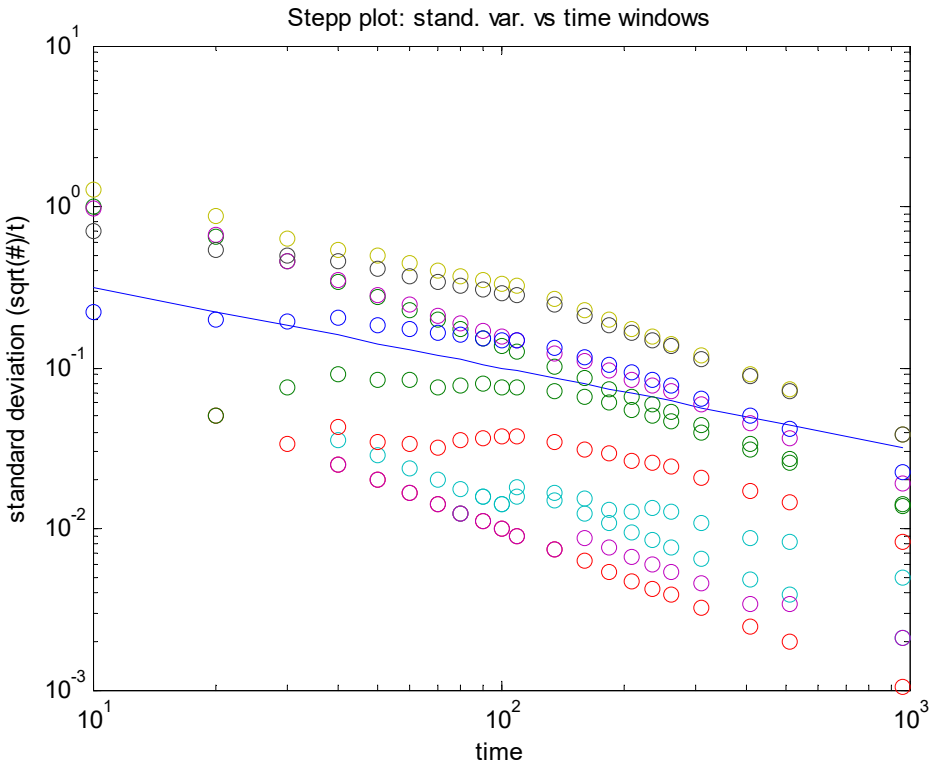

Figure 3: Cumulative number of earthquakes of each Intensity/Magnitude class.

```
% Define completeness period
```

From above figure we will define completeness time period manually and input in the program to get a- and b parameters of Gutenberg-Richter relation.

```
%Calculation of recurrence rates
```

Cumnum_t: It calculates the recurrences of individual intensity/magnitude classes (Cumulative number of earthquake events divided by the time period t).

```
 %plotting
```

We will make a semi log plot between intensity/magnitude Vs recurrence rates.

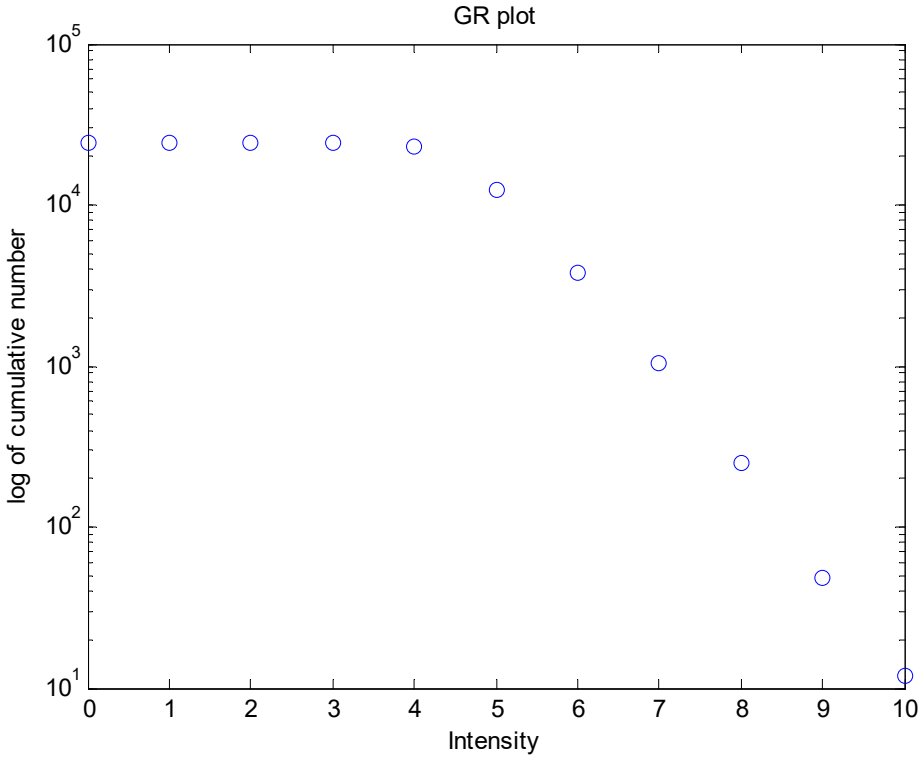

Figure 4: Gutenberg-Richter plot of the input file.

```
%Excluding data points from regression
```

In this section we exclude the data point which should not be included in regression

```
%Regression and %Plot Regression vs. Data
```

We display a semi log plot between intensity/magnitude Vs recurrence rates after regression.

The output looks like as below. The values can be different depending on the data used

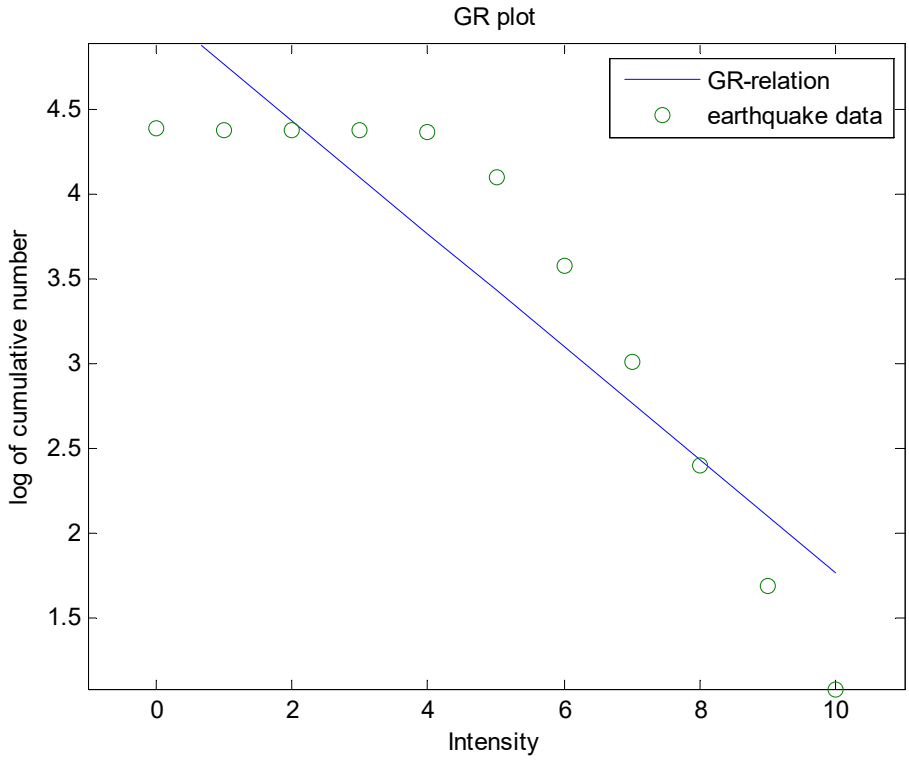

Figure 5: Regression and evaluation of Gutenberg-Richter parameters.

B =

```
 a-value:    1.2156
 b-value:   -0.2855
```

Bint =

```
    0.6372    1.7939
   -0.3832   -0.1877
```

(The minimum and maximum of a-value)
(The minimum and maximum of b-value)

R = (The distance of each data point from regression line)

```
   -0.5985
   -0.3342
   -0.0488
    0.2362
    0.4809
    0.5462
    0.3803
    0.2341
    0.0440
   -0.1982
   -0.7420
```

Rint =
(minimum and maximum of each data point from regression line)

```
   -1.3583    0.1613
   -1.2462    0.5778
   -1.0372    0.9396
   -0.7621    1.2345
   -0.4764    1.4383
   -0.3942    1.4866
   -0.6055    1.3662
   -0.7645    1.2327
   -0.9445    1.0326
   -1.1353    0.7389
   -1.4160   -0.0681
```

Stats =

```
    0.8290   43.6307    0.0001    0.2054
```

Attachment 2

Programming for the TCEF correction

1. TCEF MATLAB Script

```
clear all

%Input source file
data = xlsread(input('please enter source file   :  '));

%check for NaN
i=length(data);
while i>0,
    if isnan(data(i,2)),
       data(i,:)=[];
    end;
    i=i-1;
end;
%Define length of catalogue
t_all = data(:,2);
tmin = min(t_all);
tmax = max(t_all);
t = tmax-tmin+1;
t_year = tmin:1:tmax;

%Define I or M, we define I at the moment
%I = column 12, M = column 11
x = input('please choose Intensity (1) or Magnitude (2) ');

if x == 1, y=12;
else y=11;
end

%intensity/magnitude data
h = data(:,y);
hmin = min(h);
hmax = max(h);

%cummulative number of earthquake in every year

h_list = hmin:1:hmax+0.5;
h_count=[];
h_cumGR=[];
i=1; j=1;

 while i<=length(t_year),
      g=find(data(:,2)==t_year(i));
      h_sublist=h(g);
      %how many earthquakes of a certain intensity in a certain time
      %window
      h_subcount = histc(h_sublist,(hmin-0.5):1:(hmax+0.5));
      if length(g)== 1, h_count = cat(2,h_count,h_subcount');
      else h_count = cat(2,h_count,h_subcount);
      end;
      i = i+1;
```

```
 end;

 % TCEF Plotting
 h_cum = cumsum(h_count');
 plot(t_year,h_cum,'-')
 title('TCEF plot: Time Vs Cummulative Number of earthquakes');
xlabel('Time');
ylabel('Cummulative Number of EQ');

% Define new completeness period
tc=[]; % completeness time period
nc=[]; % number of events within the completeness time period

i=1;
t_flip=t_year';
while i<=hmax+1.5,
    for n=1:hmax+1.5
    tcmin  = input(['Please enter minimum completeness time for
',int2str(n),' intensity/Mag:']);
    tc = cat(1,tc,t_flip(find(hmax))-t_flip(find(t_flip==tcmin-1)));
    nc = cat(1,nc,h_cum(find(hmax),i)-h_cum(find(t_flip==tcmin)-1,i));
    i=i+1;
    end
end;

%Calculation of recurrence rates
num_eq=nc*t./tc;
cum_numeq=flipud(cumsum(flipud(num_eq)));

%plotting
figure(2)
semilogy(h_list,cum_numeq,'o')
if y==12,
    xlabel('Intensity'),
else xlabel('Magnitude'),
end
ylabel('log of cumulative number')
title('GR plot')

h_reg=[ones(size(h_list')), h_list'];
t_reg=log10(cum_numeq);

j=length(cum_numeq);
while j>0,
    if cum_numeq(j) == 0,
        h_reg(j,:)=[];
        t_reg(j,:)=[];
    end,
    j=j-1;
end

%Excluding data points from regression
i=input('Neglect data during regression? (1)Yes (2)No');
if i==1,
     a=input('Give number of low mag/int to exclude');,
     b=input('Give number of large mag/int to exclude');,
     if b>0,
         h_reg(length(h_list)-b+1,:)=[];,
         t_reg(length(h_list)-b+1,:)=[];,
     end,
     if a>0,
         j=1;
         while j<=a,
```

```
            h_reg(1,:)=[];,
            t_reg(1,:)=[];,
            j=j+1;
            end,
        end,
end
%Regression
[B,Bint,R,Rint,Stats]=regress(t_reg,h_reg)

%Plot Regression vs. Data
figure(3)
plot(h_reg(:,2),(h_reg(:,1)*B(1)+h_reg(:,2)*B(2)),h_list,log10(cum_nume
q),'o')
xlim([hmin-1,hmax+1]);
ylim([log10(min(cum_numeq))-0.5,log10(max(cum_numeq))+0.5]);
legend('GR-relation','earthquake data')
ylabel('log of cumulative number')
title('GR plot')
if y==12,
    xlabel('Intensity'),
else xlabel('Magnitude'),
end;
```

2. Explanation to use TCEF MATLAB Script

```
%Input source file
Input the source file which is of format given below
```

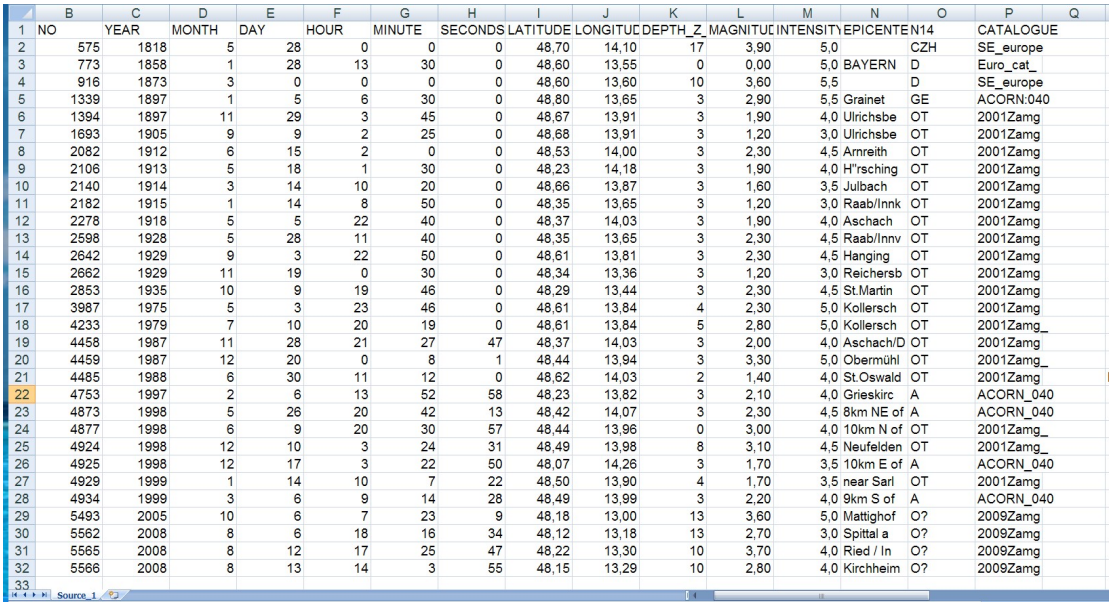

	B	C	D	E	F	G	H	I	J	K	L	M	N	O	P	Q
1	NO	YEAR	MONTH	DAY	HOUR	MINUTE	SECONDS	LATITUDE	LONGITUD	DEPTH_Z	MAGNITUD	INTENSITY	EPICENTE	N14	CATALOGUE	
2	575	1818	5	28	0	0	0	48,70	14,10	17	3,90	5,0		CZH	SE_europe	
3	773	1858	1	28	13	30	0	48,60	13,55	0	0,00	5,0	BAYERN	D	Euro_cat_	
4	916	1873	3	0	0	0	0	48,60	13,60	10	3,60	5,5		D	SE_europe	
5	1339	1897	1	5	6	30	0	48,80	13,65	3	2,90	5,5	Grainet	GE	ACORN:040	
6	1394	1897	11	29	3	45	0	48,67	13,91	3	1,90	4,0	Ulrichsbe	OT	2001Zamg	
7	1693	1905	9	9	2	25	0	48,68	13,91	3	1,20	3,0	Ulrichsbe	OT	2001Zamg	
8	2082	1912	6	15	2	0	0	48,53	14,00	3	2,30	4,5	Arnreith	OT	2001Zamg	
9	2106	1913	5	18	1	30	0	48,23	14,18	3	1,90	4,0	H"rsching	OT	2001Zamg	
10	2140	1914	3	14	10	20	0	48,66	13,87	3	1,60	3,5	Julbach	OT	2001Zamg	
11	2182	1915	1	14	8	50	0	48,35	13,65	3	1,20	3,0	Raab/Innk	OT	2001Zamg	
12	2278	1918	5	5	22	40	0	48,37	14,03	3	1,90	4,0	Aschach	OT	2001Zamg	
13	2598	1928	5	28	11	40	0	48,35	13,65	3	2,30	4,5	Raab/Innv	OT	2001Zamg	
14	2642	1929	9	3	22	50	0	48,61	13,81	3	2,30	4,5	Hanging	OT	2001Zamg	
15	2662	1929	11	19	0	30	0	48,34	13,36	3	1,20	3,0	Reichersb	OT	2001Zamg	
16	2853	1935	10	9	19	46	0	48,29	13,44	3	2,30	4,5	St.Martin	OT	2001Zamg	
17	3987	1975	5	3	23	46	0	48,61	13,84	4	2,30	5,0	Kollersch	OT	2001Zamg	
18	4233	1979	7	10	20	19	0	48,61	13,84	5	2,80	5,0	Kollersch	OT	2001Zamg_	
19	4458	1987	11	28	21	27	47	48,37	14,03	3	2,00	4,0	Aschach/D	OT	2001Zamg	
20	4459	1987	12	20	0	8	1	48,44	13,94	3	3,30	5,0	Obermühl	OT	2001Zamg_	
21	4485	1988	6	30	11	12	0	48,62	14,03	2	1,40	4,0	St.Oswald	OT	2001Zamg	
22	4753	1997	2	6	13	52	58	48,23	13,82	3	2,10	4,0	Grieskirc	A	ACORN_040	
23	4873	1998	5	26	20	42	13	48,42	14,07	3	2,30	4,5	8km NE of	A	ACORN_040	
24	4877	1998	6	9	20	30	57	48,44	13,96	0	3,00	4,0	10km N of	OT	2001Zamg_	
25	4924	1998	12	10	3	24	31	48,49	13,98	8	3,10	4,5	Neufelden	OT	2001Zamg_	
26	4925	1998	12	17	3	22	50	48,07	14,26	3	1,70	3,5	10km E of	A	ACORN_040	
27	4929	1999	1	14	10	7	22	48,50	13,90	4	1,70	3,5	near Sarl	OT	2001Zamg	
28	4934	1999	3	6	9	14	28	48,49	13,99	3	2,20	4,0	9km S of	A	ACORN_040	
29	5493	2005	10	6	7	23	9	48,18	13,00	13	3,60	5,0	Mattighof	O?	2009Zamg	
30	5562	2008	8	6	18	16	34	48,12	13,18	13	2,70	3,0	Spittal a	O?	2009Zamg	
31	5565	2008	8	12	17	25	47	48,22	13,30	10	3,70	4,0	Ried / In	O?	2009Zamg	
32	5566	2008	8	13	14	3	55	48,15	13,29	10	2,80	4,0	Kirchheim	O?	2009Zamg	
33																

Source_1

Figure 1: Example (screenshot) of input in MATLAB application file.
Assignement of colums in the code:
Column C= Column 2 = year
Column L = Column 11= magnitude
Etc.

```
%check for NaN
```

The script will check the second column (year) as shown above, empty row will not be counted.

```
%Define length of catalogue
```

t_all will select the year column and tmin, tmax find the minimum and maximum year
't' will count the time period(years).

```
%Define I or M, we define I at the moment
%I = column 12, M = column 11
```

We can choose the column of intensity by pressing 1 and by pressing 2 we can choose magnitude for calculation of GR-Relation.
hmin will find the minimum intensity/magnitude of the catalogue used.
hmax will find the maximum of intensity/magnitude of the catalogue used.

```
%cummulative number of earthquake in every year
```

h_list: It will count and display the list of intensity/magnitude clasees.

h_count: It counts the number of earthquake of individual intensity/magnitude class.
The while loop will run until the length of year, count the number of earthquake events of individual intensity/magnitude classes in each year.

h_cum: It calculates the cumulative number of earthquake events of certain intensity/magnitude.

```
% TCEF Plotting
```

We will make a plot between time Vs cumulative number of earthquake of individual intensity/magnitude classes.

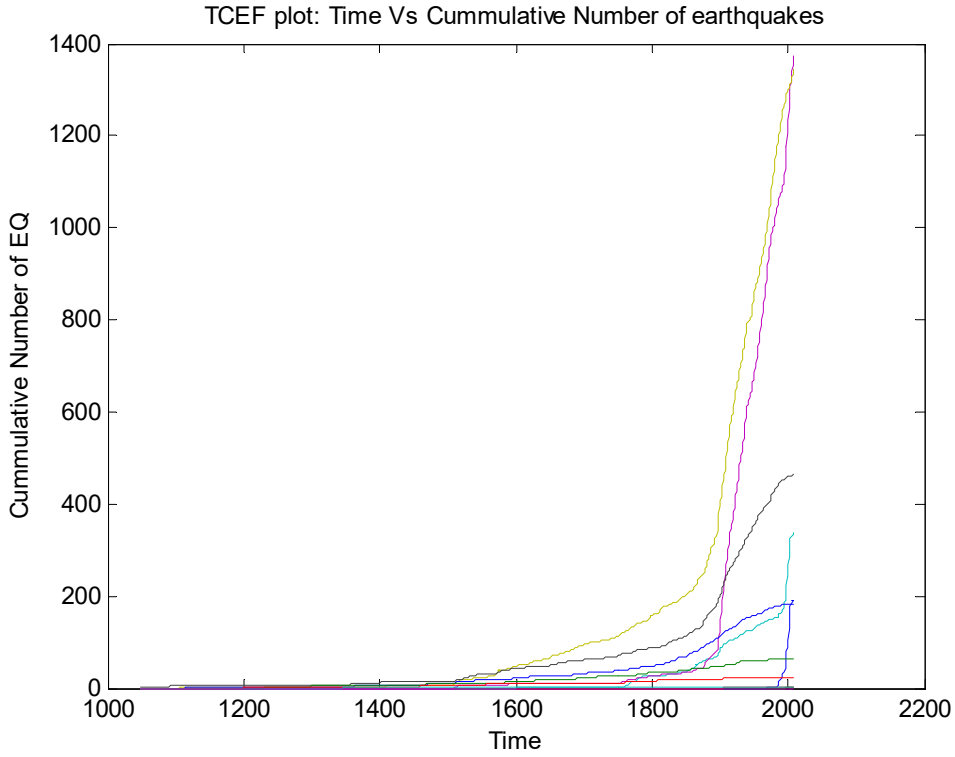

Figure 2: TCEF plot of Time Vs Cummulative number of earthquake of individual Intensity/Magnitude class.

```
% define completeness period for every intensity/magnitude class#
```

In this section we will define completeness time windows by the input in years of every intensity/magnitude class.

```
%Calculation of recurrence rates
```

It calculates the recurrences of individual intensity/magnitude classes (Cumulative number of earthquake events divided by the completeness time period t).

```
%plotting
```

We will make a semi log plot between intensity/magnitude Vs recurrence rates.

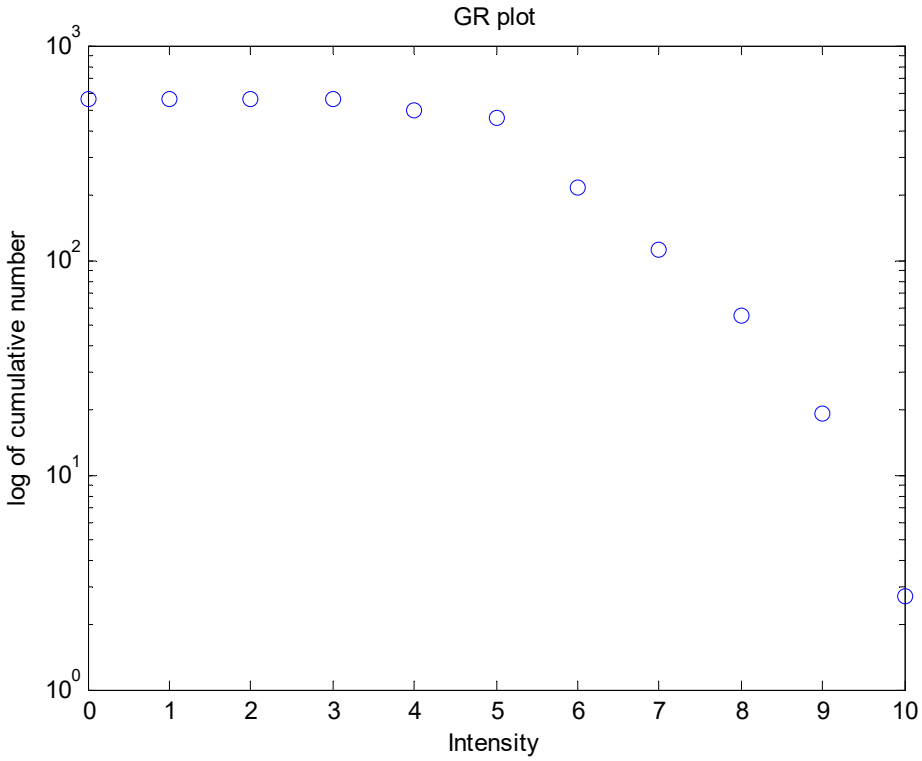

Figure 3: Gutenberg-Richter plot of the input file.

```
%Excluding data points from regression
```

In this section we exclude the data point which should not be included in regression

```
%Regression and %Plot Regression vs. Data
```

We display a semi log plot between intensity/magnitude Vs recurrence rates after regression. The output looks like as below. The values can be different depending on the data used.

See GR_Script

Attachment 3

Calculating a- and b-parameter of Gutenberg-Richter

1. G-R MATLAB Script

```
clear all
%Input source file
data = xlsread(input('please enter source file'));

%Define I or M, we define I at the moment
%I = column 12, M = column 11
x = input('please choose Intensity (1) or Magnitude (2)');

if (x == 1) y=12;
else y=11;
end

h = data(:,y);
hmin = min(h);
hmax = max(h);

%Define length of time period t
t_all = data(:,2);
tmin = min(t_all);
tmax = max(t_all);
t = tmax - tmin + 1;

%Cumulative number
h_list = hmin:1:(hmax+1);
h_count = histc(h,(hmin-0.5):1:(hmax+0.5));
h_cum = cumsum(flipud(h_count));

%Calculation of recurrence rates
cumnum_t= flipud(h_cum/t);

%plotting
figure(1)
semilogy(h_list,cumnum_t,'o')
xlabel('intensity')
ylabel('log of cumulative number')
title('GR plot')
h_reg=[ones(size(h_list')), h_list'];
t_reg=log10(cumnum_t);

j=length(cumnum_t);
while j>0,
    if cumnum_t(j) == 0,
        h_reg(j,:)=[];,
        t_reg(j,:)=[];,
    end,
    j=j-1;
end
```

```
%Excluding data points from regression
i=input('Neglect data during regression? (1)Yes (2)No');
if i==1,
     a=input('Give number of low mag/int to exclude');,
     b=input('Give number of large mag/int to exclude');,
     if b>0,
         h_reg(length(h_list)-b+1,:)=[];,
         t_reg(length(h_list)-b+1,:)=[];,
     end,
     if a>0,
         j=1,
         while j<=a,
         h_reg(1,:)=[];,
         t_reg(1,:)=[];,
         j=j+1,
         end,
     end,
end

%Regression
[B,Bint,R,Rint,Stats]=regress(t_reg,h_reg)

%Plot Regression vs. Data
figure(1)
plot(h_reg(:,2),(h_reg(:,1)*B(1)+h_reg(:,2)*B(2)),h_list,log10(cumnum_t
),'o')
xlim([hmin-1,hmax+1]);
ylim([log10(min(cumnum_t))-0.5,log10(max(cumnum_t))+0.5]);
legend('GR-relation','earthquake data')
ylabel('log of cumulative number')
title('GR plot')
if y==12,
    xlabel('Intensity'),
else xlabel('Magnitude'),
end
```

Output

```
GR_plot.m
please enter source file'stepp.xls'
please choose Intensity (1) or Magnitude (2)1
Neglect data during regression? (1)Yes (2)No4
```

2. Explanation to use the Script

```
%Input source file
```

Input the source file which is of format given below

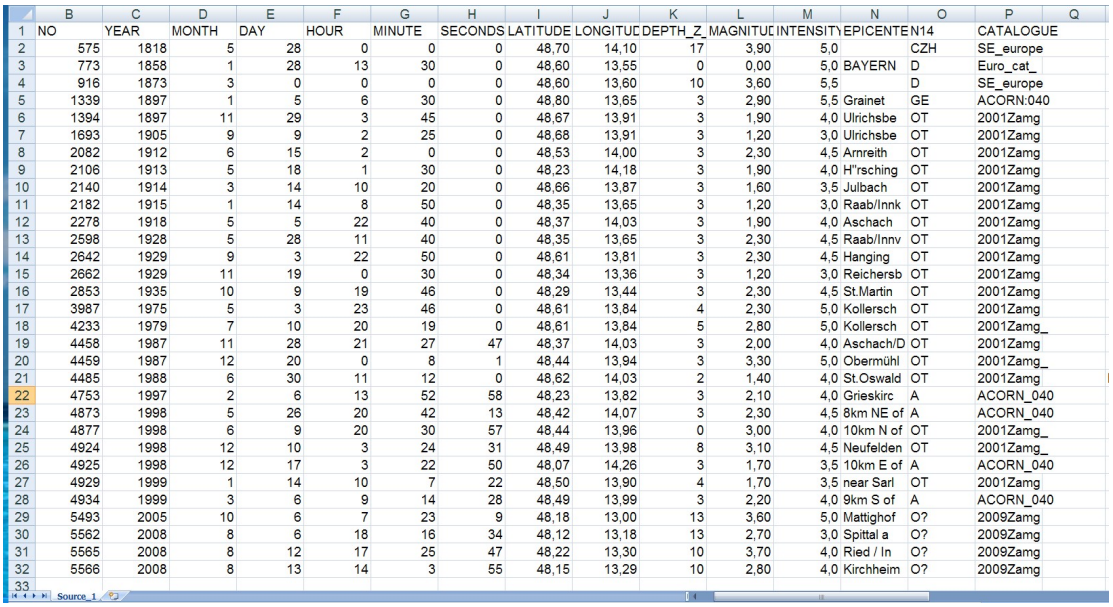

	B	C	D	E	F	G	H	I	J	K	L	M	N	O	P	Q
1	NO	YEAR	MONTH	DAY	HOUR	MINUTE	SECONDS	LATITUDE	LONGITUD	DEPTH_Z	MAGNITUD	INTENSITY	EPICENTE	N14	CATALOGUE	
2	575	1818	5	28	0	0	0	48,70	14,10	17	3,90	5,0		CZH	SE_europe	
3	773	1858	1	28	13	30	0	48,60	13,55	0	0,00	5,0	BAYERN	D	Euro_cat_	
4	916	1873	3	0	0	0	0	48,60	13,60	10	3,60	5,5		D	SE_europe	
5	1339	1897	1	5	6	30	0	48,80	13,65	3	2,90	5,5	Grainet	GE	ACORN:040	
6	1394	1897	11	29	3	45	0	48,67	13,91	3	1,90	4,0	Ulrichsbe	OT	2001Zamg	
7	1693	1905	9	9	2	25	0	48,68	13,91	3	1,20	3,0	Ulrichsbe	OT	2001Zamg	
8	2082	1912	6	15	2	0	0	48,53	14,00	3	2,30	4,5	Arnreith	OT	2001Zamg	
9	2106	1913	5	18	1	30	0	48,23	14,18	3	1,90	4,0	H"rsching	OT	2001Zamg	
10	2140	1914	3	14	10	20	0	48,66	13,87	3	1,60	3,5	Julbach	OT	2001Zamg	
11	2182	1915	1	14	8	50	0	48,35	13,65	3	1,20	3,0	Raab/Innk	OT	2001Zamg	
12	2278	1918	5	5	22	40	0	48,37	14,03	3	1,90	4,0	Aschach	OT	2001Zamg	
13	2598	1928	5	28	11	40	0	48,35	13,65	3	2,30	4,5	Raab/Innv	OT	2001Zamg	
14	2642	1929	9	3	22	50	0	48,61	13,81	3	2,30	4,5	Hanging	OT	2001Zamg	
15	2662	1929	11	19	0	30	0	48,34	13,36	3	1,20	3,0	Reichersb	OT	2001Zamg	
16	2853	1935	10	9	19	46	0	48,29	13,44	3	2,30	4,5	St.Martin	OT	2001Zamg	
17	3987	1975	5	3	23	46	0	48,61	13,84	4	2,30	5,0	Kollersch	OT	2001Zamg	
18	4233	1979	7	10	20	19	0	48,61	13,84	5	2,80	5,0	Kollersch	OT	2001Zamg_	
19	4458	1987	11	28	21	27	47	48,37	14,03	3	2,00	4,0	Aschach/D	OT	2001Zamg	
20	4459	1987	12	20	0	8	1	48,44	13,94	3	3,30	5,0	Obermühl	OT	2001Zamg_	
21	4485	1988	6	30	11	12	0	48,62	14,03	2	1,40	4,0	St.Oswald	OT	2001Zamg	
22	4753	1997	2	6	13	52	58	48,23	13,82	3	2,10	4,0	Grieskirc	A	ACORN_040	
23	4873	1998	5	26	20	42	13	48,42	14,07	3	2,30	4,5	8km NE of	A	ACORN_040	
24	4877	1998	6	9	20	30	57	48,44	13,96	0	3,00	4,0	10km N of	OT	2001Zamg_	
25	4924	1998	12	10	3	24	31	48,49	13,98	8	3,10	4,5	Neufelden	OT	2001Zamg_	
26	4925	1998	12	17	3	22	50	48,07	14,26	3	1,70	3,5	10km E of	A	ACORN_040	
27	4929	1999	1	14	10	7	22	48,50	13,90	4	1,70	3,5	near Sarl	OT	2001Zamg	
28	4934	1999	3	6	9	14	28	48,49	13,99	3	2,20	4,0	9km S of	A	ACORN_040	
29	5493	2005	10	6	7	23	9	48,18	13,00	13	3,60	5,0	Mattighof	O?	2009Zamg	
30	5562	2008	8	6	18	16	34	48,12	13,18	13	2,70	3,0	Spittal a	O?	2009Zamg	
31	5565	2008	8	12	17	25	47	48,22	13,30	10	3,70	4,0	Ried / In	O?	2009Zamg	
32	5566	2008	8	13	14	3	55	48,15	13,29	10	2,80	4,0	Kirchheim	O?	2009Zamg	
33																

Source_1

Figure 1. Example (screenshot) of input in MATLAB application.

Assignement of colums in the code:
Column C= Column 2 = year
Column L = Column 11= magnitude
Etc.

```
%Define I or M, we define I at the moment
%I = column 12, M = column 11
```

We can choose the column of intensity by pressing 1 and by pressing 2 we can choose magnitude for calculation of GR-Relation.
hmin will find the minimum intensity/magnitude of the catalogue used.
hmax will find the maximum of intensity/magnitude of the catalogue used.

```
%Define length of catalogue t
```

t_all will select the year column and tmin, tmax find the minimum and maximum year
't' will count the time period(years).

```
%Cumulative number
```

h_list: It will count and display the list of intensity/magnitude clasees.
h_count: It counts the number of earthquakes of individual intensity/magnitude class.
h_cum: It calculates the cumulative number of earthquake intensity/magnitude.

```
%Calculation of recurrence rates
```

Cumnum_t: It calculates the recurrences of individual intensity/magnitude classes (Cumulative number of earthquake events divided by the time period t).

```
 %plotting
```

We will make a semi log plot between intensity/magnitude Vs recurrence rates.

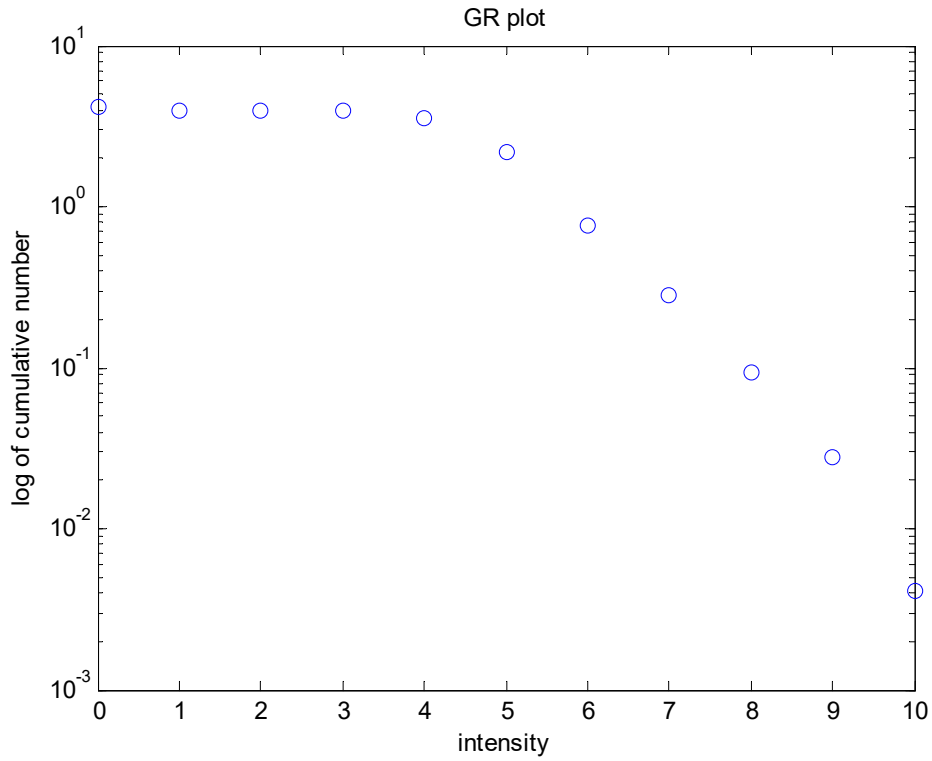

Figure 2: Evaluation of Gutenberg-Richter plot of the input file.

```
%Excluding data points from regression
```

In this section we exclude the data point which should not be included in regression

```
%Regression and %Plot Regression vs. Data
```

We display a semi log plot between intensity/magnitude Vs recurrence rates after regression.

The output looks like as below. The values can be different depending on the data used.

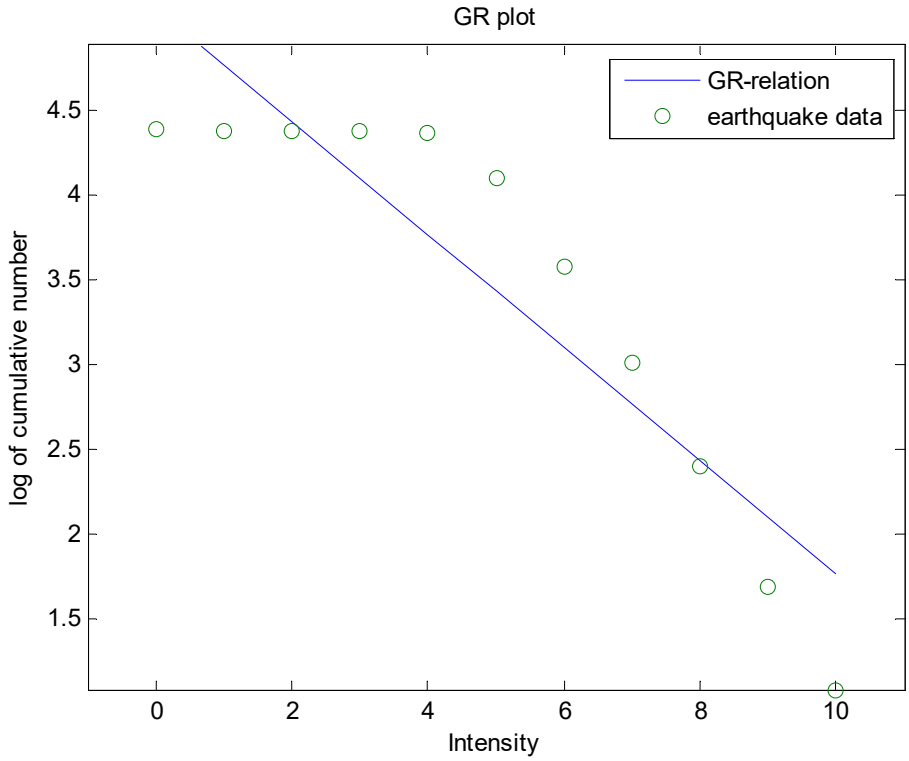

Figure 3: Regression and evaluation of Gutenberg-Richter parameters.

B =

```
a-value:     1.2156  (Average a-value)
b-value:    -0.2855  (Average b-Value)
```

Bint =

```
    0.6372     1.7939  (The minimum and maximum of a-value)
   -0.3832    -0.1877  (The minimum and maximum of b-value)
```

R = (The distance of each data point from regression line)

```
   -0.5985
   -0.3342
   -0.0488
    0.2362
    0.4809
    0.5462
    0.3803
    0.2341
    0.0440
   -0.1982
   -0.7420
```

Rint = (minimum and maximum of each data point from regression line)

```
   -1.3583    0.1613
   -1.2462    0.5778
   -1.0372    0.9396
   -0.7621    1.2345
   -0.4764    1.4383
   -0.3942    1.4866
   -0.6055    1.3662
   -0.7645    1.2327
   -0.9445    1.0326
   -1.1353    0.7389
   -1.4160   -0.0681
```

Stats =

```
    0.8290   43.6307    0.0001    0.2054
```

Appendix 1

Nasir, A. Lenhardt, W., Hintersberger, E., & Decker, K., **2013**. Assessing the completeness of historical and instrumental earthquake data in Austria and surrounding areas. Austria Journal of Earth Sciences, 106/1, 90-102. doi: 10.14470/FX099882

Austrian Journal of Earth Sciences | Volume 106/1 | 90 - 102 | Vienna | 2013

Assessing the completeness of historical and instrumental earthquake data in Austria and the surrounding areas

Asma NASIR[1)*], Wolfgang LENHARDT[2)], Esther HINTERSBERGER[1)] & Kurt DECKER[1)]

[1)] Department of Geodynamics and Sedimentology, Center for Earth Sciences, University Vienna, Althanstrasse 14, A-1090 Vienna, Austria;

[2)] Department of Geophysics, Zentralanstalt für Meteorologie und Geodynamik, Hohe Warte 38, A-1190 Vienna, Austria;

[*)] Corresponding author, asma.nasir@univie.ac.at

KEYWORDS

earthquake catalogue completeness
Gutenberg-Richter-relation
completeness analysis
Austria

Abstract

In regions with long historical earthquake records, seismic hazard assessments are additionally challenged by the large uncertainties related to the available pre-instrumental data. A major source of uncertainty is the incompleteness of historical earthquake records. Therefore, an important step in seismic hazard assessment is the check of completeness for different intensity levels and the removal of aftershock sequences. Mainly two different approaches have been proposed for checking the completeness of seismic catalogues: the temporal course of earthquake frequency (TCEF), and a completeness check based on statistical analysis of the mean earthquake recurrence interval for varying time windows. We systematically compared the effects of the different methods on the Gutenberg-Richter relation (GR-relation), as well as the influence of removing fore- and aftershocks.

For that purpose we created and declustered a new composite catalogue for Austria, the Vienna Basin and a 100 km wide region outside the boundaries of Austria and Vienna Basin based on four different earthquake catalogues. We can show that the a- and b-values for the GR-relations derived from different completeness analyses depend on the correction method used. Corrections with the TCEF seem to produce lower a- and b-values. The Stepp method, on the other hand, excludes the highest intensity class (I_0 =X) and tends to calculate lower a- and b-parameters. Based on these results, we prefer the latter.

Both completeness methods have further been applied to a subset of the composite catalogue corresponding to a source zone including the active Vienna Basin fault system. Comparison shows that completeness of the entire dataset is apparently overestimated.

Die Unvollständigkeit von historischen Erdbebenaufzeichnungen ist ein wesentlicher Unsicherheitsfaktor bei der Bestimmung der Erdbebengefährdungen in Regionen, in denen der größte Teil der aufgezeichneten Erdbeben aus historische Daten stammt. Ein wichtiger Schritt der Gefährdungsanalyse ist daher die Abschätzung der Vollständigkeit der vorhandenen Erdbebenaufzeichnungen für einzelne Intensitätsklassen. In den meisten Fällen wird die Vollständigkeit der Erdbebenkatalogen mit einer der zwei folgenden Methoden bewertet: der TCEF-Methode (Temporal Course of Earthquake Frequency; kumulative Anzahl der Erdbeben pro Intensitätsklasse), und dem Stepp Test, eine statistische Überprüfung der Vollständigkeit auf Basis der mittleren Wiederholungsintervalle von Erdbeben für unterschiedliche Zeitfenster. Unser Artikel enthält einen systematischen Vergleich der Ergebnisse der beiden Tests und ihrer Anwendung für die Erstellung einer Gutenberg-Richer-Funktion (GR). Weiters wird der Effekt der Entfernung von Vor- und Nachbeben aus dem Erdbebendatensatz untersucht.

Bei diesem Vergleich verwenden wir einen neu zusammengestellten Erdbebenkatalog, der Österreich, das Wiener Becken außerhalb Österreichs, und eine 100 km breite Zone um diese Region erfasst. Vor- und Nachbeben wurden aus dem Datensatz manuell eliminiert. Wir können zeigen, dass die Korrektur der Unvollständigkeit der Erdbebendaten nach Anwendung des TCEF-Tests und des Stepp Tests zu GR-Funktionen mit unterschiedlichen a- und b-Werten führt. Aus der TCEF-Korrektur ergeben sich kleinere a- und b-Werte. Der Stepp Test führt zu tendenziell höheren a- und b-Werten, da die höchste Intensitätsklasse (I_0 =X) durch den Test als unvollständig kategorisiert und somit nicht berücksichtigt wird. Aufgrund des durchgeführten Vergleichs bevorzugen wir die letztgenannte Korrekturmethode.

Beide Korrekturen werden in einem zweiten Schritt auf ein Teilgebiet des Gesamtdatensatzes angewandt, das der seismischen Quellzone des Wiener Becken-Störungssystems entspricht. Der Vergleich der Vollständigkeit der Daten aus diesem Teilgebiet zeigt, dass beide Analysemethoden die Vollständigkeit des Gesamtdatensatzes überschätzen.

1. Introduction

Earthquake catalogues are the most important seismological product in regions such as Central Europe, where earthquake hazard assessments exclusively rely on the analysis of historical and instrumental earthquake data (Lenhardt, 2007; Grünthal et al., 1998; 1999). Catalogues of historical and instrumental data are used for estimations of the mean annual rate of seismic activity and the determination of seismicity parameters, such as the magnitude-frequency relation coefficients (a- and b-values) in the corresponding Gutenberg-Richter relation.

Due to various reasons, historical and even instrumental data ,records are by their nature incomplete. It is therefore important that seismic hazard analysis accounts for this deficiency. The reasons for incomplete historical earthquake data are discussed by Gutdeutsch and Hammerl (1997, 1999), who defi-

ned a record threshold for historical earthquakes. For historical times, this threshold depends on the local intensity of a historical event as well as on a various other factors such as the past population density, the presence, interest and motivation of chronologists who could take note of the event, as well as social and political circumstances and other natural disasters distracting attention from earthquakes. The incompleteness of instrumental data may be due to the geometry and coverage of the seismic network, or malfunction of seismic stations. An example is the destruction of the seismographs installed at the ZAMG in Vienna during the Second World War (Hammerl et al., 2001). A thorough assessment of the data completeness is therefore a prime prerequisite for any hazard evaluation.

Several methods have been proposed to assess the intensity/magnitude above which an earthquake catalogue can be considered as reasonably complete, or alternatively to assign time intervals in which a certain intensity/magnitude range is likely to be completely reported (Stepp, 1972; Mulargia and Tinti, 1987; Grünthal et al., 1998; Stucchi et al., 2004; Wössner and Wiemer, 2005). These assessments are used for determining the completeness of the analyzed catalogues and for estimating corrected occurrence rates for earthquakes of different intensity/magnitude classes, which are then used to define intensity/magnitude-frequency relations.

Accordingly, the purpose of the study presented here is twofold. Firstly, we evaluate the completeness of earthquake records in the Central European region covering Austria and the Vienna Basin. For that, we use firstly the TCEF method (temporal course of earthquake frequency) because it is the most commonly used in Germany and Austria (e.g. Lenhardt., 1996). For comparison, we additionally assess the completeness of this data set by using the statistical approach proposed by Stepp (1972). Secondly, we use these new data to determine the effects of different correction methods on intensity-frequency relations. The results of this sensitivity study will be presented in terms of a- and b-parameters of Gutenberg-Richter relation. Finally, we compare the results of completeness analyses derived from the regional dataset (Austria, the Vienna Basin including its extension into the Czech Republic and

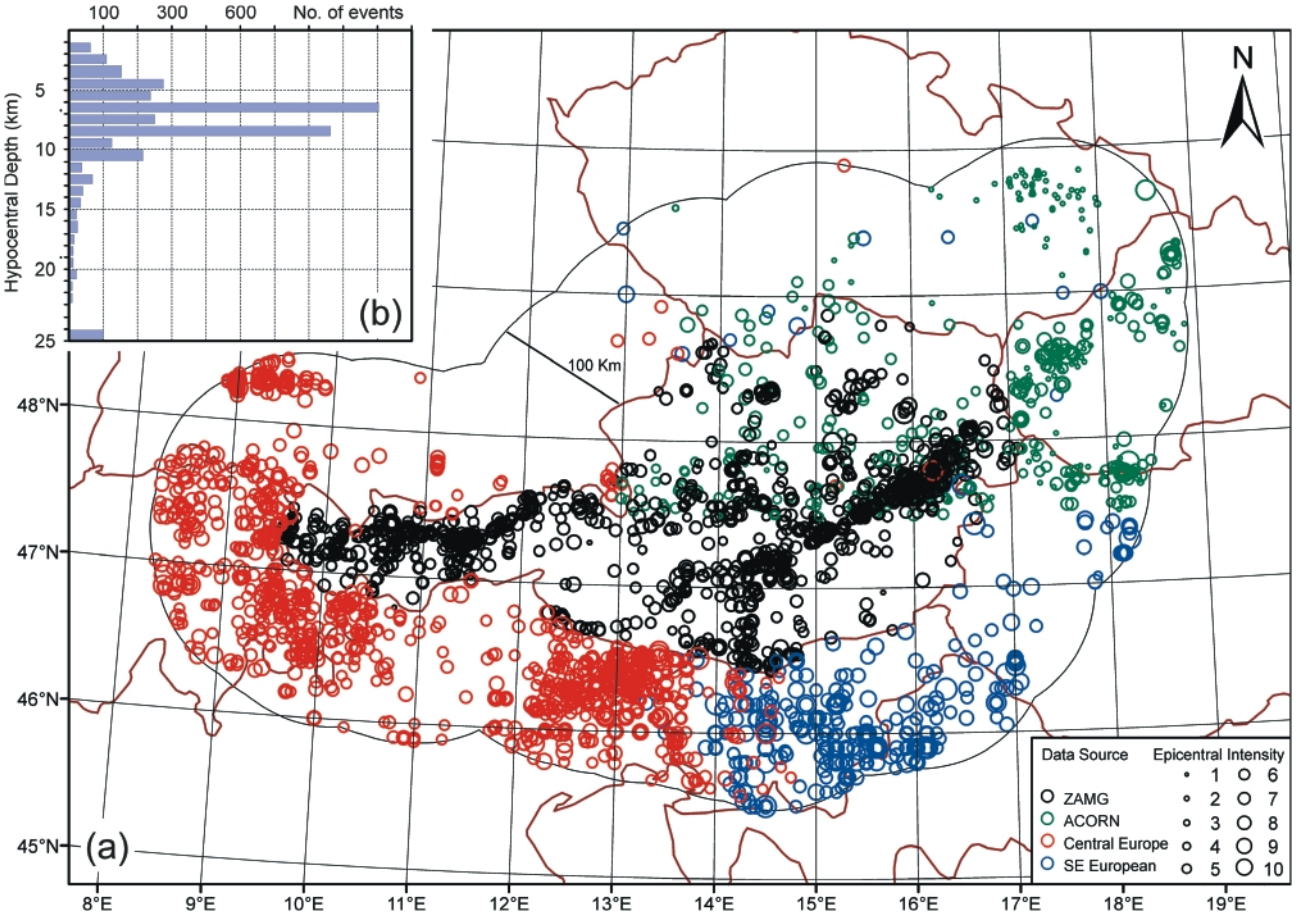

Figure 1: 1a. Compiled catalogue for Austria, the Vienna Basin and a 100 km wide region outside the boundaries of Austria and Vienna Basin (1048 -2009 AD). The intensity range is from II – X. Colours indicate the coverage of the different earthquake catalogues used for this study. (Black) ZAMG Catalogue of Felt Earthquakes (1201- 2009 AD). Data cover the area within the boundary of Austria. The intensity range is from III - IX (ZAMG, 2010); (Green) ACORN Earthquake Catalogue (1267 – 2004 AD) with an intensity range from II - VIII (Lenhardt et al., 2007); (Red) European Earthquake Catalogue for Austria and a 100 km buffer area outside the boundary of Austria (479BC - 1981 AD). The intensity range is from III - X (Van Gils and Leydecker, 1991). (Blue) Southeast European Earthquake Catalogue (342BC – 1990AD). The intensity range is from III – IX (Shebalin and Leydecker, 1998). 1b. Hypocentral depth of the region under consideration which is characterized by shallow seismicity with 90% of all events occurring in the upper crust at hypocenter depths above 12 km.

Slovakia, and a 100 km wide bounding region) to completeness analyses of a sub-sample of the region. The sub-sample has the size of a typical seismic source zone used in seismic hazard assessment and corresponds to a source zone, which may be defined for the active Vienna Basin Fault System.

2. Database: Composite earthquake catalogue

Seismicity in Austria and most of the surrounding areas is dominated by earthquakes of small to medium intensity. Earthquakes with intensities as low as I_0 =IV must be therefore taken into account for the assessment of the seismic potential and finally the seismic hazard of this region. Existing compilations of trans-national earthquake catalogues (Van Gils and Leydecker, 1991; Grünthal et al., 2009) do not meet these specific requirements. The CENEC catalogue (Grünthal et al., 2009) only lists earthquakes with Mw ≥ 3.5. Following the conversions from the originally given epicentral intensity (I_0) into moment magnitude (Mw) used by the authors, events with an epicentral intensity I_0 ≤IV-V would be associated with magnitudes in the range of 2.9 ≤ Mw ≤ 3.9, considering hypocentral depths down to 25 km (see Fig. 1b). Therefore, most events within this intensity class are eliminated in the CENEC catalogue. At this background it was decided to compile a new database, which includes all events recorded in the area of interest.

The composite catalogue used for further analyses includes Austria, a 100 km wide region beyond the national borders and the Vienna Basin Fault System in the Czech and Slovak Republic (Fig. 1a). It is compiled from four different catalogues (ZAMG, 2010; ACORN, 2004; Van Gils and Leydecker, 1991; Shebalin and Leydecker, 1998). In these catalogues the quality of entries for different areas and time periods varies significantly with respect to completeness, reliability of intensity/magnitude, homogeneity and location accuracy.

The ZAMG (2010) catalogue of felt earthquakes includes earthquakes within the national boundaries of Austria (black circles in Fig. 1a). This catalogue contains 2089 earthquakes covering the period from about 1000 until 2009 AD. The minimum intensity is III and maximum intensity is IX. This catalogue is the most complete available and includes results of careful systematic historical investigations (Hammerl et al., 2002; Hammerl, 2007). The events included in the composite earthquake catalogue within Austria are almost entirely based on the ZAMG catalogue.

The ACORN catalogue covers a rectangular region encompassing the Eastern Alps, West Carpathians and the Bohemian Massif (Czech Republic, Slovakia, Hungry and Austria; Lenhardt et al., 2007). The data set includes 1105 earthquakes from the time period between 1600 to 2004 AD. The compiled catalogue includes 607 events from ACORN, which are located in the area of interest outside of Austria (i.e., mainly the NE part of the Vienna Basin). The intensity range is from II to IX. Earthquakes from this catalogue are shown as green circles in Fig. 1a.

Earthquake data in the adjacent region of 100 km outside of the Austrian territory in Germany, Switzerland and Italy are taken from the catalogue for European countries (Van Gils and Leydecker., 1991). The catalogue is used regardless of its known inherent inaccuracies as no other suitable data be-

(a) Examples of duplicate removed from the composite earthquake catalogue

Year	Mon	Day	Hour	Min	Sec	Lat.	Long.	Z	M	I_0	Epicenter	Country	Catalogue
1979	5	1	23	32	0	47.26	11.53	6	2.90	5	Tulfes/Innsbruck	A	ZAMG
1979	5	2	0	32	0	47.20	11.55	6	2.90	5	Tyrol	A	European
1980	11	10	23	58	0	47.26	11.43	4	1.80	4	Innsbruck	A	ZAMG
1980	11	11	0	58	0	47.25	11.40	4	1.80	4	Tyrol	A	European
1981	4	12	23	18	47	47.79	16.35	4	1.80	4	Burgenland	A	ZAMG
1981	4	13	0	18	47	47.80	16.30	4	1.80	4	Burgenland	A	European

(b) Earthquakes on Austrian territory from Van Gils and Leydecker (1991)

1468	2	0	0	0	0	47.80	16.20	10	5.20	8	Lower Austria	A	European
1907	7	21	22	42	0	47.70	15.20	-	3.33	5	Styria	A	European
1917	11	2	22	5	0	47.30	11.50	-	3.33	5	Tyrol	A	European
1928	2	19	0	30	0	47.60	15.80	-	2.67	4	Styria	A	European
1945	12	25	21	25	0	47.20	11.40	-	3.33	5	Tyrol	A	European

Table 1: (a) Examples of duplicate earthquakes listed in the ZAMG earthquake catalogue and European earthquake catalogue. In the composite catalogue priority is given to the data provided by ZAMG. The grey shaded events have been removed from the composite catalogue. (b) Earthquakes on Austrian territory from the catalogue by Van Gils and Leydecker (1991). The events are considered in the completeness analysis.

came available. The database lists events for the years 479 BC - 1981 AD with intensities equal or higher than IV. The maximum intensity is X. In total, 1950 events were taken from this catalogue (red circles in Fig. 1a).

The earthquake catalogue for Central and Southeastern Europe (Shebalin and Leydecker, 1998) served as a base for compiling the seismicity in the 100 km bounding area around Austria in Slovenia, Croatia and Hungary. Seismic events from this catalogue are shown as blue circles in Fig. 1a. The catalogue covers the time period from 342 BC to 1990 AD. The compiled dataset includes 472 data from that catalogue with intensities between III and IX.

During the compilation of the regional dataset, the following priority has been given to the source data: ZAMG earthquake catalogue followed by the ACORN database, the European earthquake catalogue and the SE-European earthquake catalogue. Combining the listed earthquake catalogues resulted in some duplicate events, which have been removed manually. Events which are listed with same longitude, latitude and intensity but with a time difference of one hour in the ZAMG/ ACORN and European catalogues were also considered as duplicates and removed. Examples of such events are shown in Table 1a. In those cases, priority is given to the ZAMG and ACORN catalogues. From European and SE-European earthquake catalogues, five events have been taken for the Austrian territory, which are not listed in the ZAMG or ACORN catalogues (Tab. 1b).

The regional compilation for Austria, the Vienna Basin including its extension into the Czech Republic and Slovakia, and a 100 km wide bounding region resulted in a database of 5616 earthquakes with intensities between III to X between 1048 and 2009 AD. The distribution of seismicity and the temporal distribution of earthquake records according to the composite clustered catalogue are shown in Fig. 1a and 2, respectively.

3. Catalogue Declustering

The recognition and removal of fore- and aftershocks from the raw catalogue is a prerequisite for assessing catalogue completeness because of the general assumption that earthquakes are Poissonian-distributed and therefore independent of each other (e.g. Gardner and Knopoff, 1974; Shearer and Stark, 2011). Declustering removes dependent events such as foreshocks, aftershocks and swarm events except for the largest event in each swarm. Including these events in the database otherwise leads to major deviation from a Poissonian distribution (Gardner and Knopoff, 1974; Keilis-Borok et al., 1982; Molchan and Dmitrieva, 1992; Öncel and Alptekin, 1999).

The number of events removed by declustering is affected by the size of the main shock (Omori, 1900, Utsu et al., 1995). Typically, events that occur within a given time interval and a

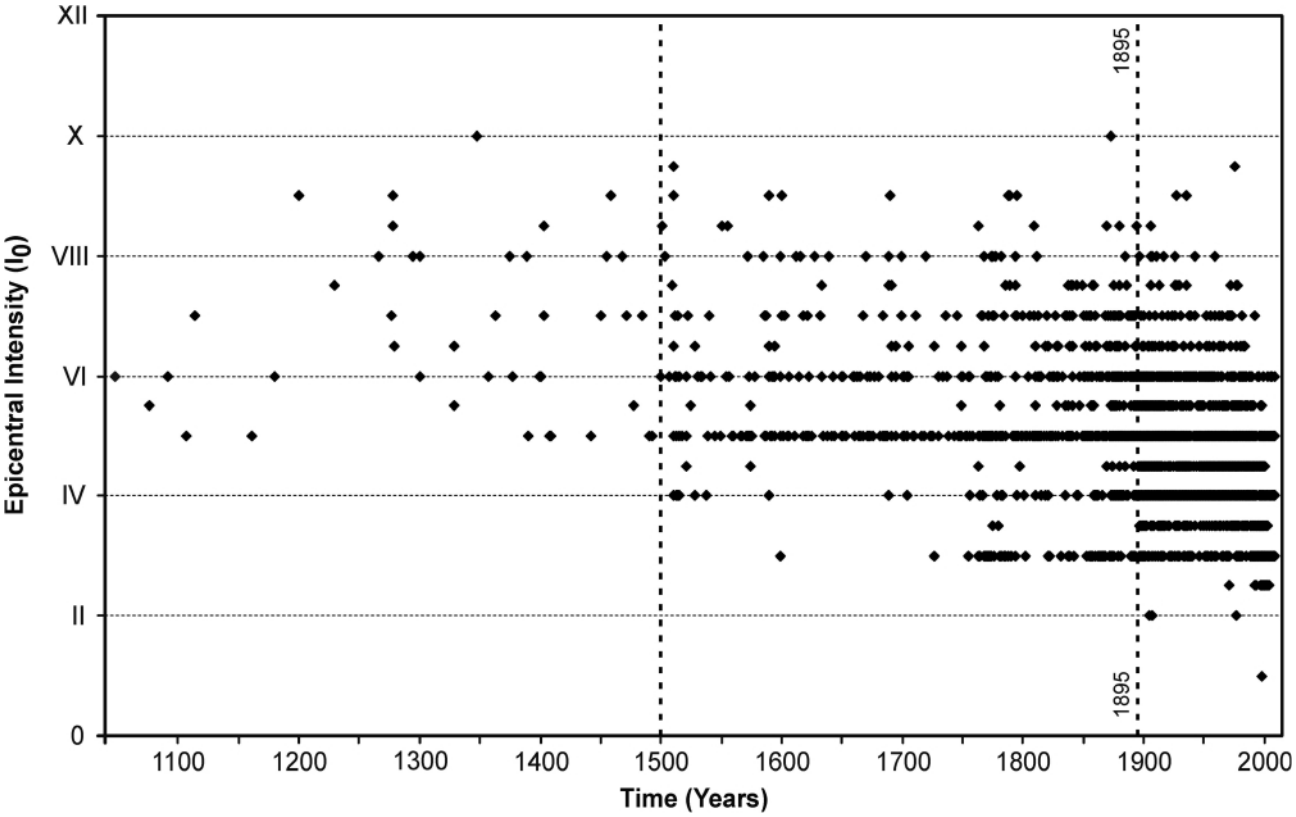

Figure 2: Intensity vs. time plot of the earthquakes listed in the clustered composite catalogue (1048 – 2009, Fig. 1a). Note the apparent increase of records around 1500, which is due to the increased number of historical chronicles available from that time onwards (Rohr, 2007, p. 118), and the major increase of earthquake records at about 1900 related to the start of systematic macroseismic data collection in the former Austro-Hungarian empire after the earthquake of Ljubljana (1895) and the installation of Wiechert seismographs (1903, 1905).

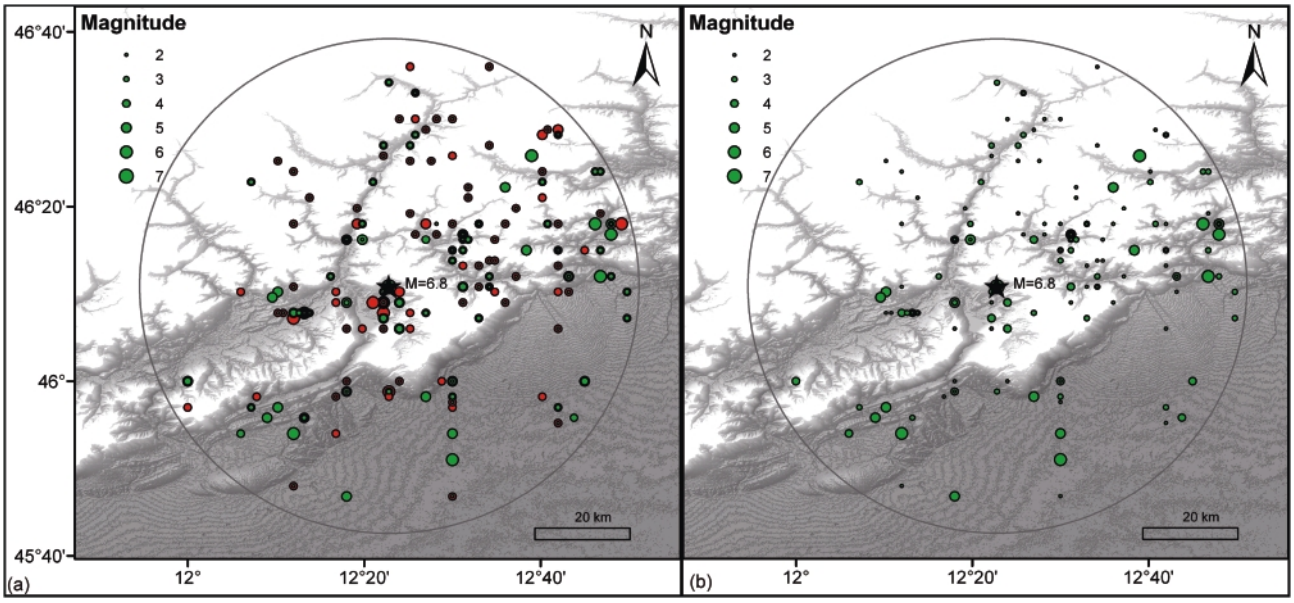

Figure 3: Determination of aftershocks of the 1873 Belluno M = 6.8 earthquake. The epicenter of the main shock is marked with star symbol. The largest distance of potential aftershocks from the mainshock is about 40 km (grey circle; see also Tab. 2). Background image is showing the DEM of the region. (a) Clustered catalogue. Aftershocks of the 1873 Belluno M = 6.8 earthquake are marked in red. (b) Declustered composite catalogue within the spatial window of the 1873 Belluno M = 6.8 main shock. The remaining events occurred outside the aftershock time window (see Fig. 4).

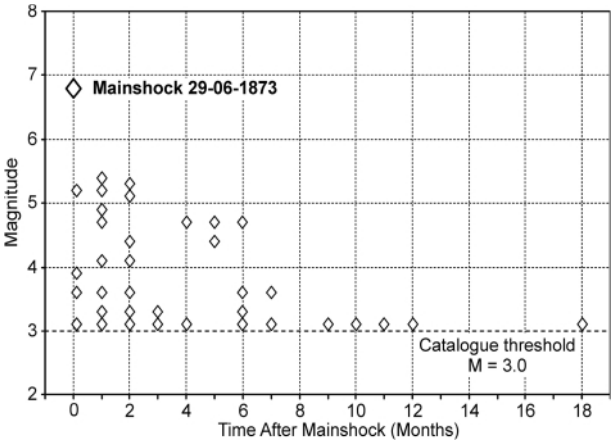

Figure 4: Aftershock sequence of the 1873 Belluno M = 6.8 main shock in the temporal window defined by the algorithm of Gardner and Knopoff (1969). The aftershock sequence of this earthquake lasted for about 18 months and includes 72 events.

Magnitude	Radius (km)	Time (days)
4.5	10	83
5.0	10	155
5.5	10	290
6.0	12	510
6.5	26	790
7.0	54	915

Table 2: Magnitude-dependent time (days after the main shock) and space windows (radius of a circle around the epicentre) used for the identification of aftershocks. Space windows follow the equation Log (Radial Distance in km) = (M - 4.32)/1.54 (Wells and Coppersmith, 1994) with a minimum radius set to 10 km. The duration of the time window is taken from Gardner and Knopoff (1969).

given distance of a larger event are regarded as dependent, where the time interval and distance vary with magnitude (Gibson and Brown, 1999). Fore- and aftershock identification in our study applies the spatial and temporal windows shown in Table 2. Both, the epicentral distance from the main shock and the time (days after/before main shock), are scaled according to the main shock moment magnitude taken from the corresponding original catalogue. The maximum epicentral distance of fore- and aftershocks from the main shock is derived from Wells and Coppersmith (1994). For historical events, the epicentral distance was increased by a factor of two in order to account for inaccurate epicenter locations. For the same reason, the minimum distance is fixed to 10 km, being the approximate hypocenter uncertainty for pre-instrumental earthquakes during the 20th century (Gangl and Decker, 2011). The duration of fore- and aftershock sequences is taken from Knopoff and Gardner (1969). All earthquakes within the defined spatial and temporal windows were identified as fore- and aftershocks and manually removed from the composite catalogue.

The 1873 Belluno earthquake (I_0 =X, M =6.8) is shown as an example of the declustering procedure. Fig. 3 shows the radial length of aftershock sequence from the main shock according to Table 2 (about 40 km for M =6.8), while the duration of the aftershock sequence of about 18 months is shown in Fig. 4. In total, 72 events have been identified as aftershocks including four events with VII< I_0 ≤VIII and seven earthquakes with VI< I_0 ≤VII (catalogue data from Van Gils and Leydecker, 1991). The analysis of the 1873 Belluno earthquake sequence further shows that its aftershock sequence accounts for about 20% of the seismicity recorded in the entire area. In total, 161 out of 373 earthquakes in this area have been identified as aftershocks of larger earthquakes, accounting for more than 40% of the recorded seismicity. This example demonstrates the

large influence of strong single events and their fore- and aftershocks on the seismicity of regions of low and moderate seismicity, and Austria in detail.

Manual declustering of the raw catalogue resulted in the removal of 1633 events with intensities between III and VIII. The declustered catalogue, cleaned of aftershocks and foreshocks, is used for completeness assessments of the regional seismicity parameters.

4. Assessing Catalogue Completeness

Two completeness analyses are performed on the composite and declustered catalogues in order to assess the differences resulting from both methodological approaches in terms of recurrence intervals and GR parameters. In order to avoid ambiguities arising from different intensity-magnitude conversions the following computations and comparisons are made for intensity. The use of intensity data in Gutenberg-Richter plots appears to be justified by the fact that the region under consideration is characterized by shallow seismicity with 90% of all events occurring in the upper crust at hypocenter depths above 12 km (Fig. 1b). Even if the depth determination for historical earthquakes might not be very accurate, the instrumentally recorded earthquakes show similar depth distribution and underscore our assumption.

4.1 Temporal course of earthquake frequency (TCEF)

TCEF is a common method applied in Central Europe to check the completeness of records for single intensity classes (e.g. Lenhardt, 1996). Data completeness levels are estimated from the earthquake catalogue using plots of the cumulative number of events of a certain intensity class versus time. Slope changes in the graphs indicate changes of the completeness of the catalogue. It is commonly assumed that the most recent change in slope occurs when the data became complete for each intensity class (Gasperini and Ferrari, 2000). Recurrence intervals are computed for the time interval corresponding to the linear segments of the curves, whose corresponding epicentral intensity data are considered complete.

Representation of the TCEF for single intensity classes in Austria and surrounding Central Europe is shown in Fig 5. Inspection of the curves shows significant increases of slopes for earthquakes with I_0<VII around 1900. This dramatically in-

TCEF Declustered Catalogue

I_0	T (years)	N	No
III < I_0 = IV	114	1357	21999
IV < I_0 = V	152	1178	10548
V < I_0 = VI	155	360	3093
VI < I_0 = VII	191	130	858
VII < I_0 = VIII	242	38	204
VIII< I_0 = IX	247	12	53
IX < I_0 = X	662	4	6

Table 3: Rate of earthquake occurrence for different intensity classes using the TCEF completeness check for the declustered composite catalogue. T: time period (completeness period) for which the catalogue is considered to be complete for an intensity class. N: number of recorded earthquakes of an intensity class within the completeness period T. No: cumulative number of earthquakes with intensities ≥ I_0 extrapolating the recurrence intervals derived for the completeness time period T to the total length of the catalogue (962 years between the first data entry and 2010).

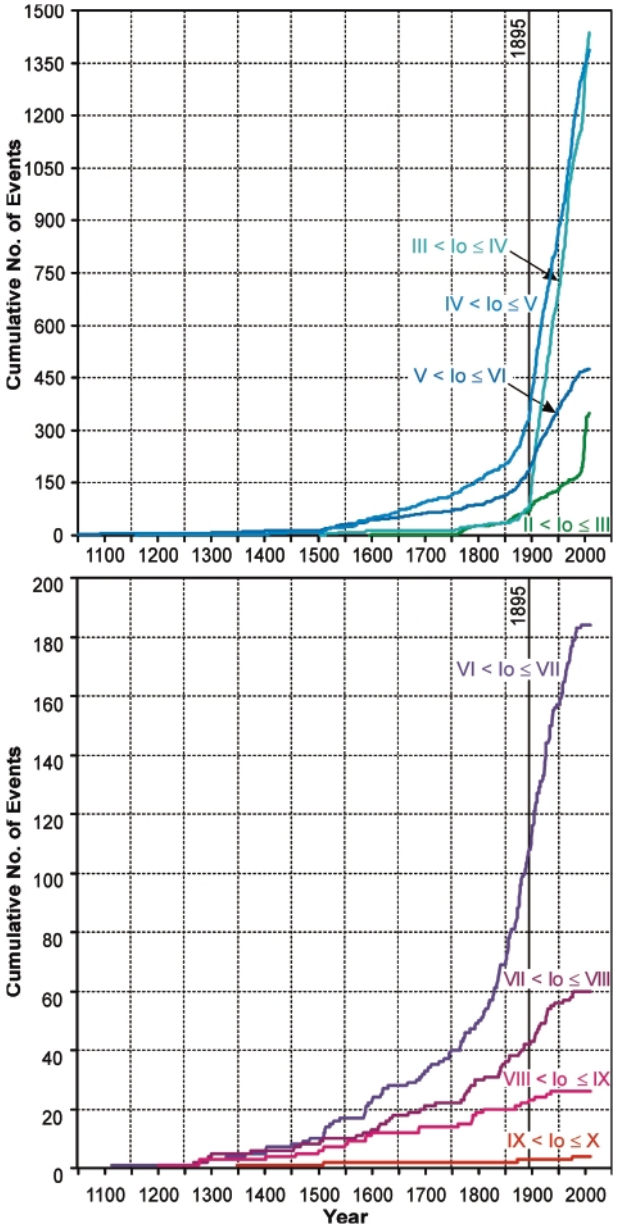

Figure 5: Temporal course of earthquake frequency (TCEF) for different intensity classes of the declustered composite catalogue. Recurrence intervals are computed for the time interval corresponding to the steepest slope of the curves. Note the significant increase of the record rate for events with I_0 = IV to VI subsequent to the earthquake of Ljubljana, 1895. Apparent plateaus of the graphs after 1990 are related to the different record lengths of the source catalogues. Note the different scales of cumulative event numbers on the upper and lower panel.

creased recording is related to the start of systematic macroseismic documentation in the former Austrian-Hungarian Empire after the earthquake of Laibach/Ljubljana in 1895 (I_0 =VIII-IX; Suess, 1887). The earthquake led to the appointment of a committee for seismology in 1895 (Erdbebenkommission der Kaiserlichen Akademie der Wissenschaften) and the installation of the first national seismographs in Pribram (1903) and Vienna (1905; Hammerl et al., 2001). Apparent plateaus of the curves in the last years, especially for smaller intensities, are related to the different recording lengths of the used catalogues. The earthquake recurrence intervals for different intensity classes are derived for the time interval of the graph showing the steepest slope (Table 3, Fig. 5). Results indicate that the time of complete records increases from 16 years for the intensity class II $<I_0 \leq$III to about 250 years for VIII $<I_0 \leq$IX. The slope of the graph for XI$< I_0 \leq$X is only defined by four single events giving rise to significant uncertainties for estimating the average recurrence interval of such events. Data of II $<I_0 \leq$III are not regarded complete even after TCEF correction, as the source catalogues have different threshold intensities and the ACORN catalogue is the only catalogue covering the II$< I_0 \leq$III intensity class.

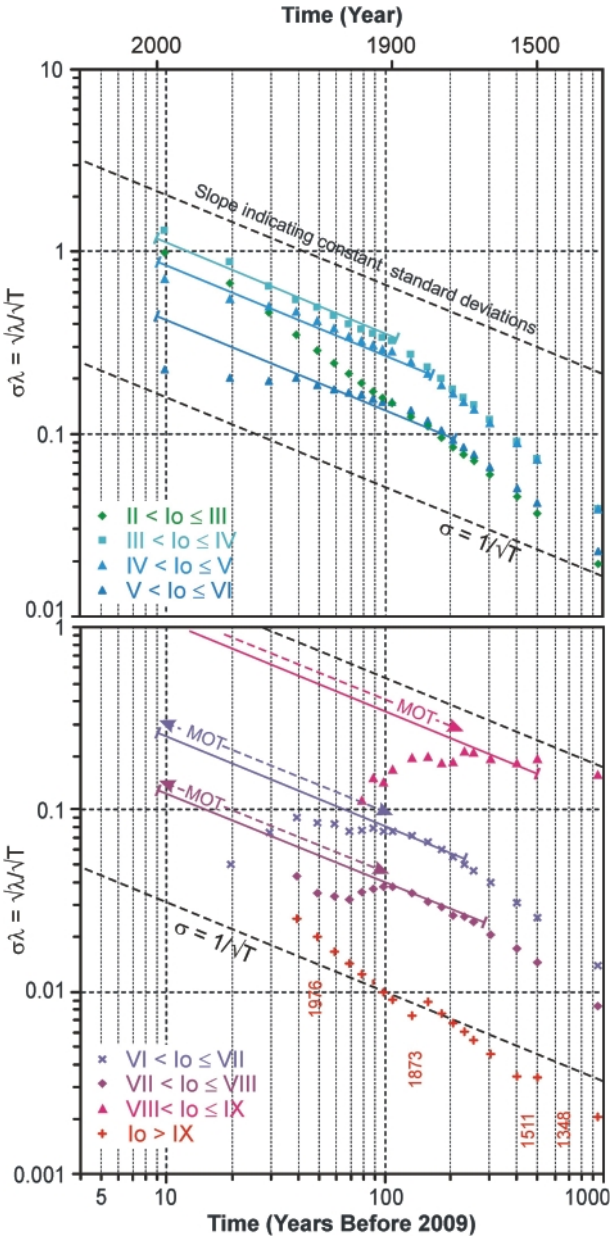

Figure 6: Completeness periods for different intensity classes determined by the method of Stepp (1972). The Stepp Test investigates the stability of the mean rate of occurrence (λ) of events in a series of time periods (T). If λ is constant, then the standard deviation (σ) varies as 1/√T, if λ is not stable, σ deviates from the straight line of the 1/√T slope. The length of the time interval at which no deviation from that straight line occurs defines the completeness period for the given intensity range. Dashed arrows in the lower diagram indicate the minimum observation time (MOT) required for deriving reliable average recurrence intervals for the intensity class indicating that ~100 years observation are required for VI $< I_0 \leq$ VIII and ~250 years for VIII $< I_0 \leq$ IX. For the intensity class $I_0 >$ IX only four events are reported (Friuli/"Villach", 1348; Slovenia, 1511; Belluno, 1873; Friuli, 1976). A completeness time period with stable σ cannot be determined for the intensity class I_0 = X.

4.2 Stepp (1972) completeness analysis (Stepp Test)

The Stepp Test (Stepp, 1972) has been used in numerous studies to obtain time intervals for which the recorded data is considered to be complete (Bollinger, 1973; Cuthbertson, 2006; Bus et al., 2009). The test relies on the statistical property of the Poisson distribution highlighting time intervals during which the recorded earthquake occurrence rate is uniform. Supposing that earthquake occurrences follow a Poisson distribution, the Stepp Test evaluates the stability of the mean rate of occurrences (λ) of events which fall in a predefined intensity range in a series of time windows (T). If λ is constant, then the standard deviation (σ) varies as 1/√T. On the contrary, if λ is not stable, σ deviates from the straight line of the 1/√T slope. The length of the time interval at which no deviation from that straight line occurs defines the completeness time interval for the given intensity range (Stepp, 1972; Fig. 6). This interval is visually determined from the plots. The test further evaluates the minimum observations length needed for establishing reliable average recurrence intervals for events of a certain intensity class (Fig. 6).

The completeness periods for various intensity classes of the declustered composite catalogue are analyzed for the time between 1048 (first data entry in the catalogue) and 2009 (962 years) using 21 time windows of different length (Fig. 6). Time windows were selected according to the number of earthquakes listed in the catalogue with 10 year time windows covering the period between 1900 and 2009. The time before 1900 is covered by windows of 25 years (1899–1750), 50 years (1749–1700), 100 years (1699–1500) and 452 years (1499–1048). The corresponding completeness time interval is estimated manually from the parts of the curves following the 1/√T slope as shown in Fig. 6. Table 4 summarizes the number of earthquakes of different intensity classes and corresponding completeness time intervals T of the declustered catalogue for I_0 = IV to IX. Completeness of records for the intensity class II $< I_0 \leq$III is not reached at any time. The results of the Stepp

Intensity	Clustered Catalogue			Declustered Catalogue		
I_0	T (years)	N	No	T (years)	N	No
III < I_0 = IV	1875-2009	1787	24790	1875-2009	1329	18666
IV < I_0 = V	1850-2009	1551	12056	1850-2009	1145	9196
V < I_0 = VI	1750-2009	523	2730	1775-2009	383	2312
VI < I_0 = VII	1700-2009	198	795	1775-2009	138	744
VII < I_0 = VIII	1500-2009	72	181	1750-2009	39	179
VIII< I_0 = IX	1600-2009	17	45	1600-2009	13	35
IX < I_0 = X	N/A	5	N/A	N/A	4	N/A

Table 4: Rate of earthquake occurrences for different intensity classes derived from the Stepp Tests of the clustered and declustered composite catalogue (Stepp, 1972). Note that declustering re-sults in significantly less events for smaller intensity classes. Intensity class IX < I_0 ≤ X is excluded since no completeness time period can be determined for this class. See text for more information. T: time period (completeness period) for which the catalogue is considered to be complete for an intensity class. N: number of recorded earthquakes of an intensity class within the completeness period T. No: cumulative number of earthquakes with intensities ≥ I_0 extrapolating the recurrence intervals derived for the completeness time period T to the total length of the catalogue (962 years between the first data entry and 2010).

Test further prove that the occurrence rate of the intensity class XI< I_0 ≤X is not stable for any time interval (Fig. 6) as the 962 years observation period is too short for constraining a stable average recurrence interval for the highest intensity class in the sample with reasonable accuracy.

5. Applying completeness analyses to a sub-region: the Vienna Basin

We applied the methodology described above to a sub-region in order to check whether the completeness time intervals derived for the whole catalogue are appropriate for sub-samples of the area or not. The evaluation is done for an area along the Vienna Basin Fault System (Decker et al., 2005; Beidinger and Decker, 2011), which could be defined as a source zone for seismic hazard assessment. The analyzed source zone is defined as that area where the active fault system separates into several fault splays, i.e. approximately between the cities of Gloggnitz (Austria) and Nove Mesto nad Váhom (Slovakia). The extent of the source zone as well as the local earthquake data for this source zone is shown in Fig 7. After declustering, the dataset comprises 707 earthquakes with epicentral intensities between II and IX occurring between 1468

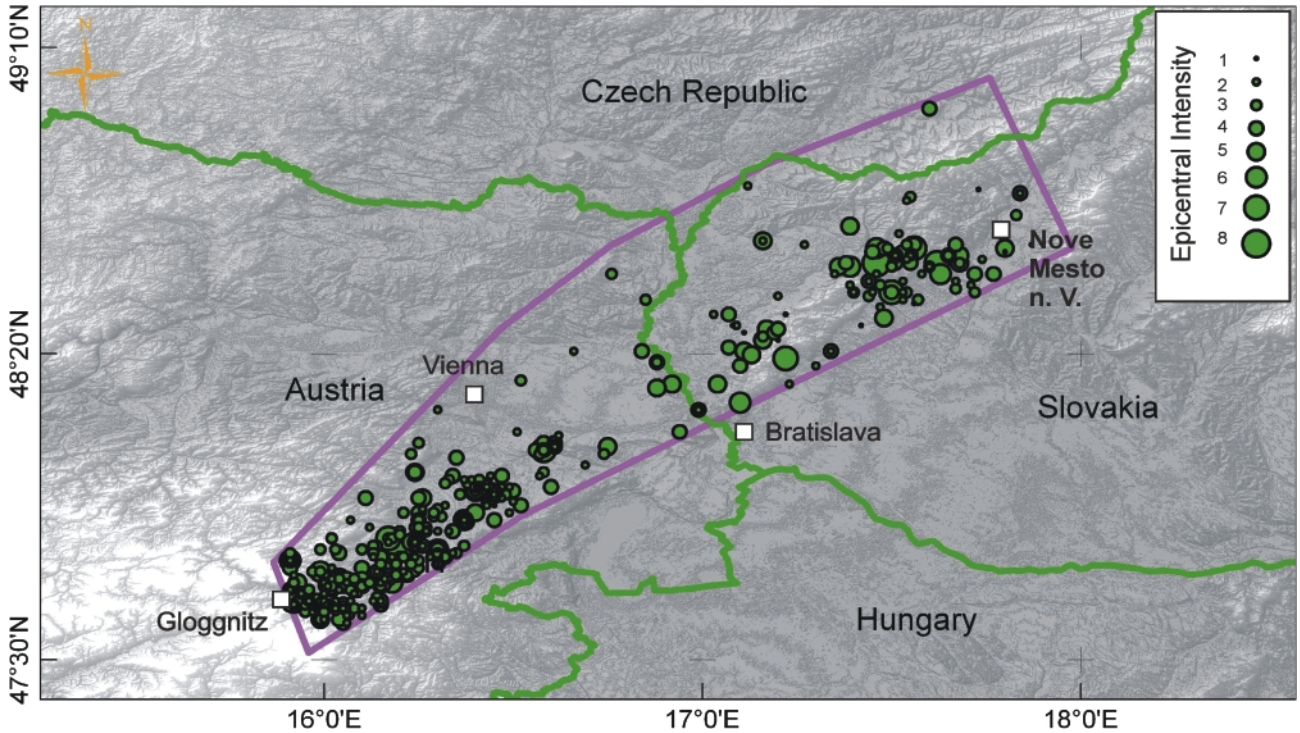

Figure 7: Seismicity recorded in the Vienna Basin source zone (Austria and Slovakia). The composite catalogue comprises 707 earthquakes with epicentral intensities II to IX in the time between 1468 and 2009 AD.

Intensity	Whole Region (Declustered Catalogue)			Vienna Basin Source Zone		
I_0	T (years)	N	No	T (years)	N	No
III < I_0 = IV	1896-2009	1357	21999	1923-2009	185	2061
IV < I_0 = V	1858-2009	1178	10548	1963-2009	65	922
V < I_0 = VI	1855-2009	360	3093	1952-2009	12	172
VI < I_0 = VII	1819-2009	130	858	1929-2009	6	61
VII < I_0 = VIII	1768-2009	38	204	1905-2009	4	21
VIII< I_0 = IX	1763-2009	12	53	1468-2009	1	1
IX < I_0 = X	1348-2009	4	6	N/A	N/A	N/A

Table 5: Earthquake occurrence rates for different intensity classes derived from TCEF completeness corrections. The table compares the completeness periods derived for the declustered composite catalogue of the whole region and the Vienna Basin source zone. Note that completeness periods for the Vienna Basin Source Zone are significantly shorter than those derived for the whole region. T: time period (completeness period) for which the catalogue is considered to be complete for an intensity class. N: number of recorded earthquakes of an intensity class within the completeness period T. No: cumulative number of earthquakes with intensities ≥ I_0 extrapolating the recurrence intervals derived for the completeness time period T to the total length of the catalogue between the first data entry and 2010 (962 years for the declustered composite catalogue and 542 years for the Vienna Basin source zone). There are no records of earthquakes with I ≥ IX for the Vienna Basin source zone.

and 2009. We consider this number of seismic events large enough for statistical analysis.

The analysis of the completeness time intervals for different intensity classes using the Stepp Test uses fourteen time windows of different lengths covering the period of 542 years between 1468 and 2009 (Fig. 8). The results indicate that different intensity classes are considered to be complete from the following years up to 2009: intensity classes III< I_0 ≤IV and IV< I_0 ≤V starting with 1900, V< I_0 ≤VI and VI <I_0 ≤VII from 1800 onwards, and finally, VII< I_0 ≤VIII for the complete time interval covered by the catalogue since 1468. Tables 5 and 6 compare the completeness time intervals obtained for the entire area with those obtained for the Vienna Basin source zone using TCEF and the Stepp Test. Data show that the completeness time intervals obtained for the subregion are significantly shorter than the estimates derived for the whole region. This result strongly suggests that completeness time intervals obtained for the sub-region are significantly shorter than those of the whole dataset.

TCEF analysis of the data from the Vienna Basin supports this interpretation. Time frequency curves show significant increases of slopes around 1900 for all intensity classes, but also several inconsistencies in the slopes after 1900 (Fig. 9). The graphs show that records of events up to intensity VI (eventually even up to VII) are not complete for the 20th century. This is well illustrated by the number of independently recorded earthquakes from the declustered catalogue for V< I_0 ≤VI showing 9 events in the period 1890-1914, only one record be-

Intensity	Whole Region (Declustered Catalogue)			Vienna Basin Source Zone		
I_0	Time(Years)	N	No	Time(Years)	N	No
III < I_0 = IV	1875-2009	1329	18666	1900-2009	246	1957
IV < I_0 = V	1850-2009	1145	9196	1900-2009	129	745
V < I_0 = VI	1775-2009	383	2312	1800-2009	29	110
VI < I_0 = VII	1775-2009	138	744	1800-2009	11	35
VII < I_0 = VIII	1750-2009	39	179	1468-2009	7	7
VIII< I_0 = IX	1600-2009	13	35	N/A	N/A	N/A
IX < I_0 = X	N/A	4	N/A	N/A	N/A	N/A

Table 6: Comparison of earthquake occurrence rates for each intensity class (e.g. IV < I ≤ V) between the declustered composite catalogue of the whole region and the Vienna Basin source zone following the completeness method of Stepp (1972). T: time period (completeness period) for which the catalogue is considered to be complete for an intensity class. N: number of recorded earthquakes of an intensity class within the completeness period T. No: cumulative number of earthquakes with intensities ≥ I0 extrapolating the recurrence intervals derived for the completeness time period T to the total length of the catalogue between the first data entry and 2010 (962 years for the declustered composite catalogue and 542 years for the Vienna Basin source zone). There are no records of earthquakes with I_0 ≥ IX for the Vienna Basin source zone. Intensity class IX < I0 ≤ X is excluded for the declustered composite catalogue since no completeness time period can be determined for this class. For more information see text.

tween 1915 and 1952, and 12 recorded events in the period 1953-2009. These changes of the apparent earthquake frequency are not imaged by the Stepp Test. We interpret the fluctuations as a result of an incomplete earthquake record rather than as a consequence of changing seismicity.

The conspicuously low number of earthquake records in the time between about 1920 and 1950 is apparently related to the contemporary social, economic and political situation, which is characterized by the decline of the Austrian-Hungarian Empire in 1918, the subsequent economical crisis and Austrian civil war, and World War II. Such circumstances distracted attention from earthquakes and led to malfunction of the previously established macroseismic reporting system that was based on the imperial administration. Also, the seismographs at ZAMG in Vienna, located in the centre of the analyzed source zone, were destroyed by war action in 1944 and not operational until 1951 (Hammerl et al., 2001). We therefore conclude that earthquake records from this time period are not complete since the "lower seismicity" period coincides with the time of dysfunctional recording system.

6. Discussion and Comparison of results

The results of catalogue declustering and the application of different completeness analyses to the entire study area show significant differences in the estimated seismicity parameters such as the mean annual rate of seismic activity, the resulting intensity-frequency relation coefficients (a- and b-values in Gutenberg-Richter relation) and the completeness level of the seismic data, above which the earthquake catalogue is considered to be complete at a certain time. The GR a- and b-values obtained from the datasets after declustering and different completeness analyses are summarized in Table 7 and Fig 10. Even if we know that GR- relations based on clustered and uncorrected data is meaningless in a strict sense, we computed it here to demonstrate the effect of declustering and the different completeness methods._

Declustering of the data has only a minor impact on the estimated seismicity parameters leaving the b-values unchanged but reducing the a-value for about 0.1 to 0.2 (Fig. 10, Table 7). The clustered catalogue therefore tends to overestimate the number of earthquakes of higher intensities. The observed effect is due to the fact that declustering removes a large number of small intensity aftershocks from the time period after about 1900. However, for the centuries before about 1900, declustering also removes a significant number of high-intensity aftershocks (aftershocks with small intensity are hardly docu-

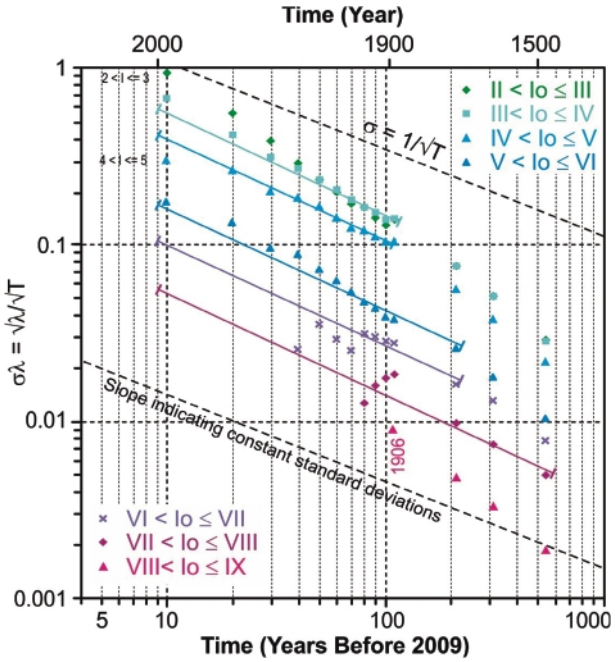

Figure 8: Stepp plots for earthquakes of different intensity classes recorded in the Vienna Basin source zone. The length of the time interval at which no deviation of σ from the straight line $1/\sqrt{T}$ occurs defines the completeness period for the given intensity class. For the intensity class I_o > VIII, only one event is reported (Dobra Voda 1906, I_o = IX).

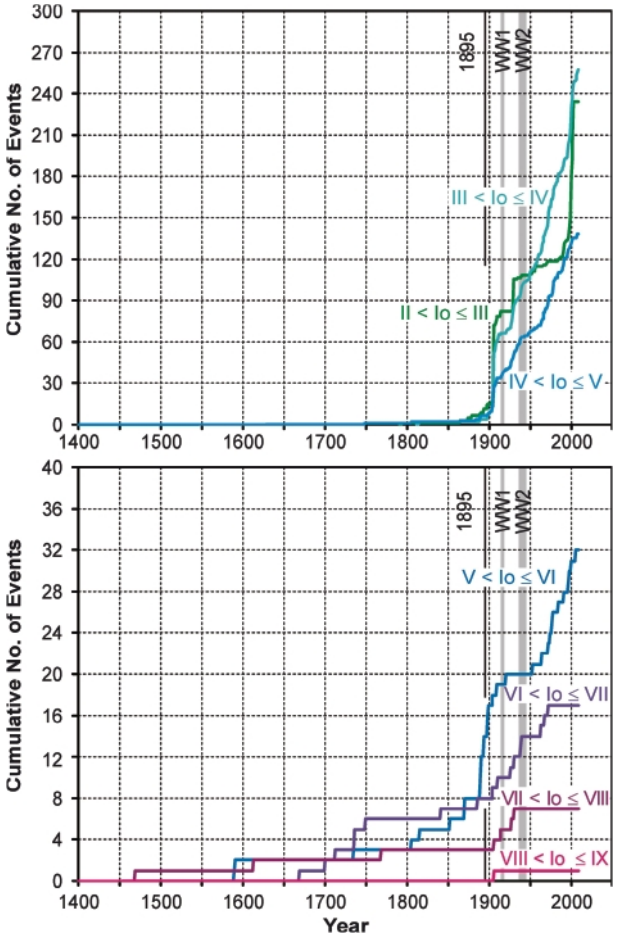

Figure 9: Temporal course of earthquake frequency (TCEF) for single intensity classes for the Vienna Basin source zone. Time intervals with the steepest slope of the curves regarded as periods with complete earthquake records of a certain intensity class. Note the prominent plateaus of the curves between about 1914 and 1950 for the intensity classes III < I_0 ≤ VI indicative for incomplete earthquake records in the time between and shortly after World War I and II. The strong increase of records of earthquakes with I_0 ≥ II is due to the implementation of a network of digital seismic stations in Austria in 1991. Note the different scales of cumulative event numbers on the upper and lower panel.

mented for that time).

When comparing correction procedures, slightly lower a- and b-values of the GR-relation corrected with the Stepp Test is caused by the fact that the highest intensity class (IX< I_0 ≤X) has been excluded from the computation of the GR-relation. Correcting completeness time periods following Stepp (1972) shows that the observation time of about 1000 years is too short to obtain reliable average recurrence intervals for this intensity class. The Stepp Test not only provides completeness time intervals, but also gives insights how many earthquakes have to be observed in order to derive reliable average recurrence intervals for a certain intensity/magnitude class. According to Stepp (1972) minimum time intervals that cover at least 5 to 15 mean return periods are required for reaching stable estimates of mean recurrence intervals. Having observed fewer earthquakes (as in the composite catalogue), the occurrence rates tend to be underestimated. Including, however, IX< I_0 ≤X data in the estimation of seismicity parameters after performing the TCEF-correction results in a slight overestimation of the number of events for lower intensities and an underestimation of larger events. The b-values of the GR-relations after using TCEF and Stepp Test differ by 0.04.

Catalogue / Correction Method	GR-parameters	
	a-value	b-value
Clustered CC uncorrected	2.84	0.49
Declustered CC uncorrected	2.70	0.48
Declustered CC TCEF Correction	3.94	0.59
Declustered CC Stepp Test Correction	3.64	0.55

Table 7: Gutenberg-Richter parameters (GR-parameters) to the clustered and declustered composite catalogues (CC = composite catalogue) and after applying different completeness corrections (TCEF and Stepp Test) on declustered composite catalogue, While the a-values vary significantly between the different applications, b-values seem to be influenced rather by the choosen completeness correction method than by declustering. Intensity I_0 = X is not included in corrections based on the Stepp Test as no completeness time period was determined for this class.

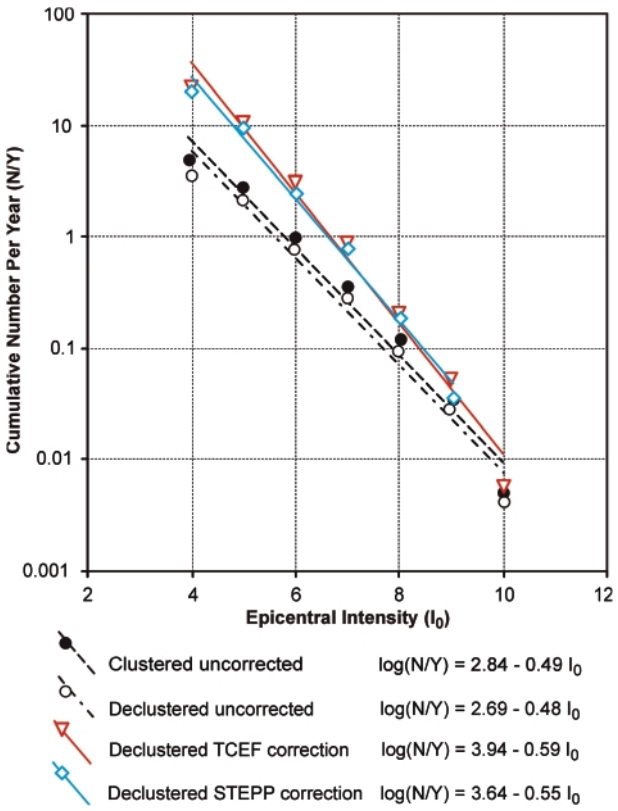

Figure 10: Comparison of Gutenberg-Richter plots derived from the raw composite catalogue (black solid dots) and the different corrections applied to the catalogue (declustering, TCEF completeness correction of the declusterd catalogue, Stepp Tests completeness correction of the declustered catalogue). Declustering of the data has only a minor effect on the a-value. Completeness corrections generally result in higher a- and b-values (compare Tab. 7). G-R regressions for the Stepp Tests do not include intensity class I_0 = X as the test shows that historical observation periods are too short for establishing reliable recurrence intervals. See text for further discussion.

Comparing the results of the composite catalogue with the composite catalogue for the Vienna Basin (Tables 5 and 6), there are two points that attract attention: Firstly, the time periods where the sub-catalogue is considered complete for most of the intensity classes are much shorter for the Vienna Basin than for the whole region. Considering that the Vienna Basin source zone is not the most active region in Austria, the shorter completeness time intervals for the Vienna Basin can also be explained by larger recurrence intervals of earthquakes with larger intensities. For example, the interevent times for intensity class VI< I_0 ≤VII are about 10 times larger for the Vienna Basin than for the whole region, therefore missing 1 event out of 7 per century (as for the Vienna Basin) affects the completeness tests more than missing 1 event out of 68 per century (as for the whole region). On the other hand, the obvious plateau during the 20th century within the cumulative number of events for the Vienna Basin (Fig. 9), shows that the earthquake record for this region is far from being complete. Even though this may only have a low impact on the average occurrence rates for the whole region, this result strongly suggests that completeness assessment of the whole dataset overestimates data completeness significantly. It therefore seems not advisable to use the completeness time intervals obtained from the whole region for single sub-regions without any additional completeness analysis. This is not obvious in many currently valid hazard assessments checking completeness from the whole area and extrapolating to seismic source zones.

7. Conclusions

Analyzing the completeness of earthquake catalogues is a necessary prerequisite for a seismic hazard assessment. We determined the completeness of a composite catalogue for Austria and the surrounding region following the TCEF as well as the method described by Stepp (1972). Comparison of both methods leads us to prefer the latter, because it also provides information on the minimum observation time required to de-

rive reliable recurrence intervals for events of a certain intensity class. As most of the catalogue's record is pre-instrumental, those completeness analyses were performed on intensity data avoiding ambiguities arising from intensity-magnitude conversion. The main difference between the TCEF and the Stepp Test is that TCEF includes also the highest intensity class because of the assumption of the TCEF that all earthquakes of the highest intensity class have been observed during the length of the catalogue. Accordingly, this intensity class is considered as complete and used in the GR calculation. GR calculation based on the Stepp Test does not consider this intensity class due to the lack of sufficiently long observation periods.

The resultant GR-relations show that:

1) Declustering has only minor effects on the a- and b-value of the GR relation.
2) Completeness analyses have large effects on lower intensity classes, which result in more realistic b-values for the whole region and lead to longer recurrence periods for most of the large events,
3) Including the highest intensity class (($IX< I_0 \leq X$ for the whole dataset,$VIII< I_0 \leq IX$ for the Vienna Basin subregion), as done using the TCEF completeness analysis, underestimates the frequency of earthquakes of higher intensities.
4) The Stepp Test seems to be more reliable regarding for assessing recurrence periods and the frequencies of strong earthquakes with high intensities.

We have shown that earthquake records in Austria and the surrounding region cover the critical minimum observation period for all intensity classes except for $IX< I_0$. Stable estimates of mean recurrence periods are derived from the following completeness time intervals: $III< I_0 \leq IV$: 1875–2009; $IV< I_0 \leq V$: 1850-2009; $V< I_0 \leq VI$: 1775-2009; $VI< I_0 \leq VII$: 1775-2009; $VII< I_0 \leq VIII$: 1750-2009; $VIII< I_0 \leq IX$: 1600-2009. Both methods, the Stepp Test and TCEF, reveal completeness time intervals. The Stepp Test, however, indicates that the catalogue length of 962 years is not sufficiently long to reach a stable estimate of the mean occurrence rate of earthquakes with epicentral intensites $IX< I_0$.

Analysis of the sub-catalogue for the Vienna Basin source zone leads to recurrence intervals that are about 10 times higher than those obtained for the whole region. The completeness time intervals for the sub-catalogue revealed from both, TCEF and Stepp Test, are much shorter than those obtained for the whole catalogue. Careful examination of the data by the TCEF method shows that data up to intensity $VI< I_0 \leq VII$ are not complete even for the 20th century. This incomplete record, which we associate on the historical evolution between WWI and WWII, is not recovered by the Stepp Test.

Comparison of the completeness time intervals derived for the whole dataset and the Vienna Basin source zone leads us to conclude that completeness time intervals estimated from a larger region generally overestimate the completeness time intervals of sub-regions.

References

ACORN, 2004. Catalogue of Earthquakes in the Region of the Alps - Western Carpathians – Bohemian Massif for the period from 1267 to 2004. Computer File, Vienna (Central Institute for Meteorology and Geodynamics, Department of Geophysics) – Brno (Institute of Physics of the Earth, University Brno.

Beidinger, A. and Decker, K, 2011. 3D geometry and kinematics of the Lassee flower structure: Implications for segmentation and seismotectonics of the Vienna Basin strike-slip fault, Austria. Tectonophysics, 499, 22-40.

Bollinger, G. A., 1973. Seismicity of the southeastern United States. Bulletin of the Seismological Society of America, 63, 1758-1808.

Bus, Z., Grenerczy, G., Toth, L., Monus, P., 2009. Active crustal deformation in two seismogenic zones of the Pannonian region - GPS versus seismologial observations. Tectonophysics, 474, 343-352.

Cuthbertson, R. J., 2006. Automatic calculation of seismicity rate in eastern Queensland. Australian Earthqake Engineering Society, 2006 Conference proceedings, 137-144.

Decker, K. Peresson, H. and Hinsch, R., 2005. Active tectonics and Quaternary basin formation along the Vienna Basin Transform fault. Quaternary Science Reviews, 24, 307-322.

Gangl, G. and Decker, K., 2011. Compilation of strong Austrian earthquakes with intensities higher than 7. Österreichische Ingenieur- und Architekten-Zeitschrift, 156, 229-237.

Gardner, J. K. and Knopoff, L., 1974. Is the sequence of earthquakes in Southern California, with aftershocks removed, poissonian? Bulletin of the Seismological Society of America, 64/5, 1363-1367.

Gasperini, P. and Ferrari, G., 2000. Deriving numerical estimates from descriptive information: the computation of earthquake parameters. In Catalogue of Strong Italian Earthquakes from 461 B.C. to 1997, Annali di Geofisica, Vol. 43, N.4, 729-746.

Gibson, G. and Brown, A., 1999. Earthquake clusters, small earthquakes and their treatment for hazard estimation. Australian Earthquake Engineering Society Annual Conference Sydney, Australia, RMIT University, Melbourne Seismology Research Centre, Bundoora. http://www.aees.org.au/Proceedings/1999_Papers/18_Gibson_Brown.pdf

Grünthal, G., Mayer-Rosa, D. and Lenhardt, W., 1998. Abschätzung der Erdbebengefährdung für die D-A-CH-Staaten - Deutschland, Österreich, Schweiz. Bautechnik, 75/10: 753-767.

Grünthal, G. and GSHAP Region 3 Working Group, 1999. Seismic hazard assessment for central, north and northwest Europe: GSHAP Region 3. Annali di Geofisicia 42, 999-1011.

Grünthal, G., Wahlström, R. and Stromeyer, D., 2009. The unified catalogue of earthquakes in central, northern, and north-

western Europe (CENEC) - updated and expanded to the last millennium. Journal of Seismology, 13, 517-541.

Gutdeutsch, R. and Hammerl, C., 1997. Über die Aufzeichnungsschwelle historischer Beben. Mitteilungen der Deutschen Physikalischen Gesellschaft, 2, 2-9.

Gutdeutsch, R. and Hammerl, C., 1999. An uncertainity parameter of historical earthquakes. The record threshold of historical earthquakes. Journal of Seismology, 3, 351-362.

Hammerl, C., Lenhardt, W., Steinacker, R. and Steinhauser, P., 2001. Die Zentralanstalt für Meteorologie und Geodynamik 1851– 2001. 150 Jahre Meteorologie und Geophysik in Österreich, 838 pp.

Hammerl, C. and Lenhardt, W., 2002. Historical earthquakes in Styria/Austria. Source investigation - Revision of the catalogue. Proceedings of the XXVIII ESC General Assembly, Genoa, Italy, 1-6 September 2002, p.133.

Hammerl, C., 2007. Die khirchen dermassen zerschmetert und zerlittert, das man nit darein darf…" – Historische Erdbebenforschung in Niederösterreich. Studien und Forschungen aus dem Niederösterreichischen Institut für Landeskunde, 46, 21-44.

Keilis-Borok, V. I., Knopoff, L. and Rotwain, I.M., 1982. Burst of aftershocks, long term precursors of strong earthquakes. Nature, 283, 259–263.

Knopoff, L. and Gardner, J. K., 1969. Homogeneous catalogs of earthquakes, Proceedings of the National Academy of Sciences, 63, 1051-1054.

Lenhardt, W., 1996. Erdbebenkennwerte zur Berechnung der Talsperren Österreichs. Bundesministerium für Land- und Forstwirtschaft, Österreichische Staubeckenkommission (Wien 1996).

Lenhardt, W., Svancara, J., Melichar, P., Pazdirkova, J., Havir, J. and Sykorova, Y., 2007. Seismic activity of the Alpine-Carpathian-Bohemian massif region with regard to geological and potential field data. Geologica Carpathica, 58, 397-412.

Molchan, G. M. and Dmitrieva, O. E., 1992. Aftershocks identification: Methods and new approaches. Bulletin of the Seismological Society of America, 109, 501–516.

Mulgharia, F., Gasperini, P., and Tinti, S., 1987. A procedure to identify objectively active seismotectonic structures. Bolletino di Geofisica teorica ed applicata, 29 (114), 147-164.

Öncel, A. O. and Alptekin, Ö., 1999. Effect of Aftershocks on earthquake hazard estimation: An Example from the North Anatolian fault zone. Natural Hazards, 19, 1–11.

Omori, F., 1900. Investigation of aftershocks. Report Imperial Earthquake Investigation Committee, 30, 4–29.

Rohr, C., 2007. Extreme Naturereignisse im Ostalpenraum. Naturerfahrung im Spätmittelalter und am Beginn der Neuzeit. Wien (Böhlau Verlag), 640 pp.

Shebalin, N. V. and Leydecker, G., 1998. Earthquake catalogue for Central and Southeastern Europe 342 BC - 1990 AD. European Commission, Report No. ETNU CT 93 - 0087, Brussels.

Shearer, P. M. and Stark, P. B., 2011. Global risk of big earthquakes has not recently increased. Proceedings of the National Academy of Sciences, 109, 717 - 721.

Stepp, J. C., 1972. Analysis of completeness of earthquake sample in the Puget Sound area and its effect on statistical estimates of earthquake hazard. National Oceanic and Atmospheric Administration Environmental Research Laboratories, Boulder Colorado, 80302.

Suess, F. E., 1887. Das Erdbeben von Laibach am 14. April 1895. Jahrbuch der k.k. geologischen Reichsanstalt 1896, 412-614.

Stucci, M., Albini, P., Mirto, C. and Rebez, A., 2004. Assessing the completeness of Italian earthquake data. Annals of Geophysics, 47, 659-673.

Utsu, T., Ogata, Y. and Matsu'ura, 1995. The centenary of the Omori formula for a decay law of aftershock activity. Journal of Physics of the Earth, 43, 1-33.

Van Gils, J. M. and Leydecker, G., 1991. Catalogue of European earthquakes with intensities higher than 4. Commission of the European Communities - Nuclear Science and Technology. 14 fig., 1 tab.- ISBN 92-826-2506-0, Catalogue number: CD-NA-13406-EN-C. Brussels - Luxembourg 1991, pp.353.

Wells, D. L. and Coppersmith, K. J., 1994. New empirical relationships among magnitude, rupture length, rupture width, rupture area, and surface displacement. Bulletin of the Seismological Society of America, 84, 974-1002.

Woessner, J. and Wiemer, S., 2005. Assessing the quality of earthquake catalogues: Estimating the magnitude of completeness and its uncertainity. Bulletin of the Seismological Society of America, 95, 684-698.

ZAMG, 2010. Earthquake catalogue of felt earthquakes 1200 – 2009 A.D. (Austria). Computer File. Central Institute of Meteorology and Geodynamics (ZAMG), Vienna, Austria.

Received: 24 February 2013
Accepted: 22 April 2013

Asma NASIR[1)*)], Wolfgang LENHARDT[2)], Esther HINTERSBERGER[1)] & Kurt DECKER[1)]

[1)] Department of Geodynamics and Sedimentology, Center for Earth Sciences, University Vienna, Althanstrasse 14, A-1090 Vienna, Austria;

[2)] Department of Geophysics, Zentralanstalt für Meteorologie und Geodynamik, Hohe Warte 38, A-1190 Vienna, Austria;

[*)] Corresponding author, asma.nasir@univie.ac.at

Appendix 2

Nasir, A., Hintersberger, E., & Decker, K., **2020**. The Dobrá Voda earthquake (M=5.7) at the Vienna Basin Transfer fault: evaluation of the ESI2007 intensity and analysis of aftershock sequence. Austria Journal of Earth Sciences,113/1, 43-58.

sciendo
Austrian Journal of Earth Sciences | Vienna | 2020 | Volume 113/1 | 43 - 58 | DOI: 10.17738/ajes.2020.0003

The 1906 Dobrá Voda Earthquake (M=5.7) at the Vienna Basin Transfer Fault: evaluation of the ESI2007 intensity and analysis of the aftershock sequence

Asma NASIR[(1)], Esther HINTERSBERGER[(2)], Kurt DECKER[(1)]

[(1)]Department of Geodynamics and Sedimentology, Center of Earth Sciences, University of Vienna, Althanstrasse 14,A- 1090 Vienna, Austria;

[(2)]Geological Survey of Austria (GBA), Neulinggasse 38, A-1030 Vienna, Austria;

*) Corresponding Author, asma.nasir@univie.ac.at

KEYWORDS 1906 Dobrá Voda earthquake; Vienna Basin; aftershock; environmental intensity

Abstract

Aftershock identification plays an important role in the assessment and characterization of large earthquakes. Especially, the length of the aftershock sequence is an important aspect of declustering earthquake catalogues and therefore impacts the frequency of earthquakes in a certain region, which is important for future seismic hazard assessment. However, in intraplate regions with low deformation rates and low to moderate seismicity, it is still questionable if aftershocks after a major event may continue for much longer time. In this study, we use one of the earliest instrumentally recorded earthquakes, the 1906 Dobrá Voda earthquake (Ms/I_{max}=5.7/VIII-IX), to compare different approaches of aftershock determination and their suitability for understanding the recorded earthquake sequence. The Dobrá Voda segment of the Vienna Basin Transfer Fault System is one of the seismically most active zones in Slovakia with the 1906 earthquake as the strongest recorded earthquake. We first assess the epicentral intensity of the earthquake according to the Environmental Intensity Scale (ESI2007) using contemporary descriptions of earthquake effects. This additional information leads to constrain the maximal intensity to IESI2007=IX. This result agrees well with first the assessment of Imax in 1907 and indicates the reliability of this intensity data. In the second step, earthquake data are plotted for two spatial windows extending 13 km and 26 km from the epicenter of the mainshock, respectively. Despite uncertainties regarding the completeness of data due to war times and lack of nearby seismic stations, the overall temporal evolution of seismicity can apparently not be described as an Omori-type aftershock sequence following the event in 1906. Instead, earthquake occurrence within 13 km of the mainshock shows elevated earthquake activity right after the 1906 event that only decays to a lower level of activity within decades after the mainshock. The decline of seismicity therefore occurs over time scales which are much longer than those predicted by the Omori relation. We conclude that today's seismic activity may still be affected by the 1906 earthquake.

1 Introduction

1.1 Background and objectives

The 1906 Dobrá Voda (M/I_{max}= 5.7/VIII-IX) earthquake is the strongest historically recorded earthquake along the Vienna Basin Transfer Fault System. It occurred in the border region between Austria, Slovakia, and Czech Republic during the transition from the macroseismic/historical recording of seismic events to instrumental recording (Réthly, 1907) (Fig. 1). The installation of seismographs and the systematic recording of macroseismic observations in the former Austro-Hungarian Empire were initiated after the 1895 Ljubljana/Laibach earthquake (Süss, 1897). The 1906 Dobrá Voda earthquake and its numerous aftershocks therefore received much scientific attention (Réthly, 1907; Kárnik, 1968; Zsíros, 2005) and instrumentally recorded earthquakes are available covering the aftermath of the mainshock until today (ACORN, 2004; Fojtikova et al., 2010).

Large earthquakes are typically followed by aftershock activity that decays hyperbolically with time after the mainshock, following the empirical Omori's Law (Ogata, 1983). The end of the aftershock activity is difficult to identify precisely, because its definition depends on several parameters, such as the area treated as the aftershock zone and the level of background seismicity before the mainshock (Stein and Liu, 2009). Therefore, one common and practical way of automatic aftershock detection is the usage of temporal and spatial windows with the window length and size depending on the magnitude of the mainshock (e.g. Gardner and Knopoff, 1974; Wells and Coppersmith, 1994). However, in diffuse plate boundaries such as the North American Basin-and-Range, or in intraplate regions with low to moderate seismicity distributed over a wide area such as Central Europe or China outside the Tibetan Plateau, the question has risen whether aftershock sequences can continue for a much longer time than predicted by the above-mentioned methods (Stein and Liu, 2009). The ongoing seismicity in the Dobrá Voda area therefore raises the question whether earthquakes today may still be related to the 1906 Dobrá Voda earthquake or if the recent seismicity observed

within the region corresponds to a level that can be interpreted as 'normal' background seismicity.

Basic information about the 1906 Dobrá Voda earthquake and its aftershocks has been obtained from the ACORN catalogue (ACORN, 2004). In addition to the catalogue data, detailed contemporaneous documentation of the damages caused by the 1906 earthquake is available that includes descriptions of earthquake effects on the natural environment (Réthly, 1907). We use these descriptions to determine the macroseismic intensities based on the Environmental Seismicity Intensity (ESI) scale (Michetti et al., 2007).

Our scope in this study is two-fold: 1) By incorporating environmental effects of the earthquake, we check if this additional information changes the assessment of the Imax (Maximum Intensity), and the assigned intensity for the Dobrá Voda earthquake. 2) By investigating the seismicity on the Dobrá Voda segment for the past 150 years, we explore whether the observed seismicity today could be still be related to the 1906 earthquake, or merely reflects background seismicity. To achieve this, we also consider how the number of recorded earthquakes is related to the development of the seismic network in the area.

1.2 Seismotectonic Setting of the Vienna Basin

The Vienna Basin Transfer Fault System (VBTF) is a seismically active sinistral fault between the Eastern Alps, the Western Carpathians and the Pannonian Basin (Fig. 1). Active seismogenic deformation along the fault is indicated by moderate historical and instrumentally recorded seismicity in a NE-striking zone paralleling the fault between the Alps (Mur-Mürz Fault System) and the Vienna Basin in Austria, and the Malé Karpaty Mountains (Little Carpathians) and Váh Valley in Slovakia (e.g., Lenhardt et al., 2007; Hammerl and Lenhardt, 2013). The hypocentre depths of the recorded earthquakes are generally between 3 and 12 km. The earliest earthquake reported from the Vienna Basin occurred in 1283 (Wiener Neustadt, I_0=V; Hammerl and Lenhardt, 2013). Moderate to relatively high seismicity occurs in the southern Vienna Basin (including the 1927 Schwadorf earthquake M/I_0= 5.2/VIII) and the Dobrá Voda segment at the northern end of the Vienna Basin (1906 Dobrá Voda earthquake). In contrast, no significant earthquakes have been observed in the central Vienna Basin in the last four centuries (Hinsch and Decker, 2003; 2011). Comparison of seismic slip calculated from seismic moment summation shows significant differences between the segments of the VBTF. Seismic slip of more than 0.7 mm/a at the seismically most active segments (Schwadorf and Dobrá Voda fault segments) contrasts with slip rates close to zero at the Lassee fault (Hinsch and Decker, 2003, 2008; Bus et al., 2009). All segments, however, show marked slip deficits for the last century when comparing seismic slip rates with geodetic data and geologically derived slip rates of about 1–2 mm/a (Decker et al., 2005; Grenerczy, 2002; Grenerczy et al., 2000).

1.3 The Dobrá Voda segment

The Dobrá Voda segment is one of the seismically most active zones in Slovakia (Fig. 1). It is located at the transition zone between the Vienna Basin and the Western Carpathians (Šefara et al., 1998; Lenhardt et al., 2007), specifically, at the Brezovské Karpaty Mountains north of the Malé Karpaty Mountains. The dominant structures of the area are ENE–WSW trending faults forming a transpressional ridge. This segment of the VBTF is interpreted as a restraining bend (Hinsch and Decker, 2011). The sinistral Brezová fault zone forms the northern margin of the Brezová elevation, while its southern border with the Dobrá Voda depression is represented by the distinctive sinistral Dobrá Voda fault zone (Marko et al., 1991). The faults separate the uplifted Mesozoic Brezová Block from Early Miocene molasses sediments to the N and S. located between two sinistral fault zones, the Brezová Block has been interpreted as a positive flower structure, which formed at the VBTF during the Miocene (Marko et al., 1991; Beidinger and Decker, 2011). Convergent sinistral strike-slip faulting along the fault segment is confirmed by fault plane mechanisms (Fojtikova et al., 2010). The predominant focal mechanisms of the small earthquakes (M=1.2-3.4) are compatible with oblique-reverse left lateral strike slip on WSW-ENE striking faults (Fojtikova et al., 2010). This data is consistent with the interpretation that earthquakes occur along the ENE-WSW trending restraining bend.

The orientation of the present-day tectonic stress calculated from focal mechanisms and other stress measurements in the Western Carpathians region and adjacent areas are summarized in the world stress map (Müller et al., 1992; Heidbach et al., 2008). The area lies in the transition zone between the Western Carpathians and the eastern Alps and is characterized a complicated stress pattern (Drimmel and Trapp, 1982; Jarosinski, 1998; Reinecker, 2000; Kováč et al., 2002; Jarosinski, 2005). The mapped maximum horizontal compression in the Dobrá Voda area has an azimuth of 30-40 °NE and lies along the strike of the Male Karpaty Mts. (Fojtikova et al. 2010).

2 Data

2.1 Seismicity data

Information about the mainshock and all reported aftershocks of the Dobrá Voda 1906 earthquake are listed in the ACORN catalogue. The ACORN catalogue contains events with I_0= II-IX, covering a rectangular area between 47.5° and 49.8° in latitude and 13.0° to 19.0° in longitude in the Czech Republic, Slovakia, Hungary, and Austria encompassing the Eastern Alps, Western Carpathians and the Bohemian Massif (Lenhardt et al., 2007). The data set includes 1968 earthquakes from the time between 1267 AD and 2004 AD. The "observation threshold" for earthquake data, i.e., the minimum magnitude/epicentral intensity for inclusion in the ACORN catalogue is M/I_0=2.5/III. Near the village of Dobrá Voda, the oldest earthquake listed in the catalogue is from 1515 (M/I_0= 5/VII). The oldest known

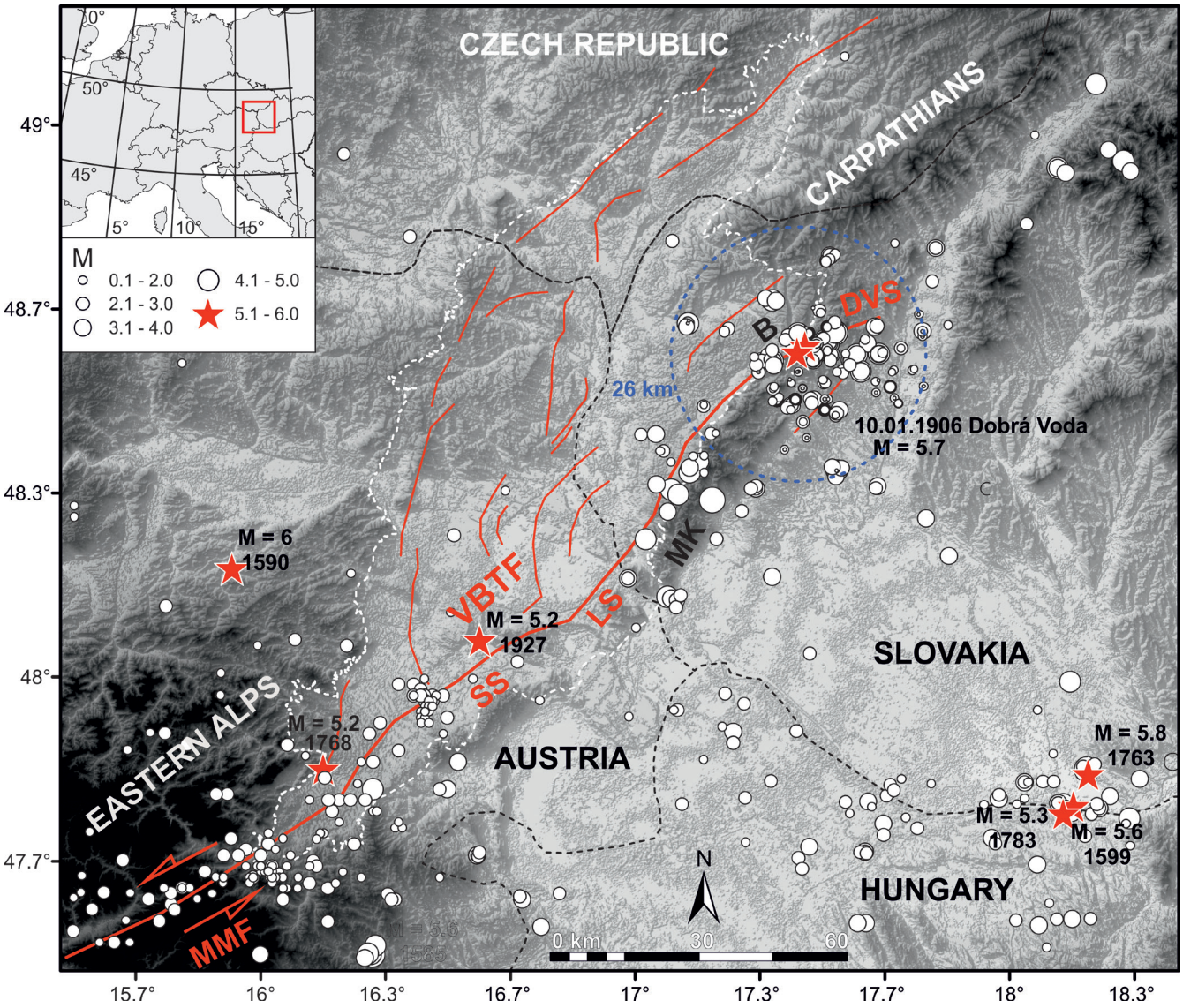

Fig. 1: Tectonic setting and earthquake scattered plot covering areas in Czech Republic, Slovakia, Hungary, and Austria (ACORN, 2004). Black stars show earthquakes with magnitudes larger than 5, red star indicates the location of the Dobrá Voda Earthquake. Blue circle marks the 26 km radius from the 16.01.1906 Dobrá Voda mainshock. Inset shows the location of the figure in Europe. MMF (Mur-Mürz-Fault); VBTF (Vienna Basin Transfer Fault); Fault segments of the VBTF: SS (Schwadorf); LS (Lassee) DVS (Dobrá Voda); MK (Male Karpaty mountains); B (Brezovské Karpaty mountains).

earthquakes along the VBTF occurred in 1267 (Kindberg/Styria, M/I_0=5.4/VIII) and 1283 (Wiener Neustadt, I_0=V; ACORN catalogue, 2004; Hammerl and Lenhardt, 2002).

The installation of the first seismographs in the former Austro-Hungarian empire commenced at the turn from the 19th to the 20th century as a consequence of the earthquake of Ljubljana (Hammerl and Lenhardt, 2013). The first seismographic station of the territory of Slovakia has been installed in 1902. However, until the early 1990's, only a few seismic stations existed in the area of interest (Lenhardt et al., 2007). The further development includes the first digital seismological station, which is in operation since 1990, and the modernisation of the network 2001-2004 (Csicskay et al., 2018). Today, the local seismic activity around the Dobrá Voda area is monitored by MKnet seismic network, installed in 1985, the Slovak National Seismic Network (Cipciar et al., 2002), and a micro displacement monitoring network (Briestenský et al., 2007).

2.2 Documentation of the 1906 Dobrá Voda earthquake

The main resource for the documentation of the 1906 Dobrá Voda earthquake and resulting damages is a report by the Hungarian seismologist Réthly (1907). The damage to buildings and the reactions of the population to the earthquake was described in detail for 180 locations and used for assessment of the local intensities and epicentral intensity. Réthly (1907) used the 12-degree extended Forel-Mercalli intensity scale (Cancani, 1904) for his assessment, which is broadly comparable to the successional intensity scales including the European Macroseismic Scale (EMS-98, see Musson et al., 2010 for a detailed discussion). Réthly's (1907) I=IX isoseismal includes 12 intensity data points and about 390 km^2. Réthly (1907, p. 60) further noted that the long axis of the I=IX isoseismal is oriented WSW-ENE (Fig. 2), which is parallel to the strike of the Dobrá Voda segment of the VBTF mapped by Beidinger and Decker (2011).

The description of the earthquake effects of the mainshock on 10.01.1906 and the largest aftershock on 16.01.1906 include also effects on the natural environment, clearly distinguishing between both earthquakes (Réthly, 1907). The environmental effects of the mainshock included temporary changes in well water level, drying out of springs and wells, changes in water chemistry and temperature, and the generation of new springs. Detailed description these occurrences are given in Tab. 1. In addition, mostly temporal effects on well water and sulphuric enrichment of spring waters were observed for the largest aftershock on 16.01.1906.

Recent EMS-based catalogues list the epicentral intensity of the Dobrá Voda mainshock as I_0=VIII-IX (Grünthal et al., 2009; ACORN, 2004; Zsíros, 2005). Re-assessment based on intensity datapoints and isoseismals lead to focal depth estimates between 2.8 km and 6.7 km (Zsíros, 2005). For precision the strongest aftershock, Réthly (1907) notes a maximum intensity of I_0= IX as well, although this intensity was only assessed at two locations. ACORN (2004) and Grünthal et al. (2009) assess the strongest aftershock with I_0=VII-VIII ("I=7.5"). As one of the first instrumentally recorded earthquakes in the Austrian-Hungarian Empire, the magnitude of the Dobrá Voda earthquake was obtained from instrumentally recorded surface-waves. The resulting surface-wave magnitude of Ms = 5.7 (Réthly, 1907; Kárník, 1968; ACORN, 2004) corresponds to a moment magnitude Mw=5.8 according to the empirical conversions by Scordilis (2006) and Kadirioglu and Kartal (2016).

3 Assessment of the epicentral intensity based on the ESI

3.1 Contemporary description of relevant secondary earthquake effects

Macroseismic intensity data points of Forel-Mercalli as well as for the EMS-98 are derived from effects of humans, objects and damage to buildings (Grünthal et al., 1998). The Environmental Seismic Intensity (ESI) scale (Michetti et al., 2007), however, focuses on environmental effects to determine intensity levels. The ESI is designed so that the intensity determined from natural effects matches the intensity derived from macroseismic observations as described in the EMS-98 (Grünthal, 1998). Here, we evaluate the descriptions of environmental effects provided by Réthly (1907) using the ESI scale for the mainshock and the strongest aftershock on 16.01.1906, and then compare the resultant intensity levels with intensity data points derived using the macroseismic Forel-Mercalli intensity scale (Fig. 2). The documented changes in hydrological conditions are important parameters for the ESI 2007 intensity evaluation.

For the mainshock on 10.01.1906, reported hydrologic anomalies include variations of spring discharge, well water levels, water turbidity, changes of water temperature, and sulphurous emissions (Tab. 1). Especially the abundance of the effects at Cerová can be assessed from the description *"all but two wells fell dry"* (Tab. 1, Fig. 2). In addition, the generation of a permanent sulphur spring is mentioned from the village Hradiste pod Vratnom. For the remaining villages, the hydrological effects are widespread, but mostly of temporal nature (Mühlmann et al., 2012).

In the Hungarian language part of the damage report, Réthly (1907) describes surface cracks that opened in the epicentral area. However, he visited the area only after the 16.01.1906 aftershock, so the features that he describes might also have been caused by the later earthquake, and not by the mainshock. One location is extensively documented by photographs. It was interpreted as being probably caused by water-saturated soil at the inclined surface that started to slide during the earthquake (Réthly, 1907). The cracks were thought to be caused by "the roughness of the subsurface". One crack is described as 33 m long with a 140 cm high scarp, an opening of 130-140 cm width and a depth of 80-110 cm. Another crack close by was 14 m long, 40 cm wide and showed a height difference from 60 cm up to 110 cm. Localized up to 3 m wide cracks were observed at several more places. In addition, local landslides were triggered by ground shaking near the village of Dobrá Voda. The total area affected by such effects is about 250 km^2 (Tab. 2a, Fig. 2). Records of environmental effects for the aftershock on 16.01.1906 are restricted to four intensity datapoints (Tab. 1, Fig. 2b) with reports from Jablonica indicating the severest effects. The total area from which hydrological effects were reported is about 80 km^2 (Tab. 2, Fig. 2b).

3.2 Interpretation of secondary earthquake effects

The size and length of the cracks described by Réthly (1907) and their occurrence in water-saturated soil helps identify them as typical secondary earthquake effects. The application of the ESI 2007 to the macroseismic report (Réthly, 1907) uses hydrological anomalies and slope movements, which are described in sufficient detail to allow assessing local intensities for five locations for the mainshock (10.01.1906) and four intensity data points for the aftershock on 16.01.1906 (Tab. 1). The locations from which secondary effects were reported define a minimum area of about 250 km^2 supporting IESI-2007=VIII-IX (Tab. 2). Tab. 1 shows that most of the reported effects refer to hydrological anomalies, all of them being indicative for ESI intensity ≥VII. Descriptions of turbid waters in wells in the villages of Bucovec and Trstín indicate that the effect was *"common"* at these sites leading to an assessment of IESI=IX (Tab. 2). For Cerová, *"all except two"* wells ran dry, including one well which remained dry until March 1906 possibly indicating a local intensity IESI-2007=X. The formation of a sulphur spring in Hradiste pod Vratnom also indicates a significant environmental impact of the earthquake. However, an intensity value cannot be assessed as the descriptions of the ESI 2007 intensities only refer to springs running dry and not to the formation of new springs.

For the aftershock on 16.01.1906, hydrologic anomalies were recorded from four locations leading to assessments

Location	Lat	Long	Intensity Forel-Mercalli	Intensity ESI 2007	Original German description by Réthly (1907)	English translation
Precursory effects						
Vrbové/ Verbó/	48.622	17.724			*„Am 8.1. in der Früh war in dem 24 m tiefen Brunnen der staatlichen Schule kein Wasser, Nachmittags um 14 Uhr war schon wieder ein bisschen trübes Wasser, während gegen 17 h der Brunnen wie gewohnt mit Wasser gefüllt war."*	*"In the morning of January, 8th, there was no water in the 24 m deep well of the school, at 2 pm there was some muddy water, and at 5 pm, the well was filled again with clear water as normal."*
Mainshock 10.01.1906						
Dobrá Voda/ Jókeö	48.599	17.541	IX	VII-IX	*„Die Blava-Quelle nahm eine rote Trübung an und klärte sich erst 4 h später. An zwei Stellen in der Umgebung von Jókeö gab es Erdrutschungen, z.B. südwestlich an einem Hang des Brezover Gebirges."* Etwa 2400 m² große *„Schichten-rutschung* … auf sanft ansteigender Lehne am Fusse des Kopec" nahe Dobra Voda auf wassergesättigtem Boden mit mehreren Spalten, 80200 cm tief, 33 m lang, 60 - 110 cm Höhenunterschied.	*"Water of the Blava spring turned turbid red and cleared only 4 hours later. Landslides occurred at two locations near Jókeö, e.g., to the SW at a slope of the Breva Mountains."* c. 2400 m² large slide in water saturated soil near Dobra Voda with cracks 80-200 cm deep, 33 m long and 60-110 cm difference of elevation
Hradiste pod Vratnom/ Hradist	48.626	17.487	IX	?	*"Nach dem Erdbeben entstand eine Schwefelquelle."* Diese liegt ca. 5-6 km vom angenommenen Epizentrum entfernt.	*"A sulfur spring formed after the earthquake"* at a distance of about 5-6 km from the assumed epicenter.
Bucovec/ Bukov	48.700	17.496	VIII	IX	*„Das Brunnenwasser wurde trüb."*	*"Well water became turbid."* Wording suggests that the effect applied to the wells in the village in general indicting that it occurred commonly.
Trstín / Nádas	48.527	17.463	IX	IX	*„Das Brunnenwasser wurde trüb."*	*"Well water became turbid."* Wording suggests that the effect applied to the wells in the village in general indicting that it occurred commonly.
Dechtice / Dejte	48.547	17.594		≥VII	*„Starkes Brausen, eine Schwefelquelle floss 2-3 Tage lang reichlicher."*	*"Laud booming, discharge of a sulfur spring increased for 2-3 days."*
Cerová/ Czerova	48.586	17.379	IX	X	*„Alle Brunnen bis auf 2 waren ausgetrocknet."* *„Das Wasser der Brunnen im Jagdschloss verschwindet völlig und taucht erst im März wieder auf."*	*"All wells but 2 fell dry."* *"Water of the well in the hunting castle disappeared, the well remained dry until March."*
Aftershock 16.01.1906						
Dobrá Voda/ Jókeö	48.599	17.541	-	VIII-IX	*"In der Blava Quelle hob sich der Wasserstand um 6 cm. Die schwächste der drei Abzweigungen, die mittlere, war sehr ergiebig. Nach dem Erdbeben war das sonst klare Wasser rostfarben und sehr heiß, 5 Tage später war es wieder normal."*	*"The water level of the Blava Increased by 6 cm. The smallest outflowing channel (the one in the middle) showed high discharge. The outflowing water was very hot, normal conditions re-established after 5 days."*
Jablonica / Jablonic	48.830	17.421	-	IX	*„Das Brunnenwasser der gesamten Umgebung war getrübt."*	*"Well water of the entire surroundings was turbid."*
Hradiste pod Vratnom / Hradist	48.626	17.487	-	≥VII	*„Der Schwefelgehalt der Quelle stieg an."*	*"The sulfur content of the spring increased."*
Bukovec / Bukóc	48.700	17.496	-	VIII-IX	*„In vielen Brunnen versiegte das Wasser."*	*"Many wells fell dry."*

Tab. 1: Contemporary descriptions of environmental effects of the 1906 Dobrá Voda / Jókeö earthquake and its strongest aftershock from Réthly (1907). Location names are given in Slovak and Hungarian language. Forel-Mercalli intensity taken from Réthly (1907). See text and Table 2 for explanation and discussion of assigned ESI 2007 intensities.

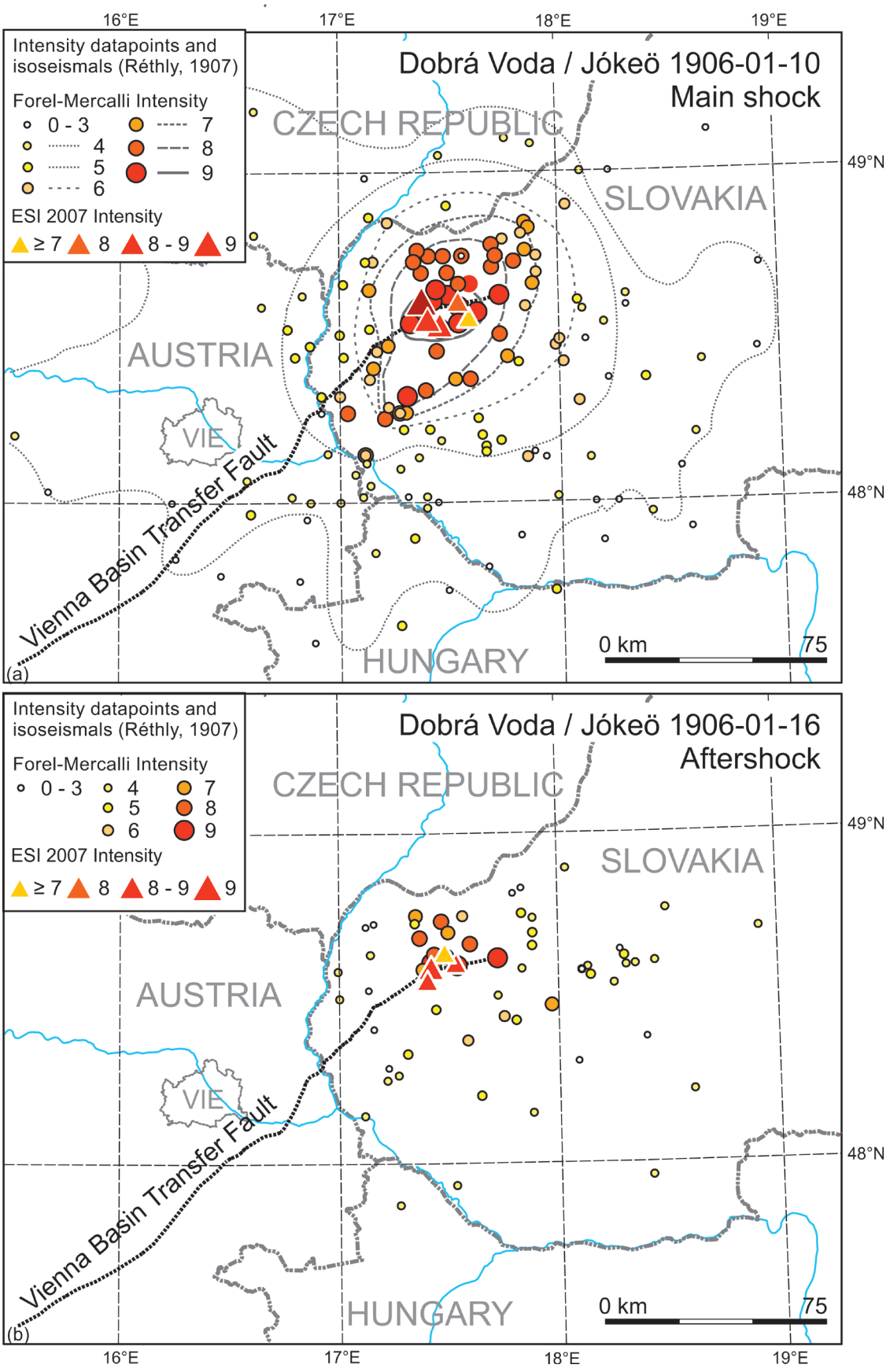

Fig. 2: Map of intensity data points for the 10.01.1906 Dobrá Voda mainshock (a) and the 16.01.1906 aftershock (b). Intensity values related to the 12-part Forel-Mercalli scale (Cancani, 1904, taken from Réthly, 1907) and to the ESI scale (Michetti et al., 2007). Original isoseismic contour lines from Réthly (1907) are included as thin black lines for reference. The felt area for the mainshock in panel (a) is almost 30.000 km². International borders are shown as dashed grey lines.

IESI	Description	Hydrological anomalies	Ground cracks	Slope movement	Area (km^2)
VII	Damaging	Significant temporary variations of the water level in wells and/or of the flow-rate of springs are locally recorded. Seldom, small springs may temporarily run dry or appear. Weak variations of chemical-physical properties of water and turbidity in lakes, springs and wells are locally observed.	Fractures up to 5-10 cm wide and up to hundred metres long are observed, commonly in loose alluvial deposits and/or saturated soils; rarely, in dry sand, sand-clay, and clay soil fractures are also seen, up to 1 cm wide.	Scattered landslides occur in prone areas, where equilibrium is unstable (steep slopes of loose / saturated soils)…	10
VIII	Heavily damaging	**Springs** may change, generally **temporarily**, their flow-rate and/or elevation of outcrop. Some small springs may even run dry. Variations in water level are **observed** in wells. **Weak variations** of chemical-physical properties of water, most commonly temperature, may be observed… Water turbidity **may appear**… Gas emissions, often sulphureous, are **locally observed**.	Fractures **up to 50 cm wide** and **up to hundreds metres long**, are **commonly** observed in loose alluvial deposits and/or saturated soils; in rare cases fractures up to 1 cm can be observed in competent dry rocks. Decimetric cracks arecommon in paved (asphalt or stone) roads, as well as small pressure undulations.	Small to moderate (10^3 - 10^5 m^3) landslides are **widespread** in prone areas; rarely they can occur also on gentle slopes; where equilibrium is unstable (steep slopes of loose / saturated soils; rock falls on steep gorges, coastal cliffs) their size is sometimes large (10^5 - 10^6 m^3).	100
IX	Destructive	**Springs** can change, generally **temporarily**, their flow-rate and/or location to a considerable extent. Some **modest** springs may even run dry. Temporary variations of water level are **commonly observed** in wells. **Variations** of chemical-physical properties of water, most commonly temperature, are observed… Water turbidity **is common** … Gas emissions, often sulphureous, are observed…	Fractures **up to 100 cm wide** and **up to hundreds metres long** are **commonly** observed in loose alluvial deposits and/or saturated soils; in competent rocks they can reach up to 10 cm. Significant cracks are common in paved (asphalt or stone) roads, as well as small pressure undulations.	Landsliding is **widespread** in prone areas, **also** on gentle slopes; where equilibrium is unstable (steep slopes of loose / saturated soils; rock falls on steep gorges, coastal cliffs) their size is frequently large (10^5 m^3), sometimes very large (106 m^3).	1,000
X	Very destructive	**Many springs significantly** change their flow-rate and/or elevation of outcrop. Some springs may run temporarily or even permanently dry. **Temporary variations** of water level are **commonly** observed in wells. Even **strong variations** of chemical-physical properties of water, most commonly temperature, are observed… **Often** water becomes **very muddy**… Gas emissions, often sulphureous, are observed.	Open ground cracks **up to more than 1 m wide** and **up to hundred metres long** are **frequent**, mainly in loose alluvial deposits and/or saturated soils; in competent rocks opening reaches several decimeters. Wide cracks develop in paved (asphalt or stone) roads, as well as pressure undulations.	Large landslides and rock-falls (> 10^5 - 10^6 m^3) are frequent, practically regardless of equilibrium state of slopes, causing temporary or permanent barrier lakes.	5,000

Tab. 2: Shortened version of the definitions of the intensity classes VII to X according to the ESI 2007. The full text of the intensity definitions provided by Michetti et al. (2007) was used for the assessment of the effects of the 1906 Dobrá Voda earthquake.

between IESI≥VII and IX. The intensity is in agreement with the minimum area of about 80 km^2 spanned by the locations mentioned by Réthly (1907), supporting IESI-2007=VIII for the aftershock. In total, the reported intensity data points of the mainshock indicate ESI intensities between VIII and X in the epicentral area of the mainshock. However, the absence of descriptions of surface faulting and the absence of descriptions of ground cracks other than those related to landsliding points to a maximum intensity of the 1906 Dobrá Voda of less than IESI=X. At the ESI intensity of X, primary effects of surface faulting should be *"leading"*, and up to more than 1 m wide and up to hundred meters long cracks should be frequent (Michetti, 2007). We therefore assess the ESI intensity of the mainshock as IESI=IX.

As seen in Tab. 1 and Fig. 2a, the ESI 2007 intensity estimations for the mainshock on 10.01.1906 are comparable to the results of macroseismic intensity assessment by Réthly (1907), but slightly higher than the assessments of Imax by Grünthal et al. (2009) and ACORN (2004), which denote intensity VIII-IX for the event. Among the four ESI 2007 intensity datapoints available for the aftershock on 16.01.1906, the one from Jablonica (*"Well water of the entire surroundings was turbid"*) indicates the highest intensity leading to assign IESI-2007=IX (Tab. 1, Fig. 2). Descriptions from two locations are indicative for IESI-2007=VIII-IX, one for IESI-2007≥VII. The area of about 80 km^2 from which hydrological effects were reported is indicative for IESI-2007=VII-VIII (Tab. 2). We conclude that I_0=VIII is more appropriately describes the maximum intensity of the event than I_0=VII-VIII as listed in ACORN (2004) and Grünthal et al. (2009).

3.3 Earthquake occurrence near the 1906 Dobrá Voda mainshock

The most common and practical way of automatic aftershock detection is the use of temporal and spatial windows with the window length and size scaled according to the magnitude of the mainshock (Gardner and Knopoff, 1974). As the proposed spatial window size (about 50

km for 5.5<M<6.0) seems too large for the investigated event, we calculated the rupture length for an earthquake with M=5.7 using the following equation (Wells and Coppersmith, 1994):

$$\text{Log (Radial distance in m)} = (M - 4.32)/1.54$$

As the aftershocks tend to occur on the ruptured fault plane, the rupture length can be used to constrain the maximum epicentral distance of aftershocks from the mainshock. The regression by Wells & Coppersmith (1994) would suggest a radius of about 10 km around the epicenter as a spatial window for aftershock of the Ms=5.7 earthquake (Tab. 3). To account for the inaccuracies of macroseismic hypocenter locations resulting from the distance between the different settlements for which intensity data points are available, we extended the region under consideration to a radius of 13 km.

For a further assessment and to account for possibly even larger uncertainties of epicentre locations of historical events, we compared the seismicity distribution for a larger region with twice the radius of the previous spatial window (26 km). This extension approximates the hypocentre uncertainty for pre-instrumental earthquakes during the 20th century (Gangl and Decker, 2011). Fig. 3 shows the seismic activity around the mainshock (red star) from the ACORN catalogue (2004). Seismicity is shown by for a radial distance of 13 km (green circles) and 26 km (blue circles) from the epicenter of the mainshock. Most earthquakes are located within 5-10 km of the mainshock (Fig. 4), justifying the definition of aftershocks within the 13 km radius of epicentral distance.

The temporal distribution of earthquakes prior and after the 10.01.1906 mainshock shows an interesting pattern (Fig. 5). Prior to the 20th century, several earthquakes with magnitudes larger than 4.0 were recorded in the study area, fitting well to the considered completeness magnitude of 4.0 for the ACORN catalogue (Nasir et al., 2013). However, no major earthquake has been recorded in the vicinity of the mainshock. Earthquakes with magnitudes of approximately M=2.7 (corresponding to I_0=IV) are reported consistently since 1850. As expected, the mainshock caused the onset of elevated earthquake activity in its vicinity, and the seismicity shifts to its close surrounding, with the strongest (M=5) event occurring on 05.03.1930. In contrast, seismicity in the wider 26 km area almost stops completely for the next 70 years after the mainshock (Fig. 6). Normally, earthquakes are considered as aftershocks as long as the seismic activity level is above the background seismicity defined as the activity level prior to the mainshock. Applying this rule to the earthquake distribution shown in Fig. 5, earthquakes with magnitudes larger than 4.0 seem to decrease to background level between the 1930s and 1950s.

In comparison, earthquakes of magnitudes between 2.5 and 4.0 were recorded only sparsely before the mainshock but are abundant in the 20th century. It is interesting to note that almost all of them occur close to the mainshock within 13 km of epicentral distance. So, compared to the pre-mainshock seismic activity level within the 13 km radius, the moderate seismic activity in this area was elevated until about 2000 AD. Using the outer area of 13-26 km distance to the mainshock as reference level for background seismicity, the seismic activity ceases to background level at around 1980 AD. Unfortunately, data gaps due the war times of WWI and WWII (1914-18 and 1939-1945) and the following decades of recovery coincide with the analyzed period. The activity rates before and after the record gaps show regular exponential patterns of decaying seismicity.

The standard length of the time window where earthquakes are considered as aftershocks according to Gardner and Knopoff (1974) would be about 380 days for the 10.01.1906 and 155 days for the 05.03.1930 (M=5) Dobrá Voda earthquakes. The time windows interpolated from the values given in Table 3 are shown in Fig. 6 as gray vertical bars. This indicates that the time window from this method seems too short to include all potential aftershocks of the 1906 earthquake. In contrast, today's apparently still elevated seismicity and the overall gradual reduction of the seismicity level following the earthquake until today closely resembles a long-lasting aftershock succession as proposed for slow intra-plate faults by Stein and Liu (2009).

Magnitude	L (km)	T (days)
4.5	10	83
5.0	10	155
5.5	10	290
6.0	13	510
6.5	26	790
7.0	54	915

Tab. 3: Values from the window algorithm for automatic detection of fore- and aftershocks based on temporal (T = days after the mainshock (Knopoff and Gardner, 1969) and spatial windows (L = radial distance from epicenter in km). Spatial windows follow the equation Log (Radial distance in km) = (M-4.32)/1.54 (Wells and Coppersmith, 1994). The lower limit for the spatial window is set to 10 km due to high uncertainties associated with macroseismically determined epicentres of historical earthquakes. For explanation for the usage of the Wells and Coppersmith (1994) relation see text.

4 Discussion

In general, the major criteria for determining aftershock duration is the change in seismicity rates from decaying aftershocks to background seismicity, which can be directly measured for short aftershock durations. However, identifying this transition becomes difficult and even impossible as the aftershock duration approaches or exceeds the length of earthquake records (Stein and Liu, 2009). In case of the Dobrá Voda earthquake, determining the pre-event background seismicity poses another challenge, as earthquake recording changes at the same time from macroseismic to instrumentally supported observations. In the following, we discuss therefore the completeness of the pre-1906 earthquake records and

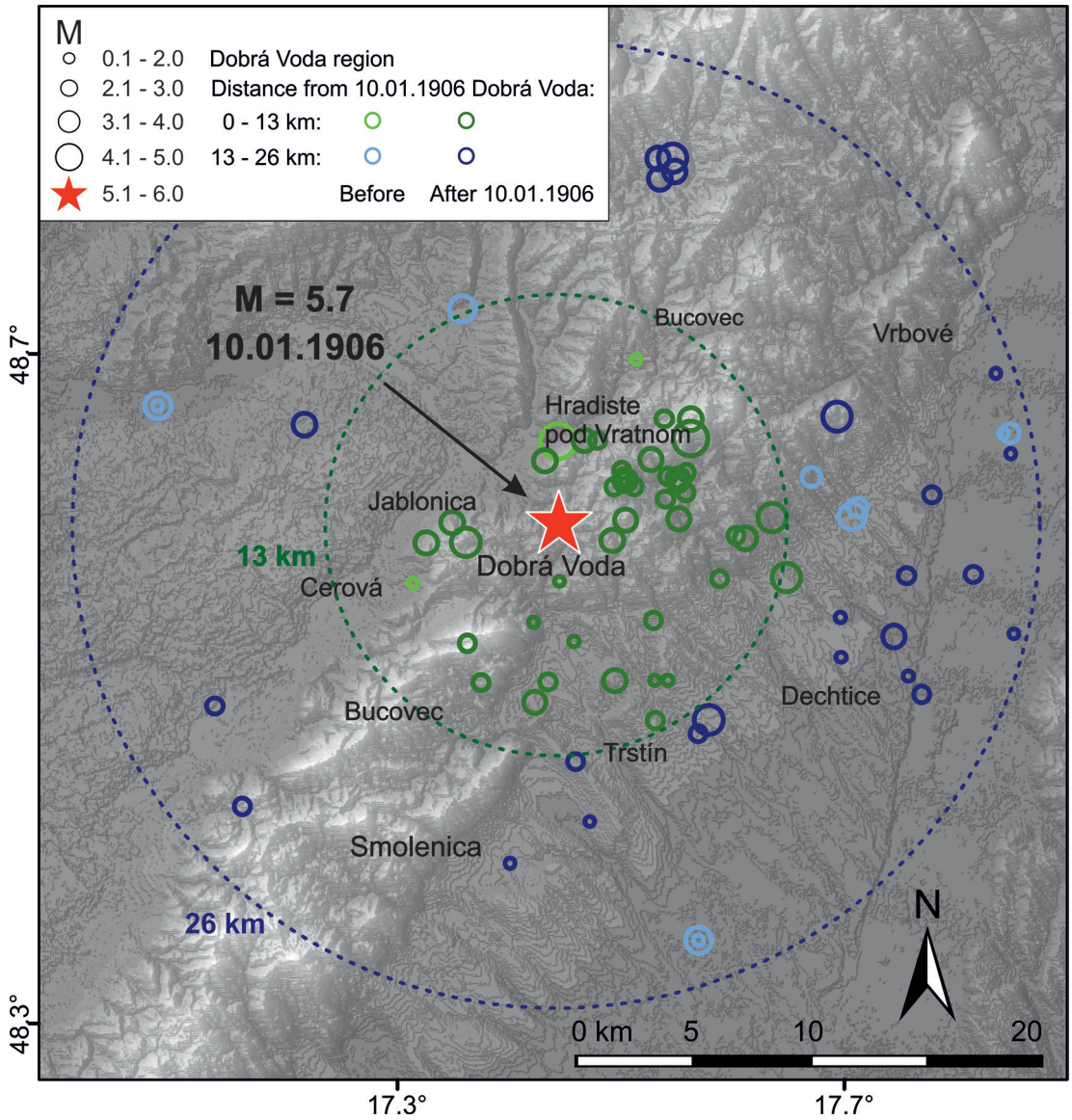

Fig. 3: Seismicity in the vicinity of the 1906 Dobrá Voda earthquake (M/I0=5.7/VIII-IX). Blue and green circles indicate earthquakes within a 0-13 km and 13-26 km distance from the mainshock. Light colors denote earthquakes before the mainshock, darker colors earthquakes after the mainshock. Data are listed in Tab. 4.

the resulting background seismicity, and then compare it to the earthquake distribution after 1906.

Fig. 5 shows that several earthquakes with M=4-5 occurred within a distance of 13-26 km from the epicenter of the 1906 Dobrá Voda mainshock between about 1500 and 1900. However, no aftershocks of these earthquakes have been recorded, most probably due to the general lack of detailed descriptions for these historical events. The observation threshold of M≈4.0 for the time before 1815 is clearly seen, with a recurrence interval of about 100 years for earthquakes larger than M=4.0. In contrast, the main Dobrá Voda earthquake was followed by several strong earthquakes on 16.01.1906 (M=5.1), 18.04.1914 (M=5.1), 05.03.1930 (M=5.0) and 06.03.1930 (M=4.6) in much shorter intervals.

The next strong earthquake after the apparent lack of data due to World War II (Figs. 5 and 6) occurred on 03.12.1967 (M=4.3) close to Dobrá Voda. As the 1967 earthquake occurred approximately 100 years after the 1852 (M=4.3) Pernek earthquake, its occurrence fits well to the level of seismicity observed before the 1906 earthquake. Considering this as background seismicity, the elevated seismicity caused by the 1906 mainshock would have lasted at least until 1930. On the other hand, considering that this earthquake occurred to close to the epicenter of the 1906 mainshock, it would be also reasonable to include it into a long-lasting aftershock sequence.

The systematic recording of smaller earthquakes with magnitudes down to M≈2.6 (I0≈IV) in the former Austrian empire started around 1895 (Nasir et al., 2013). However, the period between 1800 and 1900, and especially since 1850, may be regarded as complete enough to define the "background seismicity" before the 1906 mainshock (Fig. 5). The observational threshold for this period is M≈2.6 except for the periods of non-recording around WWI and WWII. In spite of the low record threshold, almost no earthquake larger than M=3.0 was recorded at

Date	Lat	Long	M	I_0	Epicentre
26.02.1515	48,37	17,56	5	7	Trnava
1586	48,37	17,56	4,6	7	Trnava
30.11.1660	48,37	17,56	4,4	6	Trnava
1805	48,58	17,68	4,3	6	Dobrá Voda
1815	48,6	17,65	3,2	4	Lancar
15.06.1815	48,58	17,68	3,2	4	Dobrá Voda
15.11.1852	48,64	17,16	4,3	6	Pernek -
13.04.1860	48,37	17,56	2,6	3	Trnava
13.04.1860	48,37	17,56	2,6	3	Trnava
15.11.1865	48,64	17,16	2,6	3	Sastin
15.11.1865	48,64	17,16	2,6	3	Sastin
01.02.1873	48,37	17,56	2,6	3	Trnava
02.12.1874	48,66	17,52	2,6	3	Pernek-Modra
24.03.1893	48,62	17,8	3,8	6	Dobrá Voda
28.03.1893*	48,62	17,8	2,6	6	Dobrá Voda
04.03.1894	48,6	17,51	2,6	3	Dobrá Voda
19.04.1904	48,6	17,51	2,6	3	Dobrá Voda
20.04.1904	48,62	17,46	4,5	7	Dobrá Voda
12.10.1904	48,68	17,39	4,3	6	Dobrá Voda
10.04.1905	48,55	17,35	2,6	3	Sandorfal
09.01.1906	48,58	17,46	5,7	9	Dobrá Voda
10.01.1906	48,63	17,27	2,6	3	Dobrá Voda
10.01.1906	48,75	17,54	2,6	3	Dobrá Voda
10.01.1906	48,63	17,56	3,7	5	Dobrá Voda
10.01.1906	48,57	17,6	2,6	3	Dobrá Voda
15.01.1906	48,6	17,55	3,2	4	Dobrá Voda
16.01.1906	48,6	17,51	2,6	3	Dobrá Voda
16.01.1906	48,6	17,51	2,6	3	Dobrá Voda
16.01.1906	48,6	17,51	2,6	3	Dobrá Voda
16.01.1906	48,6	17,51	2,6	3	Dobrá Voda
16.01.1906	48,6	17,51	2,6	3	Dobrá Voda
16.01.1906	48,62	17,56	5,1	8	Dobrá Voda
17.01.1906	48,6	17,51	2,6	3	Dobrá Voda
17.01.1906	48,6	17,51	2,6	3	Dobrá Voda
17.01.1906	48,6	17,55	2,6	3	Dobrá Voda
19.01.1906	48,6	17,51	2,6	3	Dobrá Voda
19.01.1906	48,6	17,51	2,6	3	Dobrá Voda
20.01.1906	48,6	17,51	2,6	3	Dobrá Voda
04.02.1906	48,6	17,51	2,6	3	Dobrá Voda
04.02.1906	48,6	17,51	2,9	4	Dobrá Voda
08.02.1906	48,6	17,51	2,6	3	Dobrá Voda
10.02.1906	48,6	17,51	2,6	3	Dobrá Voda
12.02.1906	48,6	17,55	3,2	4	Dobrá Voda
14.02.1906	48,6	17,55	2,6	3	Dobrá Voda
15.02.1906	48,6	17,55	2,6	3	Dobrá Voda
15.02.1906	48,6	17,55	2,6	3	Dobrá Voda
20.02.1906	48,6	17,55	2,6	3	Dobrá Voda
21.02.1906	48,6	17,55	2,6	3	Dobrá Voda
21.02.1906	48,6	17,55	3,7	5	Dobrá Voda
22.02.1906	48,6	17,51	2,6	3	Dobrá Voda
22.02.1906	48,6	17,51	2,9	4	Dobrá Voda
24.04.1906	48,6	17,51	2,6	3	Dobrá Voda

Date	Lat	Long	M	I_0	Epicentre
22.02.1906	48,6	17,51	3,2	4	Dobrá Voda
22.02.1906	48,6	17,51	3,4	5	Dobrá Voda
25.02.1906	48,6	17,51	2,6	3	Dobrá Voda
25.02.1906	48,6	17,51	2,6	3	Dobrá Voda
25.02.1906	48,6	17,51	2,9	4	Dobrá Voda
25.02.1906	48,6	17,51	3,2	4	Dobrá Voda
26.02.1906	48,6	17,51	2,9	4	Dobrá Voda
28.02.1906	48,6	17,51	2,9	4	Dobrá Voda
28.02.1906	48,6	17,51	2,9	4	Dobrá Voda
01.03.1906	48,6	17,51	3,2	4	Dobrá Voda
02.03.1906	48,58	17,51	3,4	5	Dobrá Voda
02.03.1906	48,6	17,51	3,2	4	Dobrá Voda
02.03.1906	48,6	17,55	3,7	5	Dobrá Voda
03.03.1906	48,6	17,51	3,2	4	Dobrá Voda
03.03.1906	48,6	17,51	3,2	4	Dobrá Voda
08.03.1906	48,6	17,51	3,2	4	Dobrá Voda
09.03.1906	48,6	17,51	3,7	5	Dobrá Voda
13.03.1906	48,6	17,51	2,9	4	Dobrá Voda
16.03.1906*	48,62	17,48	3,2	5	Jablonica
23.03.1906	48,6	17,51	2,6	3	Dobrá Voda
24.03.1906	48,63	17,54	2,9	4	Dobrá Voda
25.03.1906	48,6	17,55	3,8	5	Dobrá Voda
31.03.1906	48,6	17,51	2,8	4	Dobrá Voda
31.03.1906	48,6	17,51	2,9	4	Dobrá Voda
01.04.1906	48,6	17,51	3,2	4	Dobrá Voda
02.04.1906	48,6	17,51	2,6	3	Dobrá Voda
02.04.1906	48,6	17,51	2,6	3	Dobrá Voda
02.04.1906	48,6	17,55	2,6	3	Dobrá Voda
06.04.1906	48,6	17,51	2,9	4	Dobrá Voda
07.04.1906	48,6	17,51	2,6	3	Dobrá Voda
07.04.1906	48,6	17,51	2,6	3	Dobrá Voda
07.04.1906	48,6	17,51	3,2	4	Dobrá Voda
07.04.1906	48,6	17,51	3,7	5	Dobrá Voda
07.04.1906	48,6	17,55	2,6	3	Dobrá Voda
08.04.1906	48,6	17,51	2,6	3	Dobrá Voda
08.04.1906	48,6	17,51	2,9	4	Dobrá Voda
08.04.1906	48,6	17,51	2,9	4	Dobrá Voda
09.04.1906	48,62	17,49	2,9	4	Dobrá Voda
09.04.1906	48,6	17,51	2,6	3	Dobrá Voda
09.04.1906	48,53	17,53	2,6	3	Nahac
09.04.1906	48,61	17,53	3,7	5	Dobrá Voda
12.04.1906	48,6	17,51	2,6	3	Dobrá Voda
12.04.1906	48,6	17,51	2,9	4	Dobrá Voda
12.04.1906	48,6	17,51	3,2	4	Dobrá Voda
13.04.1906	48,6	17,51	2,6	3	Dobrá Voda
15.04.1906	48,61	17,45	3,4	5	Dobrá Voda
15.04.1906	48,6	17,51	2,6	3	Dobrá Voda
19.04.1906	48,61	17,45	3,3	5	Dobrá Voda
22.04.1906	48,6	17,51	2,6	3	Dobrá Voda
23.04.1906	48,6	17,51	3,2	4	Dobrá Voda
23.04.1906	48,6	17,51	3,2	4	Dobrá Voda
07.03.1930	48,6	17,51	2,6	3	Dobrá Voda

Date	Lat	Long	M	I_0	Epicentre
25.04.1906	48,6	17,51	2,6	3	Dobrá Voda
10.05.1906	48,6	17,51	2,6	3	Dobrá Voda
12.05.1906	48,6	17,51	2,6	3	Dobrá Voda
15.05.1906	48,6	17,51	3,4	5	Dobrá Voda
31.05.1906	48,6	17,51	2,6	3	Dobrá Voda
31.05.1906	48,6	17,51	3,2	4	Dobrá Voda
01.06.1906	48,63	17,67	3,4	5	Dobrá Voda
02.06.1906	48,6	17,51	2,9	4	Dobrá Voda
07.06.1906	48,57	17,6	3,2	4	Dobrá Voda
20.06.1906	48,6	17,51	2,9	4	Dobrá Voda
04.07.1906	48,6	17,51	2,8	4	Dobrá Voda
08.08.1906	48,6	17,51	2,6	3	Dobrá Voda
09.08.1906	48,6	17,55	2,6	3	Dobrá Voda
10.08.1906	48,6	17,55	2,6	3	Dobrá Voda
13.08.1906	48,6	17,51	2,6	3	Dobrá Voda
14.08.1906	48,6	17,51	2,6	3	Dobrá Voda
15.08.1906	48,6	17,51	2,6	3	Dobrá Voda
16.08.1906	48,6	17,51	2,6	3	Dobrá Voda
16.08.1906	48,6	17,55	2,6	3	Dobrá Voda
17.08.1906	48,55	17,58	2,6	3	Dobrá Voda
25.08.1906	48,6	17,51	3,2	4	Dobrá Voda
06.09.1906	48,6	17,51	3,2	4	Dobrá Voda
11.09.1906	48,6	17,51	3,2	4	Dobrá Voda
16.03.1908	48,6	17,51	2,9	4	Dobrá Voda
25.05.1908	48,6	17,55	2,6	3	Dobrá Voda
26.05.1908	48,6	17,55	2,6	3	Dobrá Voda
18.12.1908	48,6	17,51	3,2	4	Dobrá Voda
04.01.1909	48,6	17,51	2,6	3	Dobrá Voda
08.01.1909	48,6	17,51	2,6	3	Dobrá Voda
09.01.1909	48,6	17,51	2,6	3	Dobrá Voda
14.03.1909	48,6	17,51	3,7	5	Dobrá Voda
16.01.1910	48,6	17,51	2,6	3	Dobrá Voda
06.09.1929	48,58	17,55	3,4	5	Dobrá Voda
04.03.1930	48,46	17,47	2,3	3	Dobrá Voda
04.03.1930	48,6	17,51	3,7	5	Dobrá Voda
05.03.1930	48,6	17,51	2,2	3	Dobrá Voda
05.03.1930	48,6	17,51	2,6	3	Dobrá Voda
05.03.1930	48,58	17,62	5	8	Dobrá Voda
06.03.1930	48,5	17,45	2,6	3	Dobrá Voda
06.03.1930	48,6	17,51	2,6	3	Dobrá Voda
06.03.1930	48,6	17,51	2,6	3	Dobrá Voda
06.03.1930	48,6	17,51	2,6	3	Dobrá Voda
06.03.1930	48,6	17,51	2,6	3	Dobrá Voda
06.03.1930	48,6	17,51	2,6	3	Dobrá Voda
06.03.1930	48,6	17,51	3	4	Dobrá Voda
06.03.1930	48,6	17,51	3,2	4	Dobrá Voda
06.03.1930	48,48	17,53	2,6	3	Dobrá Voda
06.03.1930	48,55	17,63	4,6	7	Dobrá Voda
07.03.1930	48,6	17,51	2,6	3	Dobrá Voda
07.03.1930	48,6	17,51	2,6	3	Dobrá Voda
07.03.1930	48,6	17,51	2,6	3	Dobrá Voda
07.03.1930	48,6	17,51	3,2	4	Dobrá Voda
08.03.1930	48,6	17,51	2,6	3	Dobrá Voda
09.03.1930	48,6	17,51	2,6	3	Dobrá Voda
09.03.1930	48,6	17,51	2,6	3	Dobrá Voda
15.03.1930	48,6	17,51	2,6	3	Dobrá Voda
17.03.1930	48,6	17,51	2,6	3	Dobrá Voda
17.03.1930	48,6	17,51	3,4	5	Dobrá Voda
18.03.1930	48,6	17,51	2,6	3	Dobrá Voda
18.03.1930	48,6	17,51	2,6	3	Dobrá Voda
13.12.1955	48,49	17,44	3,2	4	Pernek-Modra
22.06.1957	48,5	17,4	2,6	3	Smolenice
01.07.1957	48,5	17,4	2,9	4	Smolenice
03.07.1957	48,5	17,4	2,6	3	Smolenice
04.07.1957	48,5	17,4	2,3	3	Smolenice
17.06.1967	48,58	17,38	3,7	5	Dobrá Voda
03.12.1967	48,57	17,39	4,3	7	Dobrá Voda
26.07.1976	48,76	17,55	3,2	4	Pernek-Modra
28.07.1976	48,76	17,55	3,2	4	Pernek-Modra
05.08.1976	48,76	17,55	2,9	4	Pernek-Modra
19.08.1976	48,76	17,55	2,9	4	Pernek-Modra
24.08.1976	48,57	17,36	4	6	Pernek-Modra
11.04.1977	48,5	17,5	3,4	5	Dobrá Voda
21.03.1980	48,5	17,4	2,9	4	Pernek -
13.03.1987	48,59	17,74	2,4		Dobrá Voda
22.03.1987	48,47	17,56	2,3		Dobrá Voda
30.05.1987	48,52	17,71	2,8		Dobrá Voda
01.07.1987	48,52	17,39	2,3		Dobrá Voda
12.03.1989	48,49	17,2	2,3		Plavecke
21.10.1991	48,57	17,5	3,1	4	Dobrá Voda
27.04.1992	48,44	17,22	2,3		Bratislav
14.07.1992	48,48	17,57	3,3	4	Dobrá Voda
06.11.1997	48,52	17,8	1,2		Jaslov. Bohunice
11.01.1998	48,51	17,67	1,6		Jaslov. Bohunice
03.08.1998	48,53	17,67	0,5		Jaslov. Bohunice
05.05.1999	48,5	17,72	1,2		Jaslov. Bohunice
05.05.1999	48,49	17,73	2		Jaslov. Bohunice
18.10.1999	48,55	17,72	2		Chtelnica
19.10.1999	48,41	17,42	1,1		Dolne Ore
27.04.2000	48,43	17,48	1,6		Boleráz
28.05.2000	48,53	17,44	1,9		Horná Krupá
28.05.2000	48,53	17,44	0,5		Horná Krupá
08.08.2000	48,5	17,54	1,5		Nahac
24.01.2001	48,5	17,53	1,2		Nahac
06.06.2001	48,65	17,79	1		Vrbové
28.06.2001	48,61	17,8	1,2		Trebatice
15.12.2002	48,52	17,47	1,8		Dobrá Voda
05.04.2003	48,55	17,46	1,5		W Slovakia
17.06.2003	48,55	17,77	2		W Slovakia
19.09.2003	48,59	17,54	2,5	3	W Slovakia

Tab. 4. Earthquakes within 13 km (white) and 26 km distance (grey) from the 1906 Dobrá Voda earthquake. The mainshock on 10.01.1906 is highlighted. I_0: Epicentral intensity (EMS98); M: magnitude estimated from I_0. Data source: ACORN catalogue (ACORN, 2004). Data marked with * from Shebalin and Leydecker (1998).

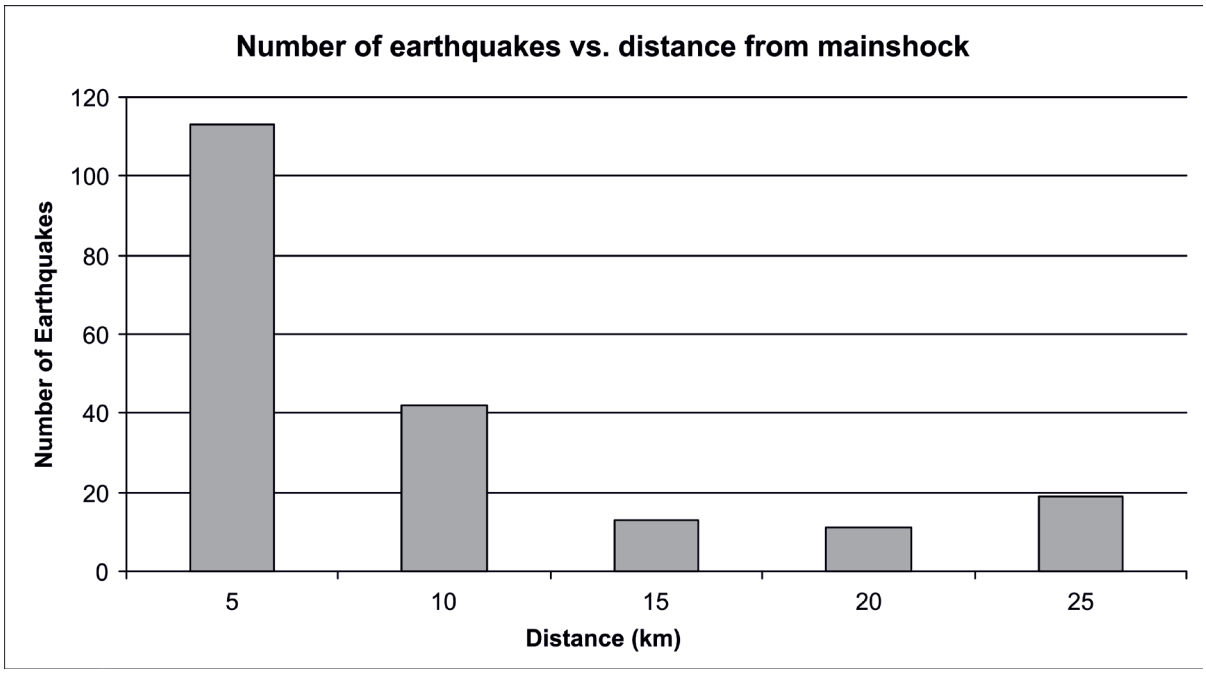

Fig. 4: Number of recorded earthquakes plotted versus epicentral distance from the 10.01.1906 Dobrá Voda mainshock (see Figure 3 for location).

distances up to 26 km from the Dobrá Voda mainshock (Fig. 5). In contrast, after the 1906 earthquake, the seismicity level significantly increased, especially within 13 km of epicentral distance. In total, 158 earthquakes were observed within 13 km from the mainshock and only 25 earthquakes in distances between 13 km and 26 km. This concentration of seismicity close to the mainshock continues until the 1990s. This evolution can be interpreted as an ongoing aftershock sequence of the 1906 Dobrá Voda earthquake. The earthquakes outside the

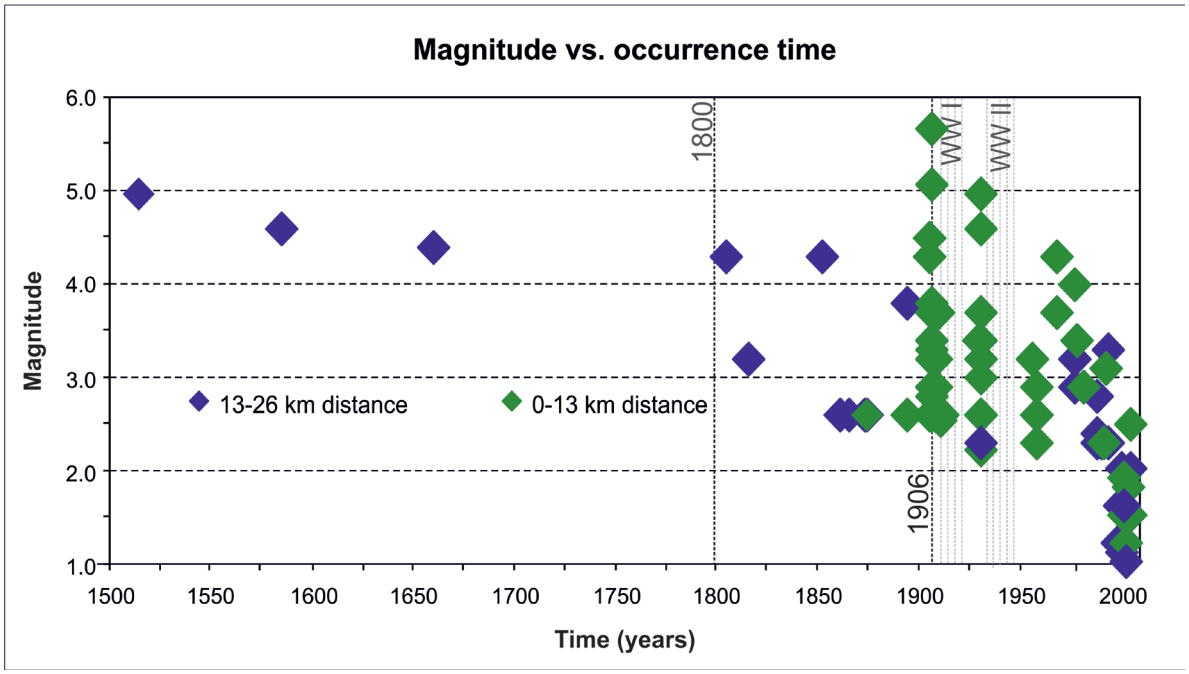

Fig. 5: Magnitude vs. occurrence time plotted for earthquakes in the vicinity of the Dobrá Voda earthquake. Blue diamonds show seismicity within 13-26 km distance, green diamonds within 0-13 km distance of the mainshock. Note the data gaps due to World War I (1914-1918) and World War II (1939-1945). 1800 indicates the onset of catalogue completeness for I_0<V (≈ M < 3.5) is marked according to Nasir et al. (2013).

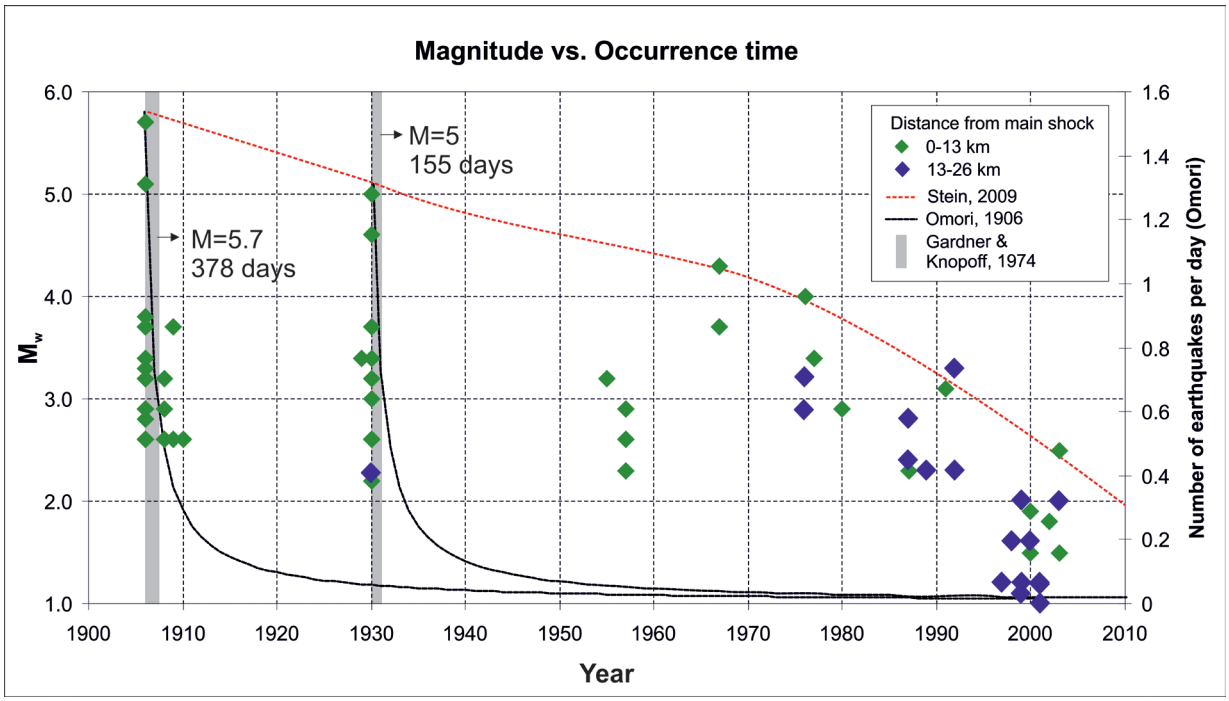

Fig. 6: Magnitude vs. time plot for earthquakes in the Dobrá Voda region between 1900 and 2004. Blue diamonds show seismicity within 13-26 km distance, green diamonds within 0-13 km distance of the mainshock. The time series includes two major events: the 10.01.1906 (M=5.7) and 03.05.1930 (M=5) earthquakes. Black lines show aftershock sequences expected from Omori's law, the red dotted line is the possible interpretation of a several-decades-long aftershock sequence following Stein and Liu (2009). The gray vertical lines indicate temporal windows following Gardener and Knopoff (1974), as interpolated from Tab. 3.

13 km radius restart again around 1975. In general, the area experiences elevated seismicity until today.

In Fig. 6, earthquakes at the Dobrá Voda Segment are plotted for the time 1900-2004. The two major earthquakes in 1906 (M=5.7) and 1930 (M=5) are shown together with expected aftershock occurrences calculated from Omori's law (black lines in Fig. 6; Ogata, 1983) and the aftershock duration based on Gardner and Knopoff (1974) in Tab. 3. Using the values in Tab. 3, the latter method indicate 155 days of aftershocks for an earthquake of M=5 and 378 days for an earthquake of M=5.7 (grey lines in Fig. 6). Both time windows and the times of increased seismicity calculated from Omori`s law are too short to cover the actual aftershock occurrences for the 1906 mainshock. Therefore, we discard the temporal windows as a suitable approach to define the aftershock sequence. Fig. 6 further indicates that Omori's law is suited to explain the aftershock occurrence for both major earthquakes. However, for the 1930 earthquake, we cannot be sure if the whole length of the aftershock sequence is recorded or if the aftershock sequence is cut short by an incomplete earthquake record. Therefore, the coincidence of data gaps due with war times (1914-18/1938-1945) and the recovery period afterwards may prevent a final conclusive interpretation of the aftershock sequences of the 1906 and 1930 events.

The temporal distribution of earthquakes within the 13 km radius around the 1906 earthquake show a long-term decay, which fits the model of Stein and Liu (2009) who proposed aftershock sequences extending over several decades to hundreds of years. Fig. 7 displays aftershock durations for selected events from three tectonic settings: plate boundary faults, broad plate boundary zones, and continental interiors (Stein and Liu, 2009). Despite the uncertainties in estimating both the duration and the rate at which tectonic slip loads the faults, the data indicate an inverse relationship between the aftershock durations and the slip rates. Faults at plate boundaries that are loaded by the rapid (typically faster than 10mm/yr) plate motion show aftershock durations of about ten years. Faults within broad plate boundary zones but off the main boundaries move at only a small fraction of the plate motion (a few millimeters per year) and have longer aftershock durations (Stein and Liu, 2009). In diffuse plate boundary zones such as the North American Basin and Range, aftershock sequences often continue for fifty years or more. Considering the geological slip rate of 1-2 mm/yr for the Vienna Basin fault (Decker et al., 2005; Grenerczy et al., 2000; Grenerczy, 2002) and the ongoing elevated seismicity level in the Dobrá Voda region, the 1906 Dobrá Voda earthquake fits well into the data presented by Stein and Liu (2009). Therefore, the observed seismicity at the Dobrá Voda area might be still be influenced by the 1906 earthquake and could be interpreted as an extended aftershock sequence of almost 100 years duration.

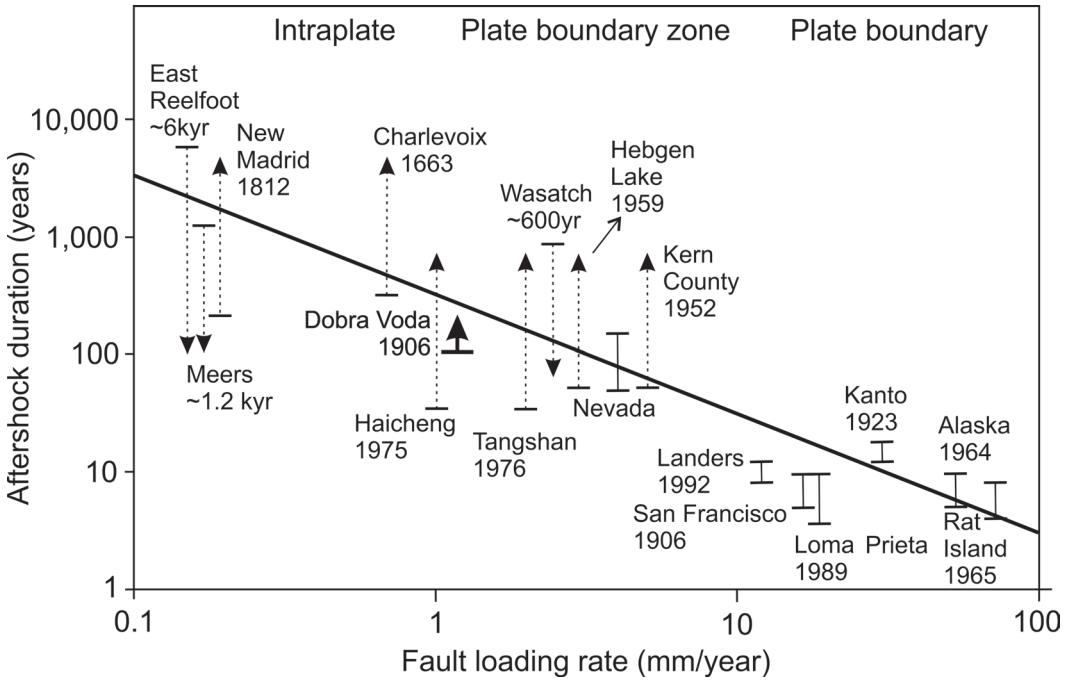

Fig. 7: Aftershock duration vs. fault loading rate for large earthquakes in different tectonic settings from Stein and Liu (2009). The solid line shows the model prediction. Aftershock durations have bars showing the span of published estimates. One-sided constraints have bars at the known value and arrows indicating the open value. For example, the New Madrid aftershocks span at least 200 years, but the upper bound is unconstrained. Similarly, the Wasatch aftershocks span less than 600 years, but the lower bound is unconstrained. Data and source for this plot obtained from the Supplementary Information of Stein and Liu (2009). The Dobrá Voda aftershock span is 100 years, but the upper bound is yet unconstrained. The graph shows that the Dobrá Voda aftershock sequence fits well to the model prediction for the slow (1-2 mm slip/yr) Vienna Basin strike-slip fault system, 1 kyr = 1000 years.

5 Conclusions

The 1906 Dobrá Voda earthquake is the dominant earthquake at the northern part of the Vienna Basin Transfer Fault and has influenced the local seismic activity throughout the 20th century. Environmental effects of the earthquake described by contemporary authors include hydrological effects and mass movements with surface cracks, which help to constrain the epicentral intensity for the Dobrá Voda mainshock and its strongest aftershock in 1906. Applying the ESI 2007 intensity scale to these effects leads to an assessment of the related epicentral intensities with I_0=IX and I_0=VIII, respectively. This new intensity estimates are regarded more appropriate to describe the maximum intensity of the events than the values listed in the ACORN and CENEC catalogues (ACORN, 2004; Grünthal et al., 2009).

Analysis of the temporal evolution of seismicity around Dobrá Voda reveals that significant earthquakes (M=4-5) that occurred in the centuries prior to the mainshock are scattered over the entire region. After the 1906 Dobrá Voda mainshock, seismicity mainly concentrates within a distance of less than 13 km from the epicentre. This seismicity pattern persists for about 70 years.

The slow regular decline of seismicity after 1906, best shown by the gradual decrease of the largest observed magnitudes (Fig. 6), suggests that the aftershock sequence might have lasted longer than predicted by the Omori law and the level of background seismicity is only reached more than about 100 years after the mainshock. The observed seismicity pattern fits to the model of century-long aftershock sequences in intraplate regions as described by Stein and Liu (2009), suggesting that the slow loading rate of the VBTF can lead to aftershock sequences of severe earthquakes that exceed 100 years duration.

6 Acknowledgements

We thank Wolf Lenhardt for supporting us with data on the seismicity of the Vienna Basin and Erika Mühlmann for her work and translations from Hungarian language. We gratefully acknowledge the careful and very constructive reviews by Seth Stein and Christoph Grützner. Their comments and suggestions helped improving the manuscript considerably.

7 References

ACORN, 2004. Catalogue of Earthquakes in the Region of the Alps - Western Carpathians – Bohemian Massif for the period from 1267 to 2004. Computer File, Vienna (Central Institute for Meteorology and Geodynamics, Department of Geophysics Brno (Institute of Physics of the Earth, University Brno

Beidinger, A., Decker, K., 2011. 3D geometry and kinematics of the Lassee flower structure: Implication for segmentation and seismotectonics of the Vienna Basin strike-slip fault, Austria. Tectonophysics 499, 22–40. http://dx.doi.org/10.1016/j.tecto.2010.11.006.

Briestenský, M., Stemberk, J., Petro, L., 2007. Displacements registered around the 13 March 2006 Vrbové earthquake M=3.2 (Western Carpathians). Geol. Carpathica, 58/5, 487–493.

Bus, Z., Grenerczy, G., Toth, L., Monus, P., 2009. Active crustal deformation in two seismogenic zones of the Pannonian region - GPS versus seismological observations. Tectonophysics, 474, 343–352.

Cancani, A., 1904. Sur l'emploi d'une double echelle sismique des intensitès, empirique et absolue. Gerlands Beiträge zur Geophysik, 2, 281–283.

Cipciar, A., Labák, P., Moczo, P., Kristeková, M., 2002. Monitoring of seismic phenomena by national seismic stations network. Publishing House D. Štúra, Bratislava, (in Slovak), 106, 123–132.

Csicskay, K., Cipciar, A., Fojtíková, L., Krsteková, M., Gális, M., Srbecký, M., Chovanová, Z., Bystrický, E., Kysel, R., 2018. The National Network of Seismic Stations of Slovakia – Current state after 13 years of operation from the project of modernization and enhancement. Contributions to Geophysics and Geology, 48/4, 337–348.

Decker, K., Peresson, H., Hinsch, R., 2005. Active tectonics and Quaternary basin formation along the Vienna Basin Transform fault. Quaternary Science Reviews, 24, 307–322.

Drimmel, J., Trapp, E., 1982. Earthquakes in Austria between 1971 and 1980. Sitzungsberichte-Österreichische Akademie der Wissenschaften, Mathematisch -Naturwissenschaftliche Klasse, Abteilung 1, 191, 73–102.

Fojtikova, L., Vavrycuk, V., Cipciar, A., Madaras, J., 2010. Focal mechanisms of micro-earthquakes in the Dobrá Voda seismoactive area in the Malé Karpaty Mts. Tectonophysics, 492(1-4), 213-229.

Gangl, G., Decker, K., 2011. Compilation of strong Austrian earthquakes with intensities higher than 7. Österreichische Ingenieur- und Architekten-Zeitschrift, 156, 229–237.

Gardner, J. K., Knopoff, L., 1974. Is the sequence of earthquakes in southern California, with aftershocks removed, poissonian?, Bulletin of the Seismological Society of America, 64/5, 1363–1367.

Grenerczy, G., Kenyeres, A., Fejes, I., 2000. Present crustal movement and strain distribution in Central Europe inferred from GPS measurements. Journal of Geophysical Research, 105 B9, 21, 835–846.

Grenerczy, G., 2002. Tectonic processes in the Eurasian–African plate boundary zone revealed by space geodesy. In: Stein, S., Freymueller J.T. (Eds.), Plate Boundary Zones. AGU Monograph Geodynamics Series, 30, 67–86.

Grünthal G. (Ed.), 1998. The European Macroseismic Scale (EMS-98). Cahiers du Centre Européen de Géodynamique et de Séismologie 15, pp. 99, (ECGS) Luxembourg.

Grünthal, G., Wahlström, R. and Stromeyer, D., 2009. The unified catalogue of earthquakes in central, northern, and north- western Europe (CENEC) - updated and expanded to the last millennium. Journal of Seismology, 13, 517–541.

Hammerl, Ch., Lenhardt, W., 2002. Historical Earthquakes in Styria/ Austria – Source Investigation – Revision of the Catalogue. Proc. of XXVIII ESC General Assembly, Genoa, Italy, 1-6 September 2002, 133.

Hammerl, Ch.,Lenhardt, W.A., 2013. Erdbeben in Niederösterreich von 1000 bis 2009 n. Chr. Abhandlungen der Geologischen Bundes-Anstalt, 67, 3–297.

Heidbach, O., Tingay, M., Barth, A., Reinecker, J., Kurfeß, D., Müller, B., 2008. The World Stress Map database release 2008. doi:10.1594/GFZ.WSM.Rel2008.

Hinsch, R., Decker, K., 2003. Do seismic slip deficits indicate an underestimated earthquake potential along the Vienna Basin Transfer Fault System? Terra Nova, 15, 343–349.

Hinsch, R., Decker, K., 2011. Seismic slip rates, potential subsurface rupture areas and seismic potential of the Vienna Basin Transfer Fault, International Journal of Earth Sciences, 100/8, 1925–1935.

Jarosinski, M., 1998. Contemporary stress field distortion in the Polish part of the western outer Carpathians and their basement. Tectonophysics, 297/1-4, 91–119.

Jarosinski, M., 2005. Ongoing tectonic reactivation of the Outer Carpathians and is impact on the foreland: Results of borehole breakout measurements in Poland. Tectonophysics, 410, 189–216.

Kadirioglu, F.T., Kartal, R.F., 2016. The new empirical magnitude conversion relations using an improved earthquake catalogue for Turkey and its near vicinity (1900–2012). Turkish J. Earth Sci., 25, 300–310.

Kárník, V., 1968. Seismicity of the European Area. Part 1. Academia, Praha.

Kováč, M., Bielik, M., Hók, J., Kováč, P., Kronome, B., Labák, P., Moczo, P., Plašienka, D., Šefara, J., Šujan, M., 2002. Seismic activity and neotectonic evolution of the Western Carpathians (Slovakia). EGU Stephan Mueller Special Publication Series, 3, 167–184.

Lenhardt, W.A., Švancara, J., Melichar, P., Pazdírková, J., Havíř, J., Sýkorová, Z., 2007. Seismic activity of the Alpine–Carpathian–Bohemian Massif region with regard to geological and potential field data. Geol. Carpathica, 58/4, 397– 412.

Marko, F., Fodor, L., Kováč, M., 1991. Miocene strike-slip faulting and block rotation in Brezovské Karpaty Mts. (Western Carpathians). Mineralia Slovaca, 23, 189– 200.

Michetti, A. M., Esposito, E. et al., Intensity Scale ESI 2007 in Mem. Descr. Carta Geologica d'Italia, Servizio Geologico d'Italia, APAT, Rome, Italy, 94

Michetti, A. M., Esposito, E. et al., 2004. The INQUA scale: An innovative approach for assessing earthquake intensities based on seismically-induced ground effects in natural environment. Special Paper Memorie Descrittive della Carta Geologica D'Italia, LXVII.

Mühlmann, E., Decker, K., Hintersberger, E. 2012. Neubewertung des Dobrá Voda Erdbebens an der Wiener Becken-Störung nach der Environmental Seismicity Intensity Scale (ESI) 2007. PANGEO Austria 2012, Abstracts, p.101, Universität Salzburg, 15-20 September 2012, Salzburg.

Müller, B., Zoback, M.L., Fuchs, K., Mastin, L., Gregersen, S., Pavoni, N., Stephansson, O., Ljunggren, C., 1992. Regional patterns of tectonic stress in Europe. J. Geophys. Res., 97/11, 783803.

Musson, R.M.W., Grünthal, G., Stucchi, M., 2010. The comparison of macroseismic intensity scales. J Seismology, 14, 413–428.

Nasir, A., Lenhardt, W., Hintersberger, E., Decker, K., 2013. Assessing the completeness of historical and instrumental earthquake data in Austria and surrounding areas, Austrian Journal of Earth Sciences, 106/1, 90– 102. doi:10.14470/FX099882.

Ogata, Y., 1983. Estimation of the parameters in the modified Omori formula for the aftershock frequencies by the maximum likelihood procedure. J. Phys. Earth, 31, 115– 124.

Reinecker, J., 2000. Stress and deformation: Miocene to Present-day tectonics in the Eastern Alps. Tübinger Geowissenschaftliche Arbeiten, Reihe A, 55, 128pp.

Rethly, A., 1907. Erdbeben in Ungarn 1906 (in Hungarian with German abstracts). K. Ungar. Reichsanstalt für Meteorologie und Erdmagnetismums (Kir. Orsz. Meteorológiai és Földmágnességi Intézet), 109pp. (Budapest)

Scordilis, E.M., 2006. Empirical global relations converting MS and mb to moment magnitude. J. Seismology, 10: 225-236.

Šefara, J., Kováč, M., Plašienka, D., Šujan, M., 1998. Seismogenic zones in the Eastern Alpine – Western Carpathian – Pannonian junction area. Geol. Carpathica, 49/4, 247–260.

Stein, S., Liu, M., 2009. Long aftershock sequences within continents and implication for earthquake hazard assessment, Nature, 462/5, 87– 89.

Süss, F. E., 1897 . Das Erdbeben von Laibach am 14. April 1895. Jahrbuch der k.k. geologischen Reichsanstalt, 1897, 412–614.

Wells, D. L., Coppersmith, K. J., 1994. New empirical relationship among magnitude rupture length, rupture width, rupture area, and surface displacement. Bull. Seismol. Soc. Amer., 84, 974–1002.

Zsíros, T., 2005. Seismicity of the Western-Carpathians. Acta Geodaet. Geophys. Hungaria, 40/3-4, 455–467.

Received: 26.10.2019
Accepted: 13.3.2020
Editorial handling: K. Stüwe

Appendix 3

Nasir, A., Hintersberger, E., & Decker, K., The temporal evolution of seismicity and variability of b-values along the Vienna Basin Transfer Fault System. (Submitted to Austrian Journal of Earth Sciences, Manuscript id: **AJES22_03**)

The temporal evolution of seismicity and variability of b-values along the Vienna Basin Transfer Fault System

Submitted to: Austrian Journal of Earth Sciences

Asma Nasir[1], Esther Hintersberger[2], Kurt Decker[1]

[1] Department of Geology, University of Vienna, Althanstraße 14, A-1090 Vienna, Austria

[2] Geological Survey of Austria, Neulinggasse 38, 1030 Vienna, Austria

Corresponding author: asma.nasir@univie.ac.at

esther.hintersberger@geologie.ac.at

kurt.decker@univie.ac.at

Vienna, 01.03.2022

Abstract

The Vienna Basin Transfer Fault System (VBTFS) is the most active fault in the region between the Eastern Alps, the western Carpathians and the Pannonian Basin. The spatial and temporal distribution of earthquakes along the fault shows a heterogeneous pattern including a long-time decay of seismicity at the northern part of the VBTFS, which was interpreted to result from a long aftershock sequence subsequent to the 1906 Dobrá Voda earthquake (M=5.7). In this paper we investigate if other strands of the VBTFS display similar long-term declines of seismicity that might indicate long aftershock sequences following strong, yet unrecorded, earthquakes in historical times.

In order to analyse the distribution of seismicity, the VBTFS is divided into arbitrary segments of about 50km length each. The segments are chosen to overlap each other to avoid missing information from neighbouring segments due to arbitrarily selected segment boundaries. For each segment we analyse the temporal evolution of seismicity and calculate the parameters of the corresponding Gutenberg-Richter (GR) relation.

The temporal seismicity patterns revealed from the segments covering the Dobrá Voda area confirm the protracted aftershock sequence following the 1906 earthquake. All but one of the other segments do not show temporal changes of seismicity comparable to the long-term Dobrá Voda aftershock sequence. Seismicity patterns, however, include short-term Omori-type aftershocks following moderate earthquakes such as the 2000 Ebreichsdorf earthquake (M=4.8). The segment covering the SW tip of the VBTFS revealed a 200 years long gradual decrease of the largest observed magnitudes starting with the 1794 Leoben (M=4.7) earthquake. The 1794 event is the oldest earthquake listed in the catalogue for the region under consideration. It therefore remains open if the recorded decay of seismicity results from the 1797 event, or a stronger earthquake before that time. The latter is corroborated by the low magnitude of the 1794 earthquake which would typically not be considered to cause long aftershock sequences.

GR a- and b-values, calculated for the individual segments, vary significantly along the VBTFS. Values range from 0.47 to 0.72 (b-values) and 0.81 to 2.08 (a-values), respectively. Data show a significant positive correlation of a- and b-values and a coincidence of the lowest b-values with fault segments with large seismic slip deficits and very low seismicity in the last about 300 years. These parts of the VBTFS were previously interpreted as “locked” fault segments which have a significant potential to release future strong earthquakes, in spite of the fact that historical and instrumentally recorded seismicity is very low. We find this interpretation corroborated by the low b-values that suggest high differential stresses for these fault segments.

1. INTRODUCTION

The Vienna Basin, a Miocene pull-apart basin between the eastern margin of the Alps and the Carpathian fold-thrust belt, is one of the most seismically active areas in intraplate Europe. The main active fault is referred to as the Vienna Basin Transfer Fault System (VBTFS), a major, about 380km long left-lateral strike-slip fault, that extends from the central Eastern Alps (Mur-Mürz Fault, Gutdeutsch & Aric, 1988; Brückl et al., 2010), crosses the entire pull-apart basin from SW to NE (e.g., Royden, 1985; Wessely, 1988; Kröll & Wessely, 1993; Decker, 1996; Decker et al., 2005; Beidinger et al., 2011) and proceeds into the Brezovské Karpaty area of the Carpathian fold-thrust belt. The fault is further traced into the area around Žilina in the Váh valley (Schenková et al., 1995; Gutdeutsch & Aric, 1988; Decker & Peresson, 1996; Sefara et al., 1998).

The spatial distribution of earthquakes along the part of the VBTFS in the Mur-Mürz valley, the Vienna Basin and the adjacent Brezovské Karpaty shows a peculiar pattern with concentrated activity in the south of the Vienna Basin and an apparent lack of earthquakes in its central and northern part (Figure 1; Hinsch & Decker, 2003; 2011). Here, we analyze the historical and instrumental records of earthquakes in this region in order to better understand the causes for this heterogeneous distribution.

The spatiotemporal correlation and energy release of earthquake occurrence is complex, but not random (Hainzl et al., 2003). The Gutenberg–Richter law states that the number of earthquakes with magnitude greater or equal to a certain magnitude occurring in a given time, decreases linearly with increasing magnitude (Gutenberg & Richter, 1942). The gradient of the Gutenberg-Richter (GR) relation, the so-called b-value, is commonly close to 1 in seismically active regions (Scholz, 2002). However, the b-value varies with respect to time, space, and magnitude ranges, since it is related to earthquake rupture dynamics, or seismic source characteristics (Senatorski, 2019). In addition, the b-value is observed to decrease with stress (Scholz, 1968). Therefore, Schorlemmer et al. (2004) proposed that spatially varying b-values can be used to forecast future seismicity more accurately than the approach in which one assumes a constant b-value equal to the average regional value.

Another possible cause of the documented heterogeneous earthquake activity might be the occurrence of long aftershock sequences. Aftershock activity is generally triggered by a strong earthquake. In the aftermath of a large earthquake, this aftershock activity leads to a local increase of seismic activity which later on decays back to a lower level labeled as ‘normal’ background seismicity (Stein & Liu, 2009). The length of an aftershock sequence can vary from a few months at plate margins to several years and even decades and centuries in intraplate regions (Stein & Lui, 2009), depending not only on the magnitude of the causing earthquake, but apparently also on the regional level of

background seismicity and the fault loading rate. At the northeast end of the Vienna Basin, the 1906 Dobrá Voda mainshock (M=5.7) has caused elevated seismicity in its near vicinity which is still visible today (Nasir et al., 2020). Therefore, we will check whether the seismic activity on other parts of the VBTFS can be explained as the result of a (pre-)historic strong mainshock.

In this publication, we will address the questions raised above using a newly compiled earthquake catalogue using the data by ZAMG (2020) and ACORN (2004) to cover the whole extent of the VBTFS. As the major part of the 754-years-long earthquake catalogue is based on intensity, we apply an empirical intensity magnitude conversion formula, which is derived from the catalogue.

2. TECTONIC SETTING

The Vienna Basin Transform Fault is an active fault system extending over a distance of some 380 km from the Eastern Alps through the Vienna Basin into the West Carpathians. Active sinistral movement is indicated by moderate seismic activity in a NE striking zone paralleling the fault, focal plane solutions and recent stress measurements (Decker et al., 2005). The Vienna Basin is regarded as one of the most prominent seismic active regions of Austria (Fig. 1). The pull-apart basin is oriented NE-SW and extends from the Semmering mountain range to the little Carpathians in Slovakia (Gutdeutsch & Aric, 1988). The VBTFS passes between the capitals of Austria (Vienna) and Slovakia (Bratislava), which are situated to the West and to the East of the fault zone, respectively

The VBTFS and the Vienna pull-apart basin started to develop in the Middle Miocene. Extension and basin subsidence initiated the Badenian (15.5 Ma) as dated by the growth strata of the basin fill (Royden, 1985; Wessely, 1988) and terminated in the Late Miocene (about 7-8 Ma; Peresson & Decker, 1997). Pull-apart basin formation was associated with about 30 km of sinistral displacement along the VBTFS which corresponds to an average Miocene sinsitral slip rate of 4 mm/y (Linzer et al., 2002; Decker et al., 2005). Since then, tectonic movement slowed down to a moderate level of 1-2 mm/a as determined by GPS geodesy (Grenerczy et al., 2000; 2005; see also Möller et al., 2011, for discussion). Geological data derived from the age and thickness of Quaternary sediments that accumulated in a Quaternary pull-apart basin (Mitterndorf Basin) indicate a slip rate between 1.5 and 2.6 mm/a (Decker et al., 2005).

Several studies have been carried out to evaluate the seismic energy release of the fault and compare it to geologically and geodetically derived slip rates, considering both, pre-instrumental and instrumental earthquake data (Hinsch & Decker, 2003; 2011). The cited studies revealed significant seismic slip deficits for the VBTFS as a whole, and several fault segments in particular. The largest slip

deficits were recorded for the Lassee- and Zohor Segments (see Fig. 1 (b) for location) and the SW part of the Mur-Mürz Fault which released virtually no seismic energy in historical times. These parts of the VBTFS were interpreted as currently locked segments.

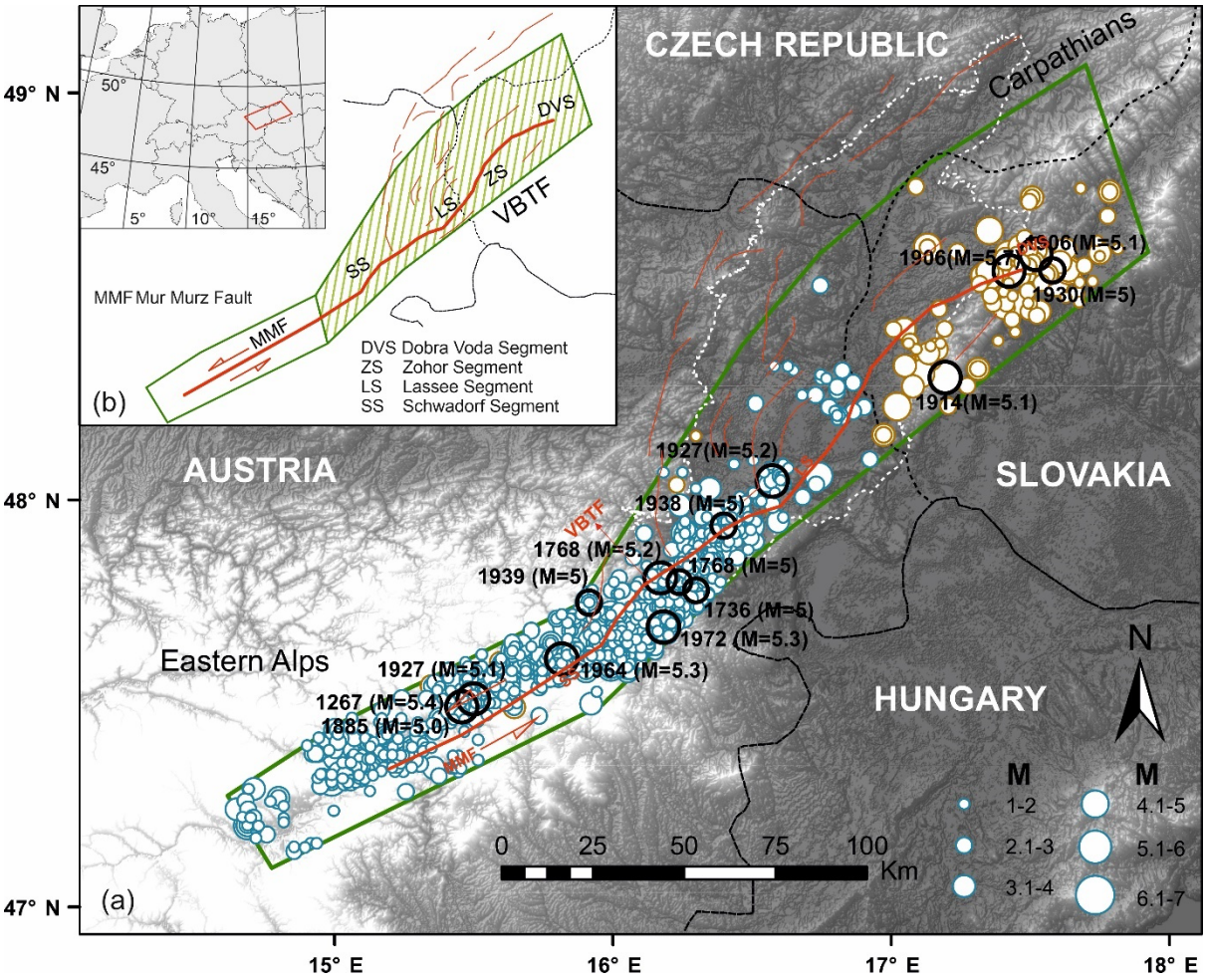

Figure 1: (a) Distribution of earthquakes along the Vienna Basin Transfer Fault System (VBTFS). Blue circles show earthquakes from the Austrian earthquake catalogue (ZAMG, 2020), brown circles are earthquakes listed in the ACORN (2004) catalogue. Black circles denote earthquake with M≥5. Green polygon indicates the extent VBTFS. Note the uneven distribution of seismicity with very low seismicity along the Lassee (LS) and Zohor (ZS) segments in the Vienna Basin as well as close to the SW termination of the Mur-Mürz-Fault (MM; see inset (b for location of the named segments). White stippled line marks the outline of the Miocene pull-apart basin. (b) Overview maps showing the extent of the VBTFS and locations of fault segments mentioned in the text.

Earthquakes of magnitude 5 tend to happen on average every 25 years along the VBTFS in the last about 250 years (Figure 1). The strongest recorded events are the earthquakes of 1267 Kindberg (I_0=VIII/M=5.4) and 1907 Dobra Voda (I_0=VII-IX/M=5.7). These magnitudes are well below the magnitude of Maximum Credible Earthquakes (MCE) estimated from the length and fault area of geologically defined fault segments (Decker & Hintersberger, 2011; Hinsch et al, 2011). The latter reveal MCE magnitudes between about M=6.0-6.8 for the different fault segments. The MCE estimates are supported by paleoseismological evidence (Hintersberger et al., 2014).

3. SEISMIC DATA AT VIENNA BASIN

Earthquake catalogues are one of the most important products of seismology. Before any scientific analysis it is necessary to assess the quality, consistency, and homogeneity of the data (Woessner & Wiemer, 2005). As the Vienna Basin is located partly in Austria and Slovakia, two earthquake catalogs have to be considered in order to cover the entire length of the VBTFS. The Austrian earthquake catalog includes both historical and instrumental data from 04.05.1201 to 06.05.2020 having a magnitude range of M_w=1-6.1 (ZAMG, 2020). However, in comparison to an older version that we used in earlier completeness studies (Nasir et al., 2013), one historical earthquake (27.08.1668; M= 4.6) at Wiener Neustadt and one instrumental earthquake (05.07.1973; M=0.7) have been removed from the new Austrian earthquake catalog.

The ACORN (2004) earthquake catalog covers a rectangular region encompassing the Eastern Alps, West Carpathians and Bohemian Massif (Czech Republic, Slovakia, Hungary and Austria; Lenhardt et al., 2007). The temporal span of the ACORN earthquake catalog is between 1267 to 2004 with a magnitude range from 0.5 to 5.7.

Both, the Austrian earthquake catalogue (ZAMG, 2020) as well as the ACORN earthquake catalogue, are dominated by pre-instrumental earthquake data. Generally, historical earthquake data is reported with intensity, which is then converted into magnitude. For this conversion different formulas and empirical correlations were suggested for countries in Central Europe (Grünthal et al., 2009). The conversion of intensity into magnitude for the Austrian catalogue is obtained by the formula M= $2/3I_0$ (Lenhardt, 2007). Conversion for the ACORN earthquake catalog is given by the following formula (Grünthal et al., 2009).

$M_w = 0.682I_0 + 0.16$ (not considering focal depth)

$M_w = 0.667I_0 + 0.3\log(h) + 0.1$ (considering focal depth)

Where h is the focal depth and I_0 is the macroseismic intensity.

In the region of the VBTFS, the majority of earthquakes are listed with hypocenter depth up to 10 km. The maximum depth is 35km. Comparison of both catalogs in the overlapping region (Figure 2a) shows the effect of the use of different intensity-magnitude conversions. Intensity to magnitude conversions for historical earthquakes for intensities $3 \leq I_0 \leq 6$ in the ACORN catalog reveal magnitudes that are significantly higher than the values listed in the Austrian earthquake catalogue (Figure 2a; ZAMG, 2020). The same things are true for comparison of earthquakes recorded in the Figure 2b.

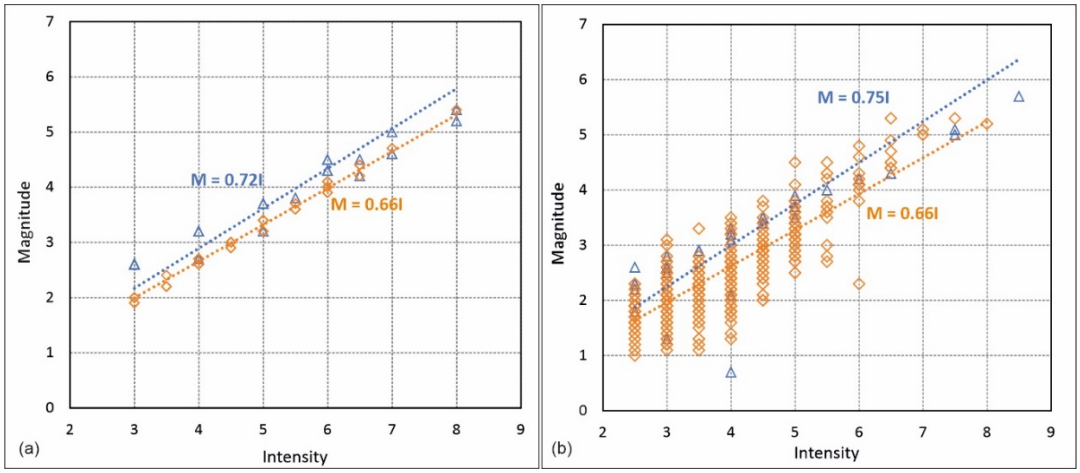

Figure 2: Intensity vs magnitude plot for earthquakes in the overlapping region of the ACORN (2004, blue triangles) and ZAMG (2020, orange diamonds) earthquake catalogues for historical earthquakes covering the time of 1267-1905 (a), and instrumental data covering the length of 1906-2020 (b). The ACORN earthquake catalogue stops in 2004.

Comparison of the intensity-magnitude correlations in the ACORN catalogue for historical earthquakes ($M=0.72I_0$) and instrumental earthquakes ($M=0.75I_0$) reveals very little differences. Both correlations differ significantly from intensity-magnitude correlation ($M=0.66I_0$) used in the Austrian earthquake catalogue for both, historical and instrumental earthquake data (Figure 2a,2b). Intensity-magnitude correlations in the Austrian catalogue therefore reveal systematically lower magnitude values for earthquakes, which were only recorded by their epicentral intensity. For intensity VI to VII earthquakes the difference is about 0.5 magnitude scales.

The observed discrepancy between the two catalogues poses some limitations to the evaluation of the a- and b-values of GR relations derived from the combined catalogues because the calculations are based on magnitude, not on intensity. As both of the used catalogue are dominated by historical data, these limitations may be significant.

4. COMPILATION, DELUSTERING AND COMPLETENESS ANALYSIS OF THE COMPILED CATALOGUE COVERING THE VBTFS

The recognition and removal of fore- and aftershocks from the raw catalogues is mandatory for further work based on the earthquake data such as the calculation of GR parameters and the assessment catalogue completeness because it is generally assumed that earthquakes are poissonian-distributed and therefore independent of each other (Gardner & Knopoff, 1974; Shearer & Stark, 2011).

The earthquake data used in the current study was compiled from the Austrian and ACORN earthquake catalogues to cover the whole extent of the VBTFS (Fig. 1). The compilation became necessary as existing regional catalogues such as the catalogue by Grünthal et al. (2003) set the lower magnitude level for the catalogue entries at Mw=3.50. For the area of the VBTFS such a lower cut-off removes a large part of the recorded seismicity.

The seismic data for the VBTFS in ZAMG (2020) and ACORN (2004) comprise a magnitude range M=0.5-5.7 and cover a nominal time period of 754 years from 1267-2020 (738 years for the ACORN data). The clustered compiled earthquake catalogue records 1739 seismic events. Duplicate earthquakes have been removed manually for the area as shown in Figure 1. For the overlap area the Austrian earthquake catalogue has been given priority and duplicate earthquakes were removed from the ACORN catalogue.

Figure 3 shows the distribution of earthquakes at VBTFS with respect to time. The figure clearly shows that, although the nominal time coverage of the combined catalogue is about 750 years, only eight earthquake records are available from the period prior to 1800. Marked increases of the numbers of recorded earthquakes are observed around 1900 and close to the end of the 20th century.

Using same method as in Nasir et al. (2013), the compiled data set was declustered manually using fault length-magnitude correlations to determine the maximum distance of aftershocks from the magnitude of the preceding main shock (Wells & Coppersmith, 1994) and standard time windows after the mainshock according to Gardner & Knopoff (1974). To account for possible inaccurately determined earthquake locations the minimum distance is set to 10km for the spatial window. For more detail we refer to Nasir et al. (2013; 2020). The earthquake data after declustering comprises of 1603 earthquakes including 12 earthquakes with magnitudes greater than or equal to 5 (Figure 3). 9 of these strong earthquakes were recorded in the last about 150 years.

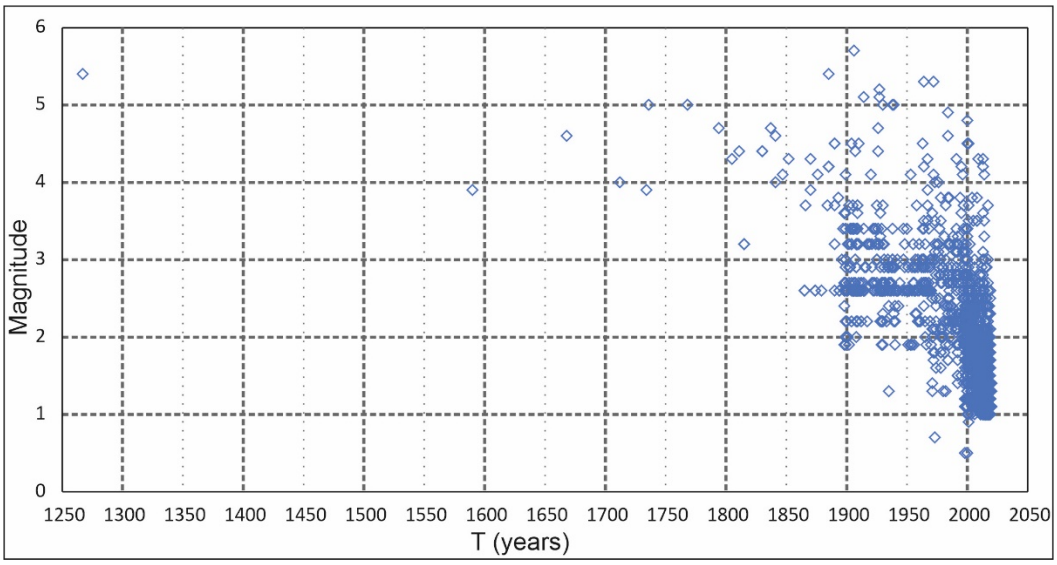

Figure 3: Magnitude vs. time plot from the combined catalog (ZAMG, 2020; ACORN 2004).

The compiled catalogue was subjected to completeness checks using two different methods. The reasons for repeating the completeness analyses reported by Nasir et al. (2013) are the use of an updated catalogue for Austria, which now extends up to 2020 and includes revisions made according to the historical earthquake research by Hammerl & Lenhardt (2013). Secondly, the region analyzed in this study is considerably larger than the area examined by Nasir et al. (2013), which did not extend to the Mur Mürz Fault.

4.1 TCEF completeness analysis

TCEF (Temporal Course of Earthquake Frequency) is the most widely used method for completeness analyses in Central Europe (e.g., Lenhardt, 1996; Grünthal et al., 1998). In this method, the cumulative number of earthquakes of a magnitude class is plotted versus time. Slope changes in the plot illustrate changes of the completeness of the catalogue (Nasir et al., 2013, Grünthal et al., 1998). It is common presumption that the latest steepening of the slope occurred when the data became complete for the magnitude class under consideration (Gesperini & Ferrari, 2000). Completeness-corrected recurrence intervals for each magnitude class are then calculated from the time interval corresponding to the latest linear segment of the curves and the number of records in this time interval (Nasir et al., 2013).

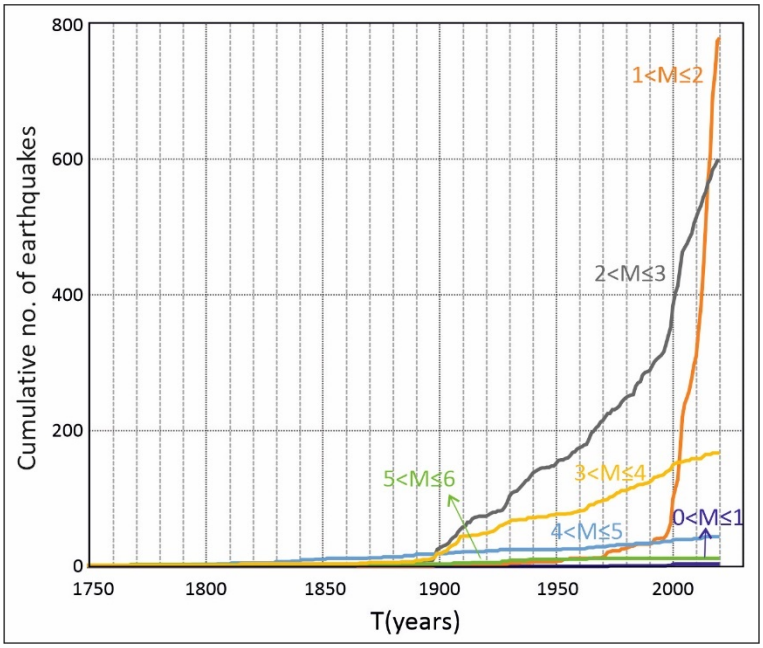

Figure 4: Cumulative number of earthquakes vs. time (TCEF) for the combined catalog covering the VBTFS. The steepest slope in the plot for an individual magnitude class indicates that the catalogue is complete for that period of time. Note that the magnitude class 0≤M<1 never reaches completeness. Changes in slope for the intensity classes of 1≤M<2 and 2≤M<3 in 2004 are due to the ending of the ACORN catalog in this year.

M	Completeness period (TCEF)
1<M≤2	1897-2020
2<M≤3	1897-2020
3<M≤4	1885-2020
4<M≤5	1793-2020
5<M≤6	1885-2020

Table 1: TCEF derived periods of complete earthquake records along the VBTFS.

The overall analysis in Figure 4 shows significantly steepening slopes for all magnitude classes M<4 around 1900. These changes relate to the onset of regular earthquake records in the former Austro-Hungarian Empire in the aftermath of the 1895 Ljubljana earthquake.

TCEF results further show that records of magnitude class 0≤M<1 cannot be regarded complete at any time because the slope of the corresponding curve is much lower than the one of intensity class 1≤M<2 indicating that by far not all events with M<1 were recorded in recent years. Periods of complete records along the VBTFS range from 24 years for magnitude class1≤M<2 to 223 years for magnitude class 4≤M<5. For magnitude class 5≤M<6, which contains only 12 earthquakes, complete records are estimated to start in 1884 (Table 1).

4.2 Stepp completeness analysis

Stepp (1972) proposed a statistical approach to analyze catalogue completeness. The test relies on the statistical property of the Poisson distribution highlighting time intervals during which the recorded earthquake occurrence rate is uniform (Stepp, 1972). The method was described in detail by Nasir et al. (2013). The magnitude classes are analyzed for completeness using time windows of different length in the time period between 1267 and 2020 (754 years; Figure 5). The calculation uses ten time windows of 10 years (1901-2020), two time windows of 50 years (1801-1900) and one time-window covering 534 years (1267-1800). The corresponding completeness of all magnitude classes are estimated manually from the parts of the calculated curves that follow a linear trend parallel to 1/√T line. For the corresponding time intervals, the mean rate of occurrence of earthquakes of the analyzed magnitude class is stable.

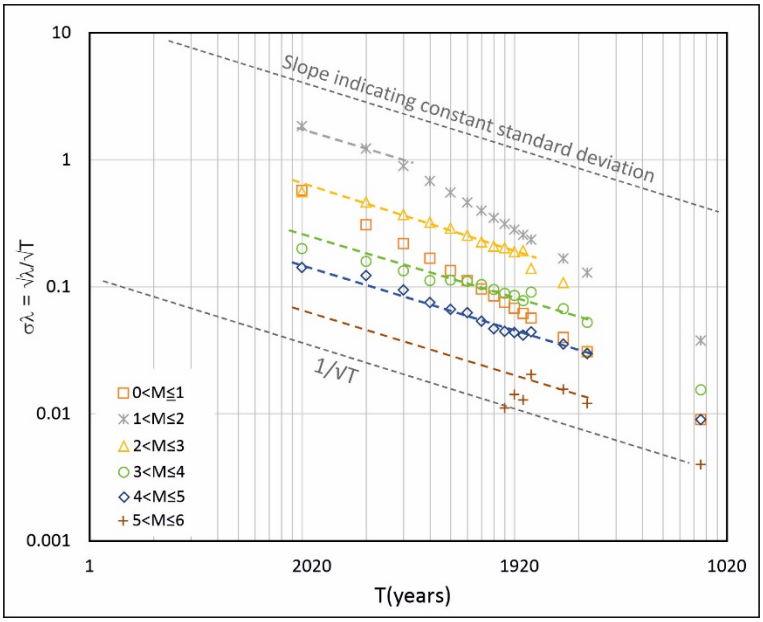

Figure 5: Stepp completeness analysis of the combined catalog covering the VBTFS. The graph shows the standard deviation of mean rate of earthquakes occurrences plotted vs. time. Colours indicate individual magnitude classes. The catalogue is regarded complete for the time period for which the

standard deviation (σ) of the mean recurrence rate (λ) of earthquakes of a given magnitude class follows the dashed 1/√T trend line. Where it deviates from that line, the catalogue is considered incomplete. Note that the magnitude classes of 0≤M<1 and 5≤M<6 never reach completeness.

Magnitude	Completeness period (Stepp Test)
1<M≤2	-
2<M≤3	1911-2020
3<M≤4	1801-2020
4<M≤5	1801-2020
5<M≤6	1875-2020

Table 2: Comparison of VBTFS, Stepp analysis in Nasir et al, 2013 with Stepp analysis in 2020. This completeness analysis was with intensity and now analysis is with magnitude of VBTFS.

The completeness period for 1≤M<2 is only 20 years (2001-2020), for 2≤M<3is 110 years (1911-2020), for 3≤M<4 and 4≤M<5 is 220 years (1801-2020). For the highest magnitude class 5≤M<6 in the catalogue is regarded complete since 1875. The intensity-based completeness analysis for VBTFS (Nasir et al., 2013) in comparison revealed 109 years to 209 years completeness time windows for the III<I_o≤IV and VI<I_o≤VII and the intensity class. Intensity class VII<I_o≤VIII did not include enough earthquakes to calculate a stable recurrence interval (Table 2).

5. LONG- AND SHORT-DURATION AFTERSHOCK SEQUENCES

Large earthquakes are typically followed the aftershock activity, which generally is assumed to decay hyperbolically as stated by Omori's law (Ogata, 1983). Based on empirical data, Stein & Liu (2009), on the other hand, suggested that large earthquakes may have much longer aftershock sequences, which depend on the slip rate of faults and may last for decades or even centuries. At the VBTFS, the 1906 Dobrá Voda was identified as an example of such a long aftershock sequence (Nasir et al., 2020). Deciding whether the earthquake activity in a defined region can be related to a long aftershock activity subsequent to a strong earthquake is challenging because the definition of aftershock activity depends on numerous parameters such as the definition of the area treated as aftershock zone and the level of background seismicity before the mainshock (Stein & Liu, 2009).

Figure 6 illustrates two examples of short- and long-term patterns of decaying earthquake forming aftershock sequences. Seismicity subsequent to the 1906 Dobrá Voda earthquake (Figure 6a) has been described in detail by Nasir et al. (2020). The Dobrá Voda earthquake of 09.01.1906 (M=5.7) at the VBTFS in Slovakia initiated earthquake activity in vicinity of the mainshock which is gradually decaying since 1906. The pattern shown in Figure 6a suggests that aftershock activity extends to the present. Figure 6b, on the other hand, shows the seismicity in the time before and after the 11.07.2000 (M=4.8) Ebreichsdorf earthquake. In this case the aftershock activity decayed hyperbolically and reached the level of background seismicity within about 300 days after the mainshock.

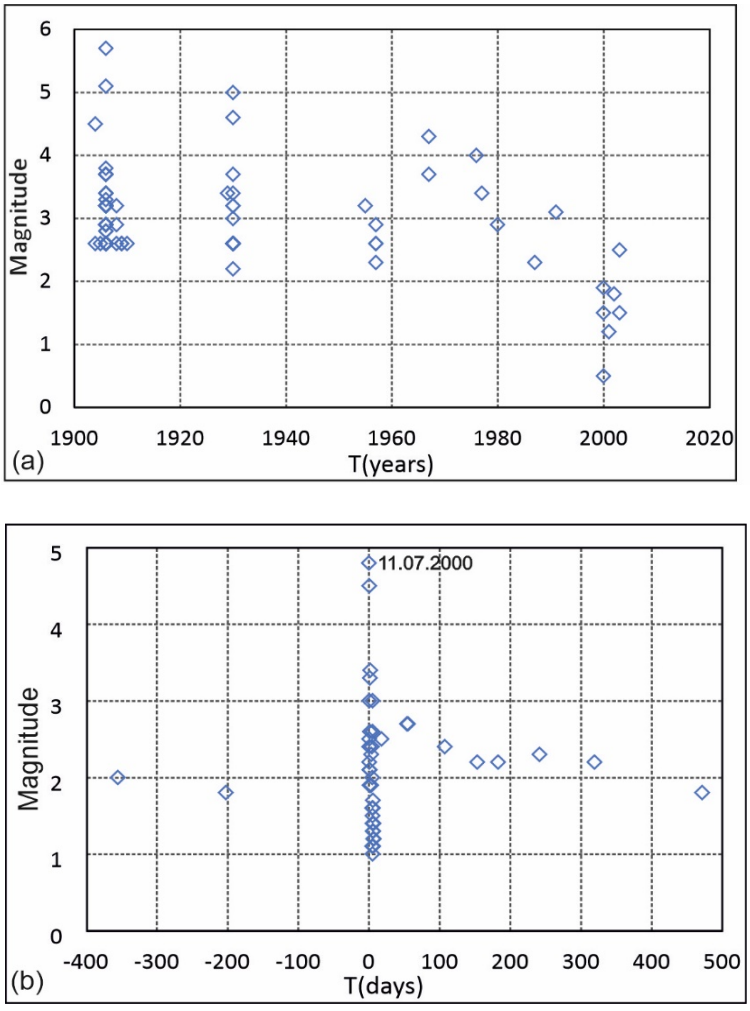

Figure 6: Different pattern of decaying earthquake activity. (a) Long aftershock sequence of 09.01.1906 (M=5.7) earthquake. (b) Short (Omori-type) aftershock sequence subsequent to the 11.07.2000 (M=4.8) Ebreichsdorf earthquake.

In order to identify seismicity patterns that may be indicative of long-term aftershock sequences comparable to the 1906 Dobrá Voda example, we divide the VBTFS into arbitrarily selected segments. Seismicity recorded for each of these segments is further analyzed to check whether it shows distinctive patterns of decaying earthquake activity which may be related to long aftershock sequences. The purpose is to identify possible strong earthquakes which occurred before the start of records in the earthquake catalogue, and which may become "visible" due to their aftershock sequences.

6. SEISMICITY OF ARBITRARILY SELECTED SEGMENTS OF THE VBTFS

The VBTFS is divided into eight segments of approximately 50km length. Segments are selected to overlap each other for not missing possible aftershock sequences which followed earthquakes that occurred close to one of the segment boundaries (Figure 7). The arbitrarily selected segment boundaries do not agree with the kinematic fault segments of the VBTFS defined on the basis of fault geometry (Hinsch & Decker, 2011; Beidinger & Decker, 2011). The selection of segment lengths of about 50 km is driven by the MCE estimates of M=6.0-6.8 for the VBTFS (Decker & Hintersberger, 2011). Earthquakes with such magnitudes are broadly associated with slip on <50 km long faults (Wells & Coppersmith, 1994). It is therefore assumed that for each possible strong earthquake the full length of the slipped fault is contained by one of the segments. The selection of segment length and overlaps is further guided by the consideration of inaccuracies of epicenter locations of historical earthquake data and the necessity of a minimum number of earthquakes for defining GR relations.

Segments 1 and 2 are located in Slovakia and include the strongest earthquake recorded at the VBTFS (1906 Dobrá Voda, M=5.7). The segments contain 207 and 96 earthquakes with M=0.5-5.7, respectively. Time coverage is 1805-2004 (segment 1) and 1794-2017 (segment 2). The first data entry in segment 2 (1794, M= 2.6) is followed by a data gap until 1852 (M=4.3). Time series of both overlapping segments 1 and 2 show a general decay of seismicity which starts with the 1906 Dobrá Voda (M=5.7) earthquake (Figure 8). The temporal evolution of seismicity in segment 1 around Dobrá Voda reveals a level of background seismicity with M=2.6-4.3 (11 earthquakes) recorded between about 1800 and 1906. While the significant earthquakes (M=4-5) in the time before 1906 are scattered over the entire region, seismicity concentrates within a distance of less than 13 km from the epicenter after the 1906 Dobrá Voda mainshock, (Nasir et al., 2020). The time-magnitude plot includes a second strong earthquake in 1914 (M=5.1) which is regarded as an aftershock of the 1906 event. The distance between the epicenters of the two events is 33km. The slow regular decrease of the largest observed magnitudes over time until 2004 (end of the ACORN catalogue) suggests that the aftershock sequence

lasted much longer than predicted by the Omori law. The level of background seismicity with M=2.6-4.3 (11 earthquakes) recorded before the 1906 Dobrá Voda earthquake between about 1800 and 1900 is only reached about 100 years after the mainshock.

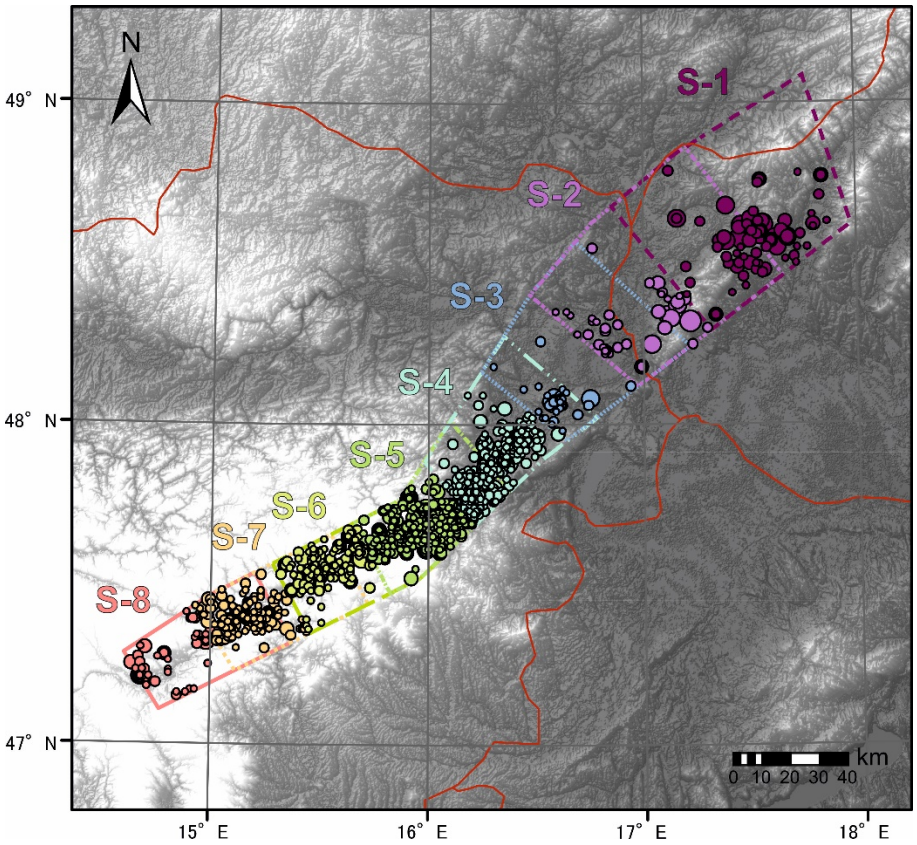

Figure 7: Subdivision of the VBTFS into 8 arbitrary overlapping segments of about 50 km length used for the analysis of aftershock sequences and calculation of GR-parameters. See text for further explanation.

Segment 3 of covers the border region between Austria and Slovakia. It includes 78 earthquakes with M=1-5.2 for the time period 1890 to 2017 (Figure 8). The time plot shows 4 earthquakes in 1890 including a main shock (M=4.5) and three aftershocks with different epicenter locations within distances of 5 km from mainshock (Figure 8). The 1927 Schwadorf earthquake (M=5.2) is followed by a short aftershock sequence. The apparent long-term decay of seismicity in the temporal window cannot be regarded to be related to aftershock activity due to the distance of events from the Schwadorf mainshock (Figure 8).

Magnitudes recorded in segment 4 range from M=1-5.2 with data length from 1590-2019 and a total number of 487 earthquakes (Figure 8). This segment shows no temporal seismicity pattern that could indicate gradual decays of seismicity except for the 1927 Schwadorf (M=5.2) earthquake (see above).

For segment 5 magnitudes between M=1-5.3 were recorded for 673 events between 1668 and 2020. Records start from 1668 with M=4.6 at Wiener Neustadt (ACORN, 2004) followed by another earthquake in 1712 having M=4 at the same epicenter (Figure 8). It must be noted that the 1668 event has been excluded from ZAMG (2020) based on the assessment by Hammerl & Lenhardt (2013). The next earthquake occurred in 1736 of M=5 is 5km away from Wiener Neustadt at Neudörfl. For the next stronger event on 1768 (M=5) ZAMG (2020) also lists an epicenter at about 5 km distance from Wiener Neustadt. In sum, 5 out of 7 earthquakes recorded between 1668 and 1841 are listed with epicenters in close proximity to each other. It can, however, not be judged if the observed clustering correctly reflects the spatial distribution of seismicity, or it is due to inaccurate location of the historical events (compare Gangl & Decker, 2011). In the time before 1898 only 7 earthquakes were recorded in a period of 230 years. Seismicity patterns indicative of aftershock sequences are not evident. Distances between the epicenters of earthquakes between 1898 and 1964 that might indicate an apparent increase of the maximum recorded magnitudes from about M=4 to M=5.3 are too large to identify the events as fore- or aftershocks.

Segment 6 includes 506 earthquakes with M=1-5.4 that occurred between 1267 and 2020. The significant recorded earthquakes are 1267 Kindberg (M=5.4), 1811 Krieglach (M=4.4), 1830 Mürzzuschlag (M=4.4) and 1837 Mürzzuschlag (M=4.7; Figure 8). The magnitude-time plot does not include any pattern indicative of aftershocks. All earthquakes are randomly distributed over the approximately 50 km long segment.

The nominal record length for segment 7 covers is 754 years (362 earthquakes). Records, however, contain no data for the 527 years between 1267 (Kindberg, M=5.4) and 1794 (Leoben, M=4.7). The next notable earthquakes followed in 1811 (Krieglach, M=4.4), 1830 (Leoben, M=4.4) and 1847 (Kindberg, M=4.1). The earthquakes in 1794 and 1830 are placed to epicenters with 1.3 km distance (Leoben). The other three events mentioned above occurred at the distances of 10km from each other. The distance of 40 km between the two groups, however, does not suggest linkage.

For segment 8, ZAMG (2020) lists 259 earthquakes with a first data entry of the 1794 Leoben earthquake. From the time between 1794 and 1899 only two earthquakes are secured by historical records. In spite of the poor data coverage, the time-magnitude plot shows a gradual decrease of the largest observed magnitudes between 1794 and the 1980ies. The strongest events of this row (1794 Leoben; 1830 Leoben; 1899 St. Stefan) occurred at a nominal distance of some 10km not contradicting

an interpretation as aftershocks. Interpreting the declining seismicity as a long aftershock sequence of a strong earthquake must, however, remain uncertain at the background of the poor earthquake record and the inaccuracies inherent in the determination of the historical epicenters.

In addition to the temporal distribution of seismicity along the VBTFS, we analyzed the frequency-magnitude correlation of earthquakes for the whole fault and the 8 selected fault segments. The correlation is stated by the GR relation which can be, written as

$$\log N(Mc) = a - bM$$

where N is the number of events with magnitudes larger than the magnitude of completeness Mc and a is the corresponding level of seismic activity (Gutenberg & Richter, 1942).

Figure 9 shows the results of calculating GR relations for the entire VBTFS. The graph shows that the actual values of the GR a- and b-values differ when using different completeness corrections. Without applying any correction, the b-value obtained from the declustered catalogue of the VBTFS is 0.57 which is low for a seismically active region. Applying the Stepp and TCEF corrections leads to a significant increase of the a-values. The b-values after TCEF and Stepp correction are 0.85 and 0.74 (Figure 9). The b-value calculated for the VBTFS from the catalogue without completeness correction leads to underestimate the number of earthquakes with smaller and medium magnitude. The frequencies of small magnitude earthquakes resulting from TCEF and Stepp correction is almost identical. The TCEF correction, however, seems to underestimate the frequency of earthquakes of higher magnitudes by the higher b-value because TCEF includes the highest magnitude earthquakes based on the assumption that records of these earthquakes are complete for the whole length of the catalogue. Stepp completeness analysis, however, shows that the number of earthquakes of the highest magnitude class ($5<M\leq6$) is too small to calculate a reliable recurrence rate. The corresponding data is therefore not considered in the GR calculation (see Nasir et al., 2013, for a more detailed discussion). We regard the results obtained after Stepp correction to be more reliable for extrapolating the recurrence periods of large magnitude earthquakes.

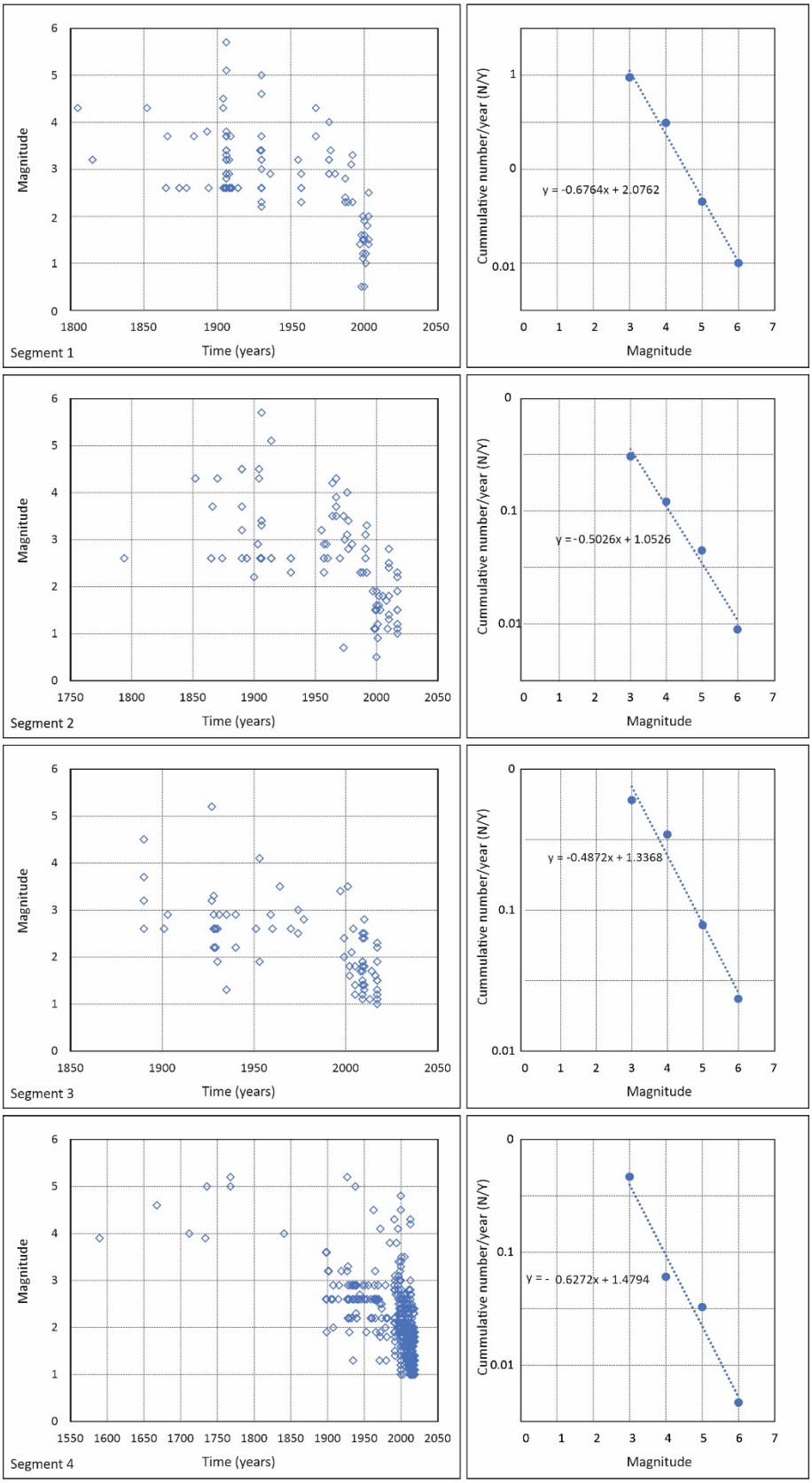

Figure 8: Figure caption on next page.

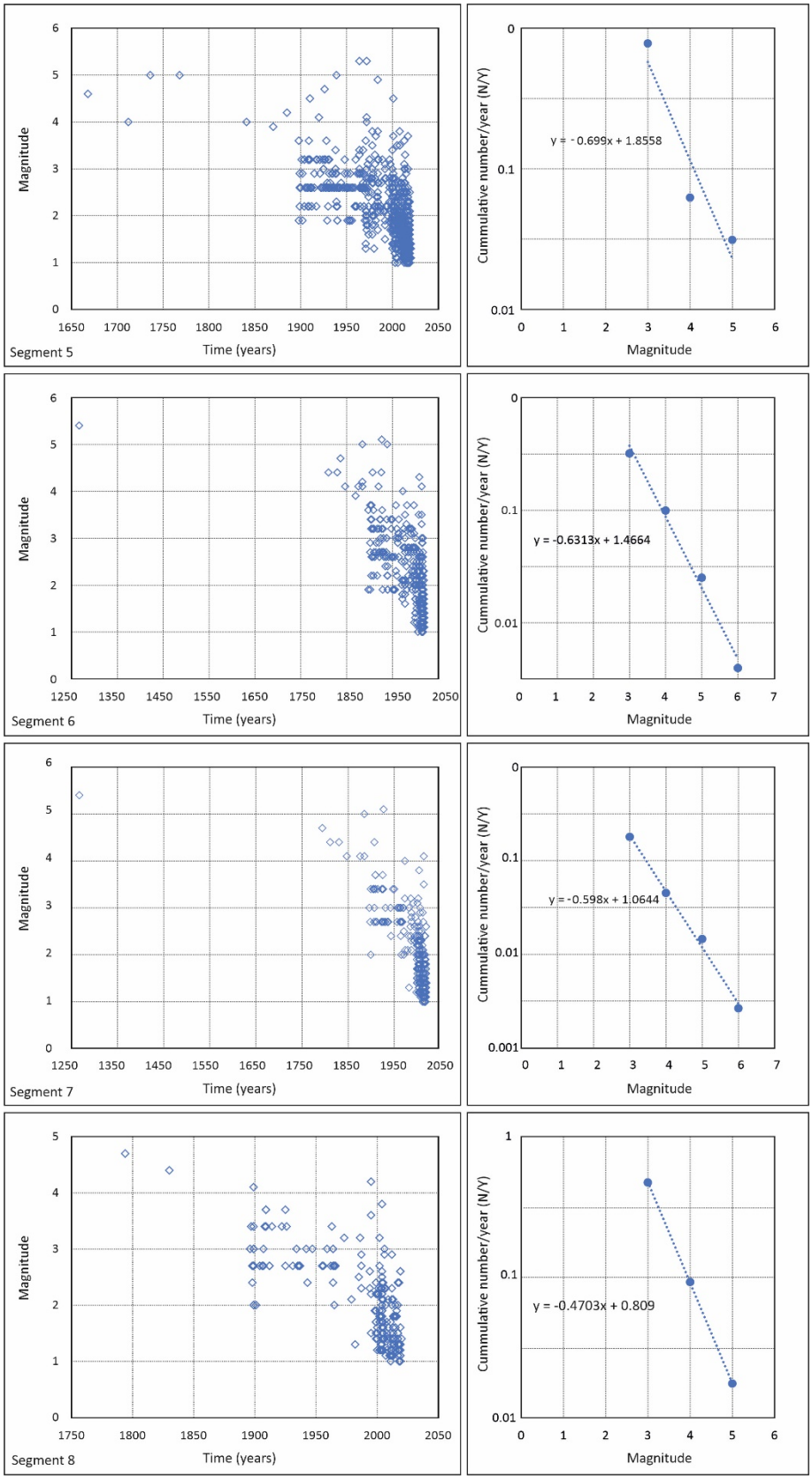

Figure 8 (continued): Figure caption on next page.

Figure 8: Time vs. magnitude plots (left column) and Gutenberg-Richter diagrams (right) for segments 1-8 of the VBTFS. See Fig. 7 and 10 for location segment locations. Segment 1 and the overlapping segment 2 show the 1906 Dobrá Voda long aftershock sequence. The time-magnitude diagram for segment 3 shows decaying seismicity after the 1927 Schwadorf earthquake. Segment 4 is includes the short aftershock sequence following the 2000 Ebreichsdorf mainshock (compare Figure 6b). Note that segments 3 to 7 do not show temporal seismicity patterns comparable to the long-term decay after the 1906 Dobrá Voda earthquake (segment 1 and 2). Segment 8 shows a regular decrease of the largest recorded magnitudes after the 1794 Leoben earthquake that is comparable to the patterns subsequent to 1906 Dobrá Voda and might indicate a long aftershock sequence.

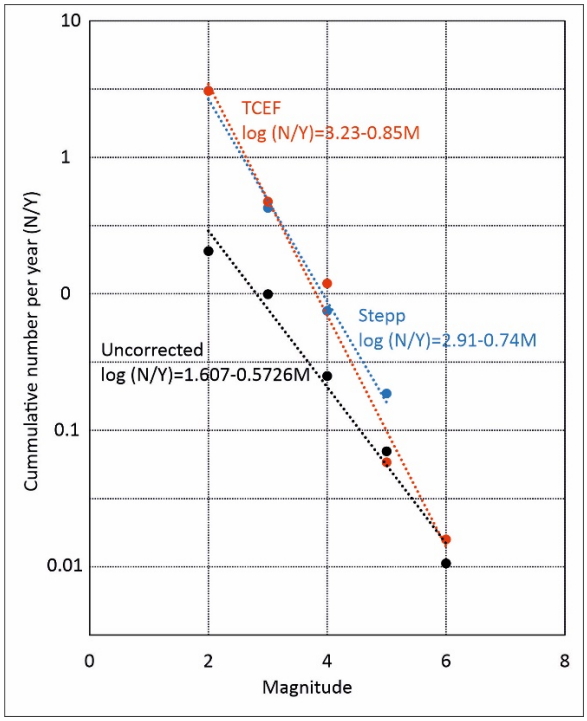

Figure 9: Comparison of Gutenberg-Richter relations obtained for the VBTFS from the declustered compiled catalogue without applying completeness correction (black), after TCEF completeness correction (red) and after Stepp correction (blue). See text for discussion.

The GR relations calculated for the 8 arbitrarily selected segments of the VBTFS are shown in Figure 8. The values were calculated from the uncorrected declustered catalogue as it was not possible to apply completeness correction on individual segments. The numbers of recorded earthquakes in the individual segments proved insufficient for applying the TCEF or Stepp method for each magnitude class.

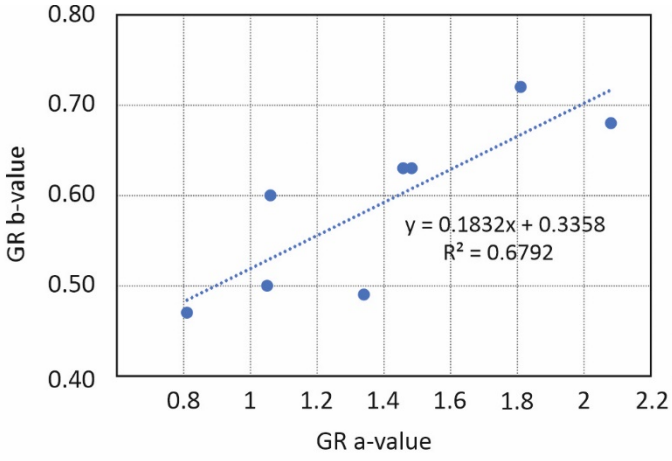

Segment	GR a-value	GR b-value
1	2.08	0.68
2	1.05	0.50
3	1.34	0.49
4	1.48	0.63
5	1.81	0.72
6	1.47	0.63
7	1.06	0.60
8	0.81	0.47

Figure 10: a- and b-values of the Gutenberg-Richter relations calculated for 8 segments of the VBTFS. See Figure 10 for segment location.

The GR relations calculated for the 8 arbitrarily selected segments of the VBTFS are shown in Figure 8. The values were calculated from the uncorrected declustered catalogue as it was not possible to apply completeness correction on individual segments. The numbers of recorded earthquakes in the individual segments proved insufficient for applying the TCEF or Stepp method for each magnitude class.

The results show that both, GR a- and b-values vary significantly between the segments, reaching from 0.81 to 2.08 (a-values) and 0.47 to 0.72 (b-values; Figure 10). The smallest b-values (0.47-0.50) are calculated for segments 2, 3 and 8. Visual inspection of the seismicity along the VBTFS shows that these segments are characterized by the lowest earthquake activity in historical times (Figure 11).

7. DISCUSSION AND CONLUSIONS

The analyses of time sequences of earthquakes recorded in 8 arbitrarily selected segments of the VBTFS was performed to identify possible long aftershock sequences subsequent to major earthquakes. Analyses were stimulated by Stein & Liu (2009) who suggest aftershock durations of tens to several hundreds of years for slow moving faults with fault loading rates of few mm/year. Nasir et al. (2020) show that this model is at least applicable to the 1906 Dobrá Voda (M=5.7) earthquake, which is followed by a century-long aftershock sequence.

Assessments of earthquake time sequences along the VBTFS is strongly limited by the length and completeness of available earthquake records. TCEF and Stepp completeness tests show that tolerably complete records only exist for the last about 200-300 years.

With exception of segment 8, time sequences obtained for fault segments apart from the 1906 Dobrá Voda (M=5.7) earthquake did not reveal long-term decays of seismicity that might be interpreted as long aftershock sequences. Segment 8, covering the southwestern tip of the VBTFS, revealed a 200 years long gradual decrease of the largest observed magnitudes starting with the 1794 Leoben (M=4.7) earthquake. Epicentral distances of the largest events in the row allow an interpretation as aftershocks. The 1794 event is the oldest earthquake listed in the catalogue for the region under consideration. It must therefore remain open if the recorded decay of seismicity results from the 1797 event, or a still older, possibly stronger earthquake before. The latter is corroborated by the low magnitude of the 1794 earthquake which would typically not be considered to cause long aftershock sequences. The 2000 Ebreichsdorf (M=4.8) earthquake, contained in segment 4, was followed by an Omori-type aftershock sequence which lasted for a few hundred days only.

Calculations of the GR relations for the 8 analyzed fault segments reveal important differences between the a- and b-values of the individual segments (Figure 10, 11). Segments 2,3 and 8 with the lowest b-values 0.49, 0.50 and 0.47, respectively, coincide with those parts of the VBTFS for which Hinsch & Decker (2011) calculated the largest highest seismic slip deficits by comparing the seismic energy release and geodetically/geologically derived slip rates of the VBTFS. For the part of the VBTFS in segment 3 of this study Hinsch & Decker (2011) state seismic slip rates between 0 and 0.1mm/a. These rates compared to geodetically/geologically derived slip velocities in the range of 1-2mm/y. The highest b-values of 0.68 and 0.72 calculated for segments 1 and 5, on the other hand, include parts of the VBTFS with seismic slip rates of about 0.5mm/a (Dobrá Voda area) and 0.7-1.1mm/a (northeastern part of the Mur-Mürz fault and southwestern Vienna Basin). Data therefore indicate that GR b-values correlate negatively with the seismic slip deficit of the VBTFS. A similar negative correlation of b-values and the slip deficit rate was reported by Nanjo & Yoshida (2018).

Variations of the GR b-value are commonly related to different states of stress in the deformation zone (Scholz, 1968; 2015) with low b-values indicating high differential stress (Farrell et al., 2009; Scholz, 2015). GR b-values are therefore considered to be proxies of stress which identify highly stressed fault segments or asperities that resist slip (Schorlemmer & Wiemer 2005; Nuannin, 2006). Low b-values were also related to knickpoints and changes of fault strike (Öncel et al., 1996). It is assumed that such highly stressed segments are locations where future ruptures are likely to occur (Schorlemmer & Wiemer, 2005; Bayrak & Bayrak, 2012; Hussain et al., 2020). At least for plate

boundaries, this assumption is corroborated by the finding that small b-values characterized the focal areas of strong earthquakes prior to fault rupture (Nanjo et al., 2012; Nanjo & Yoshida, 2021).

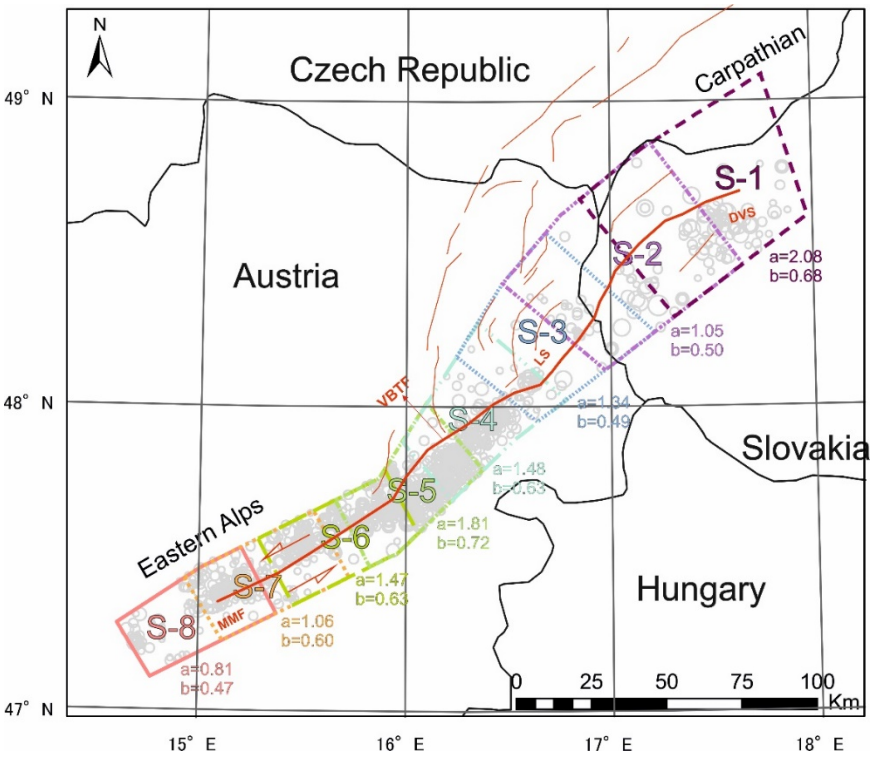

Figure 11: Gutenberg-Richter a- and b-values calculated for 8 arbitrarily selected overlapping fault segments. Note the variation of b-values ranging from 0.47 to 0.72. Fault segments with low levels of historical and instrumental seismicity (S2, S3 and S8) are characterized by low GR b-values.

For the VBTFS, fault strands with high seismic slip deficits such as the ones next to the Lassee- and Zohor segment (see Figure 1 for location) were previously interpreted as “locked” fault segments which have a significant potential to release future strong earthquakes, in spite of the fact that historical and instrumentally recorded seismicity is very low (Hinsch & Decker, 2003; 2011). This interpretation is corroborated by the low b-values that suggest high differential stresses for these segments.

REFERENCES:

ACORN, **2004**. Catalogue of Earthquakes in the Region of the Alps - Western Carpathians– Bohemian Massif for the period from 1267 to 2004. Computer File, Vienna (Central Institute for Meteorology and Geodynamics, Department of Geophysics). Brno (Institute of Physics of the Earth, University Brno.

Bayrak, Y., & Bayrak, E., **2012**. Regional variations and correlations of Gutenberg–Richter parameters and fractal dimension for the different seismogenic zones in Western Anatolia. Journal of Asian Earth Sciences 58, 98–107.

Beidinger, A., & Decker, K., **2011**. 3D geometry and kinematics of the Lassee flower structure: Implications for segmentation and seismotectonics of the Vienna Basin strike–slip fault, Austria. Tectonophysics, 499, 22-40. doi: 10.1016/j.tecto.2010.11.006

Brückl, E., Behm, M., Decker, K., Grad, M., Guterch, A., Keller, R., & Thybo, H., **2010**. Crustal structure and active tectonics in the Eastern Alps. Tectonics 29, 279–295.

Decker, K., **1996**. Miocene tectonics at the Alpine–Carpathian junction and the evolution of the Vienna Basin. Mitteilungen der Gesellschaft der Geologie- und Bergbaustudenten 41, 33–44.

Decker, K., & Hintersberger, E., **2011**. Assessing Maximum Credible Earthquake (MCE) Magnitudes for a Slow Intra-Plate fault system in the Vienna Basin, Austria. Seismological Research Letters, 82/2, 300.

Decker, K., & Peresson, H., **1996**. Tertiary kinematics in the Alpine-Carpathian-Pannonian system: links between thrusting, transform faulting and crustal extension, In: Wessely, G., Liebl, W. (Editors), Oil and Gas in Alpidic Thrustbelts and Basins of Central and Eastern Europe, European Association of Geoscientists and Engineers, 5, 69-77.

Decker, K., Persson, H., & Hinsch, R., **2005**. Active tectonics and Quaternary basin formation along the Vienna Basin Transform fault. Quaternary Science Reviews, 24,307-322.

Farrell, J., Husen, S., & Smith, R.B., **2009**. Earthquake swarm and b-value characterization of the Yellowstone volcano-tectonic system. Journal of Volcanology and Geothermal Research, 188, 260-276.

Gangl, G., & Decker, K., **2011**. Österreichische Starkbeben mit Intensität ab Grad 7. Österreichische Ingenieur- und Architekten-Zeitschrift, ISSN: 0721-9415, 156, 229-237.

Gardner, J.K., & Knopoff, L., **1974**. Is the sequence of earthquakes in southern California, with aftershocks removed, poissonian? Bulletin of the seismological Society of America, 64, 1363-136

Gasperini, P., & Ferrari, G., **2000**. Deriving numerical estimates from descriptive information: the computation of earthquake parameters. In Catalogue of Strong Italian Earthquakes from 461 B.C. to 1997. Annali di Geofisica, 43/4, 729-746.

Grenerczy, G., Kenyeres, A., & Fejes, I., **2000.** Present crustal movement and strain distribution in Central Europe inferred from GPS measurements. Journal of Geophysical Research, 105/B9, 21835-21846.

Grenerczy, G., Sella, G., Stein, S., & Kenyeres, A., **2005** Tectonic implications of the GPS velocity field in the northern Adriatic region. Geophysical Research Letters 32, L16311, doi:10.1029/2005GL022947

Grünthal, G., Mayer-Rosa, D., & Lenhardt, W., **1998**. Abschätzung der Erdbebengefährdung für die D-A-CH-Staaten - Deutschland, Österreich, Schweiz. Bautechnik, 75/10, 753-767.

Grünthal, G., & Wahlström, R., **2003**. An Mw based earthquake catalogue for central, northern and northwestern Europe using a hierarchy of magnitude conversions. Journal of seismology, 7(4), 507-531.

Grünthal, G., Wahlström, R., & Stromeyer, D., **2009**. The unified catalogue of earthquakes in central, northern, and northwestern Europe (CENEC)—updated and expanded to the last millennium. Journal of Seismology, 13, 517-541. doi:10.1007/s10950-008-9144-9

Gutdeutsch, R., & Aric, K., **1988**. Seismicity and neotectonics of the East Alpine–Carpathian and Pannonian area. American Association Petroleum Geologists, Memoir 45, 183-194.

Gutenberg, B., & Richter, C.F., **1942**. Earthquake magnitude, intensity, energy and acceleration. Bulletin of the Seimological Society of America, 32, 163-191.

Hainzl, S., Zöller, G., & Scherbaum, F., **2003**. Earthquake clusters resulting from delayed rupture propagation in finite fault segments. Journal of Geophysical Research, 108, doi:10.1029/2001JB000610

Hammerl, C., & Lenhardt, W., **2013**. Erdbeben in Niederösterreich von 1000 bis 2009 n. Chr. Abhandlungen der Geologischen Bundesanstalt, 67, 3-297.

Hinsch, R. & Decker, K., **2003**. Do seismic slip deficits indicate an underestimated earthquake potential along the Vienna Basin Transform Fault System? Terra Nova 15 /5, 343-349.

Hinsch, R., & Decker, K., **2011**. Seismic slip rates, potential subsurface rupture areas and seismic potential of the Vienna Basin Transfer Fault. International Journal of Earth Science, 100, 1925-1935. doi: 10.1007/s00531-010-0613-3

Hintersberger, E., Decker, K., Lüthgens, C., & Fiebieg, M., **2014**. Geological evidence for earthquakes close to the destroyed Roman city of Carnuntum. Schriftenreihe der der Deutschen Gesellschaft für Geowissenschaften, 85, 443.

Hussain, H., Shuangxi, Z., Usman, M., & Abid, M., **2020**. Spatial variation of b-values and their relationship with the fault blocks in the western part of the Tibetan Plateau and its surrounding area. Entropy, MDPI, 22, 1016. https://doi.org/10.3390/e22091016

Kröll, A., & Wessely, G., **1993**. Wiener Becken und angrenzende Gebiete - Strukturkarte-Basis der tertiären Beckenfüllung. Geologische Themenkarte der Republik Österreich 1:200.000.

Lenhardt, W., **1996**. Erdbebenkennwerte zur Berechnung der Talsperren Österreichs. Bundesministerium für Land- und Forstwirtschaft. Österreichische Staubecken kommission, Wien 1996.

Lenhardt, W., Freudenthaler, C., Lippitsch, R., & Fiegeil, E., **2007**. Focal depth distribution in the Austrian Eastern Alps based on macroseismic data. Austrian Journal of Earth Sciences, 100, 66-79.

Lenhardt, W., Svancara, J., Melichar, P., Pazdirkova, J., Havir, J., & Sykorova, Y., **2007**. Seismic activity of the Alpine-Carpathian-Bohemian massif region with regard to geological and potential field data. Geologica Carpathica, 58, 397-412.

Linzer, H. G., Decker, K., Peresson, H., Dell'Mour, R., & Frisch, W. **2002**. Balancing lateral orogenic float of the Eastern Alps. Tectonophysics, 354(3-4), 211-237.

Möller, G., Brückl, E., & Weber, R., **2011**. Active tectonic deformation at the transition from the European and Pannonian domain monitored by a local GNSS network. Vermessung & Geoinformation, 2/2011: 138-148.

Nanjo, K. Z., Hirata, N., Obara, K., & Kasahara, K., **2012**. Decade-scale decrease in b value prior to the M9-class 2011 Tohoku and 2004 Sumatra quakes. Geophysical Research Letters, 39, L20304, doi:10.1029/2012GL052997.

Nanjo, K. Z., & Yoshida, A., **2018**. A b map implying the first eastern rupture of the Nankai Trough earthquakes. Nature communications, 9/1, 1-7. DOI: 10.1038/s41467-018-03514-3

Nanjo, K. Z., & Yoshida, A., **2021**. A b map implying the first eastern rupture of the Nankai Trough earthquakes. Nature Communitactions, 9: 1117, DOI: 10.1038/s41467-018-03514-3

Nasir, A., Hintersberger, E., & Decker, K., **2020**. The 1906 Dobrá Voda Earthquake (M=5.7) at the Vienna Basin Transfer Fault: evaluation of the ESI2007 intensity and analysis of the aftershock sequence. Austrian Journal of Earth Sciences, 113/1, 43-58. doi:10.17738/ajes.2020.0003.

Nasir, A., Lenhardt, W., Hintersberger, E., & Decker, K., **2013**. Assessing the completeness of historical earthquake and instrumental data in Austria and the surrounding areas. Austrian Journal of Earth Sciences, 106/1, 90-102.

Nuannin, P., **2006**. The Potential of b-value Variations as Earthquake Precursors for Small and Large Events. Digital Comprehensive Summaries of Uppsala Dissertations from the Faculty of Science and Technology 183, Uppsala Universitet, ISBN 91-554-6568-4.

Ogata, Y., **1983**. Estimation of the parameters in the modified Omori formula for the aftershock frequencies by the maximum likelihood procedure. Journal of Physics Earth, 31, 115-124.

Öncel, A.O., Main, I., Alptekin, Ö., & Cowie, P., **1996**. Spatial variations of the fractal properties of seismicity in the Anatolian fault zones. Tectonophysics 257, 189-202.

Peresson, H., & Decker, K., **1997**. Far-field effects of Late Miocene subduction in the Eastern Carpatians: E-W compression and inversion of structures in the Alpine–Carpatian–Pannonian region. Tectonics, 16/1, 38-56.

Royden, L.H., **1985**. The Vienna Basin: a thin-skinned pull-apart basin. In: Biddle, K.T., Christie-Blick, N. (Eds.), Strike–slip deformation, basin formation and sedimentation: Society for Sedimentary Geology, Special Publication, 37, 319-338.

Schenkova´, Z., Schenk, V., Pospisil, L., & Kottnauer, P., **1995**. Seismogeological pattern of a transition area between the Eastern Alps and the Western Carpathians. Tectonophysics, 248, 235-245.

Scholz, C.H., **1968**. An experimental study of the fracturing process in brittle rock. Journal of Geophysical Research, 73, 1447-1454.

Scholz, C. H., **1968**. The frequency–magnitude relation of microfracturing in rock and its relation to earthquakes. Bulletin of Seismological Society of America, 58, 399-415.

Scholz, C. H., **2002.** The Mechanics of Earthquakes and Faulting. Cambridge University Press, ISBN-13: 978-0521655408

Scholz, C. H., **2015.** On the stress dependence of the earthquake b value. Geophysical Research Letters, 42, 1399-1402.

Schorlemmer, D., & Wiemer, S., **2004**. Earthquake statistics at Parkfield: 1. Stationarity of b values. Journal of Geophysical Research, 109, B12307. doi:10.1029/2004JB003234

Schorlemmer, D., & Wiemer, S., **2005**. Microseismicity data forecast rupture area. Nature, 434, 1086.

Sefara, J., Kovac, M., Plasienka, D., & Sujan, M., **1998**. Seismogenic zones in the Eastern Alpine–Western Carpathian–Pannonian junction area. Geologica Carpathica 49/4, 247-260.

Senatorski, P., **2019**. Gutenberg–Richter's b Value and Earthquake Asperity Models. Pure and applied Geophysics, 177, 1891-1905. doi:10.1007/s00024-019-02385-z

Shearer, P., & Stark, P., **2011**. Global risk of big earthquakes has not recently increased. Proceeding of the National Academy of Sciences, 109, 717-721. doi:10.1073/pnas.1118525109

Stein, R.S., Barka, A.A., & Dieterich, J.H., **1997**. Progressive failure on the North Anatolian fault since 1939 by earthquake stress triggering. Geophysical Journal International,1997, 128: 594-604.

Stein, S., & Liu, M., **2009**. Long aftershock sequences within continents and implications for earthquake hazard assessment. Nature, 462/5, 87-89. doi:10.1038/nature08502

Stepp, J.C., **1972**. Analysis of completeness of earthquake sample in the Puget Sound area and its effect on statistical estimates of earthquake hazard. National Oceanic and Atmospheric Administration Environmental Research Laboratories. Boulder Colorado, 80302.

Wells, D. L., & Coppersmith, K. J., **1994**. New empirical relationship among magnitude rupture length, rupture width, rupture area, and surface displacement. Bulletin of Seismological Society of America, 84, 974-1002.

Wessely, G., **1988**. Structure and development of the Vienna basin in Austria. In: Royden, L.H., Horváth, F. (Eds.), American Association of Petroleum Geologists, Memoir 45, 333-346.

Woessner, J., & Wiemer, S., **2005**. Assessing the quality of earthquake catalogues: Estimating the magnitude of completeness and its uncertainty. Bulletin of the Seismological Society of America, 95, 684-698. doi:10.1785/0120040007

ZAMG, **2020**. Earthquake catalogue of felt earthquakes 1200– 2020 AD. (Austria). Computer File. Central Institute of Meteorology and Geodynamics (ZAMG), Vienna, Austria.